THE REFERENCE CURRENT CONTROLLER AND COMPARISON WITH OTHER TECHNIQUES OF PRODUCING PWM WAVEFORMS

by

AHMAD MOHAMED ASAAD MAHMOUD

A thesis
presented to the University of Manitoba
in partial fulfillment of the
requirements for the degree of
PH.D
in

DEPARTMENT OF ELECTRICAL ENGINEERING
THE UNIVERSITY OF MANITOBA

Winnipeg, Manitoba

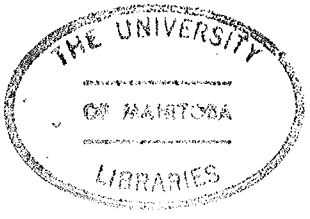

THE REFERENCE CURRENT CONTROLLER AND COMPARISON WITH OTHER TECHNIQUES OF PRODUCING PWM WAVEFORMS

BY

AHMAD MOHAMED ASAAD MAHMOUD

A thesis submitted to the Faculty of Graduate Studies of the University of Manitoba in partial fulfillment of the requirements of the degree of

DOCTOR OF PHILOSOPHY

ABSTRACT

A variety of pulse width modulation (PWM) strategies are now available for practical induction motor drive systems. Several of these are shown to be superior only over a limited part of the frequency range of interest. A simple bang-bang reference current controller is suggested and compared to the sinusoidal PWM and optimum PWM strategies, throughout a wide frequency range. The controller produces a PWM voltage waveform based on a comparison of the actual phase current with a reference current. Simulation techniques are used in the study to include the effects of saturation of mutual and leakage inductances and the deep bar effects. The overall efficiency of the system is calculated with these effects being included. The performance indices to be compared are the stator harmonic current content, the harmonic torque pulsations, and the motor efficiency. The current controller shows quite evident advantages over the other simple PWM techniques. Better values of the reference current are achieved in respect to improving the efficiency. Two disadvantages of the current controlled induction motor drive; namely the low starting torque and the proximity of the maximum torque to the rated torque were pointed out and discussed. These two problems were solved by using a simple flux linkage controller.

ACKNOWLEDGEMENT

I wish to express my heartfelt gratitude to Dr. R.W. Menzies, whom I admire, for his fruitful discussions, inspiring guidance and encouragement throughout the course of this research. Dr. R.W. Menzies, the Thesis advisor, must receive praise and grateful thanks for suggesting the idea of the reference current controller, for his sound expectations and for his precise supervision and revision.

The author acknowledges gratefully the thorough Thesis evaluation, the recommendations and the help of Dr. T.A. Lipo, the External Examiner. The assistance of Dr. R.M. Mathur, the Head of the Electrical Engineering Department, Dr. A.M. Gole and Dr. G.W. Swift at the final stage of the research is not forgotten.

The author gratefully appreciates the financial support of the Natural Science and Engineering Research Council of CANADA and the MANITOBA Department of Economic Development. Many thanks should be forwarded to the University of Manitoba Computer Center staff and advisors who have helped the author in different phases of this thesis. I would like also to thank the technical staff of the Electrical Engineering Department, who helped in some stages of this work.

Finally, sincere thanks and appreciation go to my wife for her unceasing encouragement, patience and love.

DEDICATED

TO

MY PARENTS

TABLE OF CONTENTS

LIST OF FIGURES

LIST OF TABLES

LIST OF SYMBOLS

LIST OF VARIABLES

$\hat{B}$	is the maximum flux density per pole
C	is a constant coefficient for load torque
D	is the filtered signal
DI	is the distortion index
e	is the induced e.m.f
E	is the dc line or bus voltage
ED	is the difference in motor efficiency
f	is the frequency
H	is the integration time increment
I	is the root mean square current
i	is the instantaneous current
J	is the polar moment of inertia
K	is the gain constant or proportionality constant
L	is the self, mutual or leakage inductance
LD	is the difference in total motor losses
m	is the number of discrete points in a cycle
M	is the mutual inductance
n	is the harmonic order
N	is a number of (harmonics or commutations)
Nu	is the rotor speed ($Nu=\dot{\theta}$)
p	is the differental operator
P	is the power
Q	is the quality factor
R	is a resistance or stability ratio
s	is the slip
S	is the slope
t	is the time
T	is the periodc time or torque
TML	is the total motor losses
V	is the root mean square voltage
v	is the instantaneous voltage
$\overline{U}$	is the mean value of a quantity
WE	is the energy loss per commutation
X	is the reactance
Y	is the original signal
Z	is the impedance
Δ	is a small deviation or increment
η	is the motor efficiency
θ	is the rotor angle
$\dot{\theta}$	is the rotor angular speed
$\ddot{\theta}$	is the rotor angular acceleration
λ	is the flux linkage
ν	is a ratio

π	is 22/7
σ	is the standard deviation
ψ	is the flux
ω	is the radian frequency or speed

LIST OF SUBSCRIPTS

1	for fundamental quantities
2	for lumped short circuit rotor quantities
a	for phase a quantities
	for air dependent part of leakage inductance
b	for phase b quantities
c	for phase c quantities
	for harmonic contents
	for friction coefficient
cs	for stator copper power loss
cr	for rotor copper power loss
d	for stator direct axis quantities
do	for constant term of load torque
d1	for friction or velocity term of load torque
d2	for fan type load torque
D1	for rotor first cage direct axis quantities
D2	for rotor second cage direct axis quantities
e+h	for eddy plus hysteresis power loss
eq	for equivalent short circuit reactance
f+w	for friction and windage power loss
g	for air gap quantities
i	for ideal efficiency
	for input voltage
	for iron dependent part of leakage reactance
I	for integral gain
l	for leakage inductance
	for load impedance angle
m	for magnetizing branch quantities
mr	for rotor mutual inductance
o	for running equivalent resistance or reactance
out	for output shaft power
p	for proportional gain
q	for stator quadrature axis quantities
Q1	for rotor first cage quadrature quantities
Q2	for rotor second cage quadrature quantities
r	for rotor quantities
R	for reference value of current or flux
r1	for rotor first cage quantities
r2	for rotor second cage quantities
Rmax	for max value of reference current
Rmin	for minimum value of reference current
Rset	for set value of reference current
s	for stator quantities
Tmax	for slip at maximum torque

Chapter I

INTRODUCTION

Electric drives of all types are heavy consumers of energy; indeed, studies[1,2] have shown that in the United States, 64% of the generated electricity goes to power drive systems. Much of this energy is wasted and many processes could be run with greater economy if an adjustable speed drive prime-mover was employed.

The objective of this research work is to achieve a wide range of speed control for the squirrel cage induction motor, with ratings in the 2kW to 200kW range. One of the important usages of these adjustable speed motors (prime-movers) is to control the flow of pumps and fans. The majority of the users now are investigating the replacement of inefficient variable speed drives, such as eddy current couplings, hydraulic couplings or the primary voltage control of Nema D induction motors. Other methods of flow control that should also be replaced are those using constant speed prime-movers and valves for controlling the fluid flow or dampers for controlling the air flow. All these variable speed drives consume large amounts of slip energy while with constant speed the flow controls involve high throttling losses. The same studies suggest that widespread use of efficient adjustable-speed drive technology could accrue energy savings to the United States by 1990, equivalent to one million barrels of oil per day.

It was recommended in the previous literature[3,4], that, in periods of energy shortage, rising energy costs and reduced drive costs through new technologies, it makes sense to check on applications periodically even if they were not considered worthwhile in the past. When energy is in tight supply and there is a demand for plants product, another factor to which consideration should be given is the amount of extra product that might be made in the plant if the losses on the various drives were reduced. In other words, during these times of fierce competition, the cost of a product can be reduced by improving production techniques. In conclusion, replacing inefficient drives with new types of adjustable speed drives will result in reduced operating costs.

The decision whether to apply ac or dc for some variable speed drive applications has been extensively discussed in the literature[4,5]. An important additional point to report here is the location of the repair facilities. Many service shops are simply not familiar with dc machines and therefore are incapable of repairing them. Important items like position of brushes, air gap, interpole, and shunt pole connections are sometimes done incorrectly.[4] In addition to that, the ac motor is always recommended over the dc in severe environments such as those where pumps and fans are often installed.

1.1 AN APPLICATION EXAMPLE

Let us take a pumping system to show how the adjustable speed flow control could be more efficient than the valve flow control in a constant speed system. Fans have similar operating characteristics[5]. The head/flow requirements are functions of the overall system configuration. All the secondary losses will be neglected in this discussion.

1.1.1 Valve Control

Figure 1.1 shows the effect of closing a valve in controlling the flow from a pumping system. The total system head curve is the sum of static head and friction losses. The friction losses, between the system head and the static head, in general vary as the square of the flow rate. If the flow is to be controlled to 50 percent by a valve, the overall head must be increased by partially closing the valve until the artificial system head intersects the pump head curve at 50 percent flow as shown by the marked line. The difference between pump head and original system head then represents the energy loss due to throttling. It is quite clear that the throttling energy loss is very large. This is more emphatically shown in the power versus flow characteristic shown on the same figure, where a reduction of 65% in flow results in a reduction of only 23% in the power input to the motor.

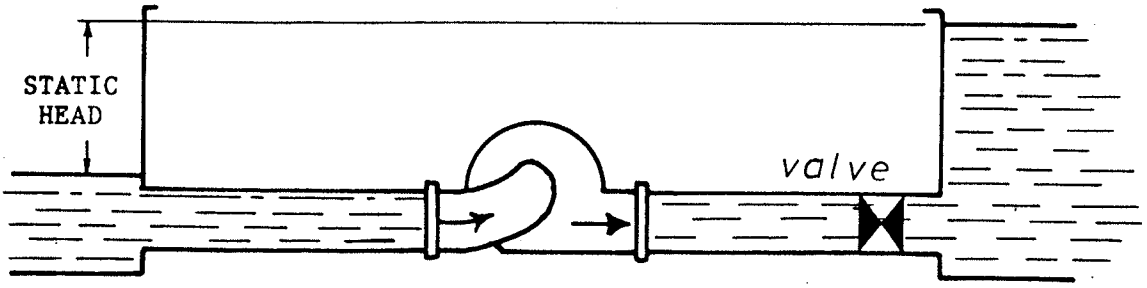

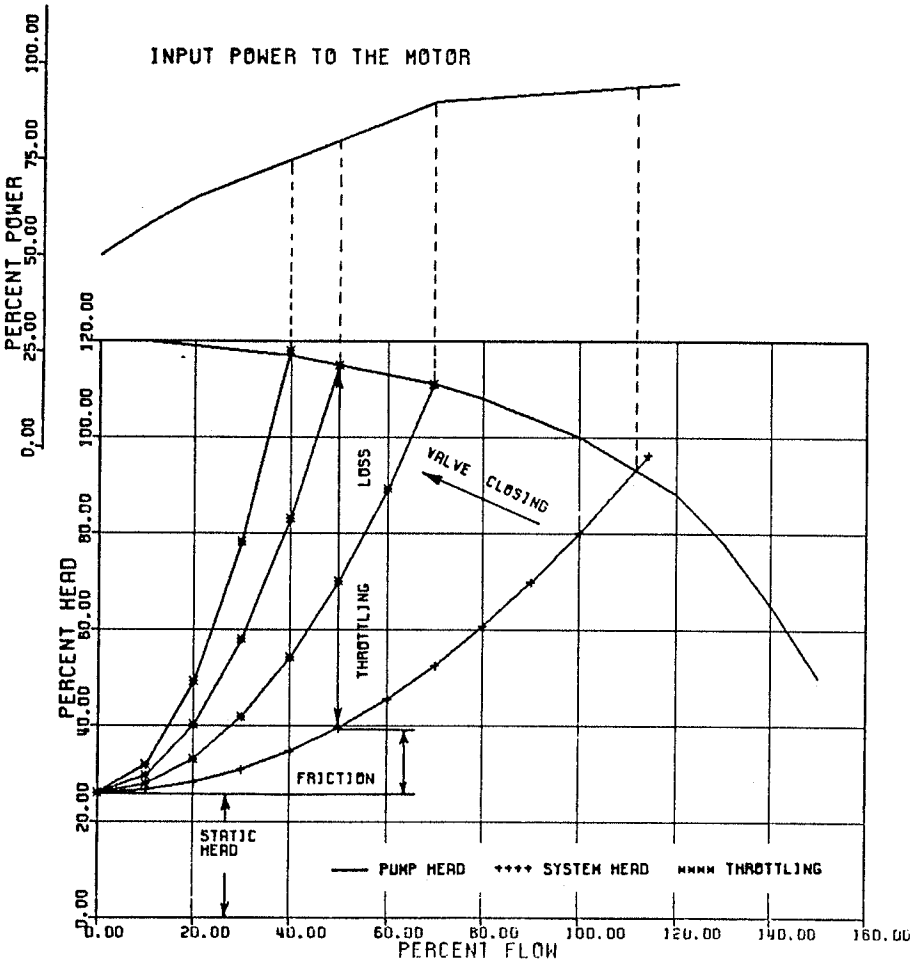

Figure 1.1: Valve Control.

1.1.2 Speed Control

When the head curve is of the type shown in Figure 1.1, the throttling losses are appreciable if reduced flow is required for long periods. Then the economical way to control flow is by speed control of the pump. Figure 1.2 shows the speed control curves along with the system head curve. If flow is to be controlled by speed, it can readily be seen that all that is needed is to reduce the speed of the pump until its characteristic intersects the system head curve at the desired flow. It is shown in the power curves that the same reduction in flow (65%) has resulted in a 75% reduction in the power input to the motor.

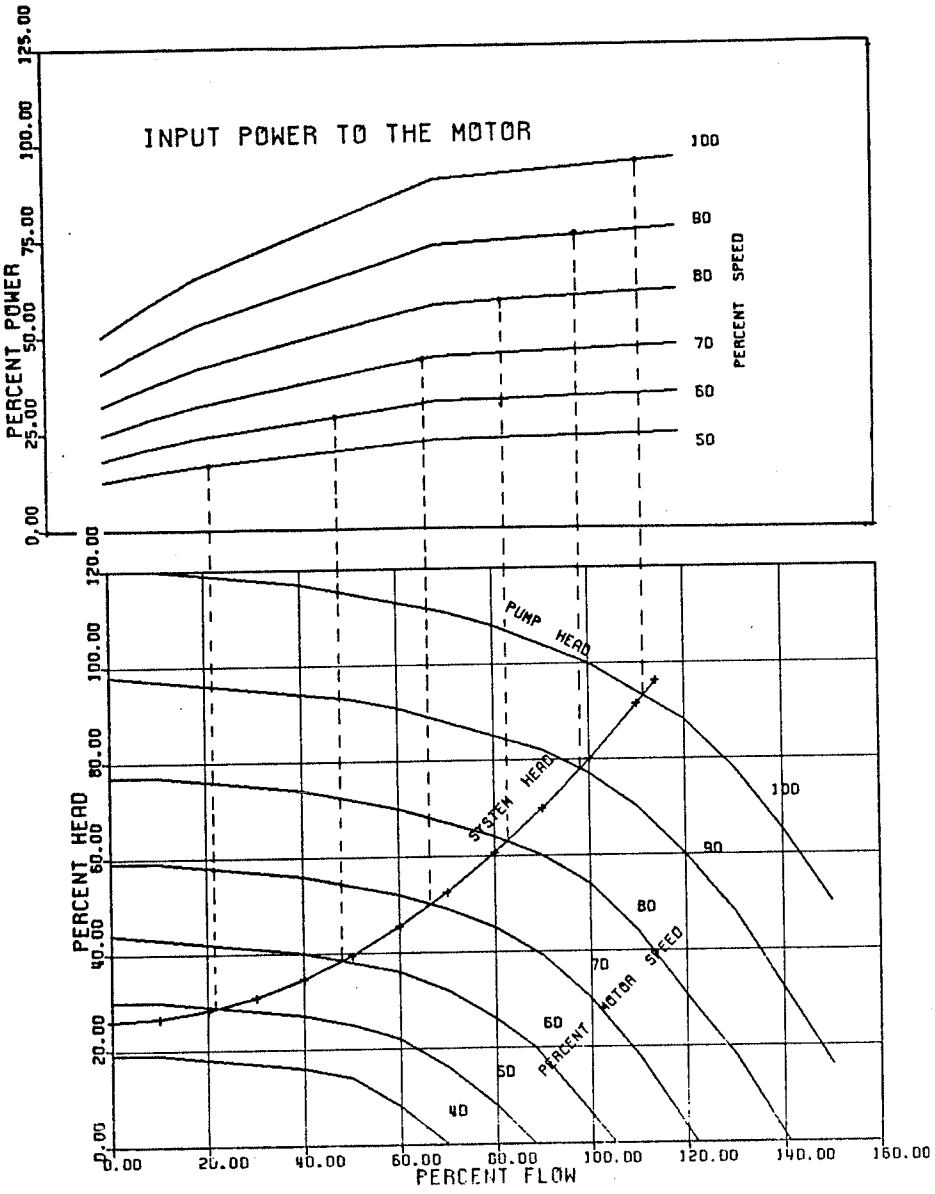

Figure 1.2: Typical System Head/Flow/Speed Curves.

1.1.3 Comparison between Valve Control and Speed Control

Let us consider the example when the flow is controlled by adjusting the speed of the pump rather than being throttled to the desired rate. Figure 1.3 shows a comparison between these two types of flow control. The pump has a constant static head H_s. In order to reduce the flow from

115% by an amount q_1 at constant speed (n_1), an artificial system curve (THROTTLING) is created by partially closing a throttling valve and consequently increasing the head losses by an amount h_s (point B to point C). On the other hand, by reducing the pump speed from n_1 to n_2 to reduce the flow by the same amount q_1, the head losses will be reduced from H_1 to H_2 (point A to point C) and the power required by the pump at the reduced speed at the reduced flow will be reduced from point B_1 (85%) to point C_1 (35%) on the power curves. Hence the reduction in input power is about 50%, which is truly significant.

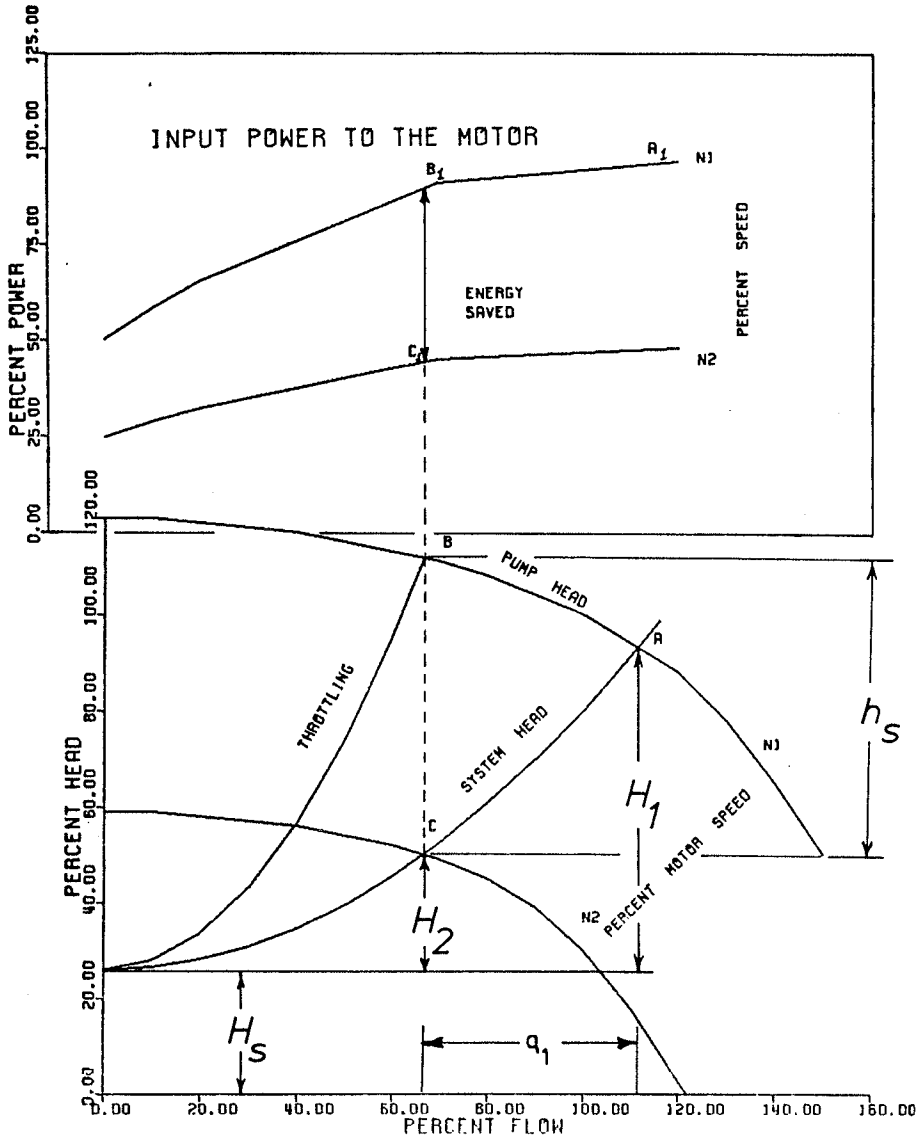

Figure 1.3: The Flow Control By The Two Methods

1.1.4 Objective of Thesis

The main objective of this thesis is to investigate the existing PWM strategies for controlling the speed of the induction motor, and to find the most suitable strategy for controlling the speed of pumps and fans. It is also the aim of the Thesis to study the different strategies and to compare them with respect to different performance indices, so that

the selection of one of the strategies over the others will be documented. A final model of the proposed strategy and the motor is to be studied with respect to different operating conditions to ensure that the scheme is reliable and applicable.

1.2 PWM INVERTERS FOR INDUCTION MOTOR DRIVES:

Actually it is the high efficiency of the variable speed drives comprising a dc-link inverter and conventional squirrel cage induction motor that is attracting most current attention, in the power range of interest. This type of speed control encounters reduced slip energy losses when compared with other types of speed control such as hydraulic coupling, eddy current coupling or stator voltage control. The pulse width modulated (PWM) voltage source inverter has these well recognized advantages: the inherent ability to provide continuous variable frequency and/or voltage control in a single power stage; in contrast to the variable voltage dc-link inverter, the commutating ability of the PWM inverter remains substantially constant since the dc-link voltage is constant irrespective of the voltage-frequency setting. Figure 1.4 shows the standard configuration, of a modern inverter drive in which the utility supply is rectified to form a constant voltage dc-link and the inverter stage drives the variable voltage and frequency supply to excite the induction motor from the link by using pulse width modulation techniques[6]. A single dc rectifier supplying a common bus-bar serving a number of inverters with motor loads is an application clearly favouring PWM. However, the main disadvantage of this type of supply is the additional loss arising from the harmonic voltages applied to the motor

windings. Therefore, it is obviously desirable for the inverter output to have a low harmonic content superimposed on the fundamental component that ensures the required flux density. This should be achieved with minimum complexity in the inverter control logic, and with a low switching frequency to keep the associated inverter losses small.

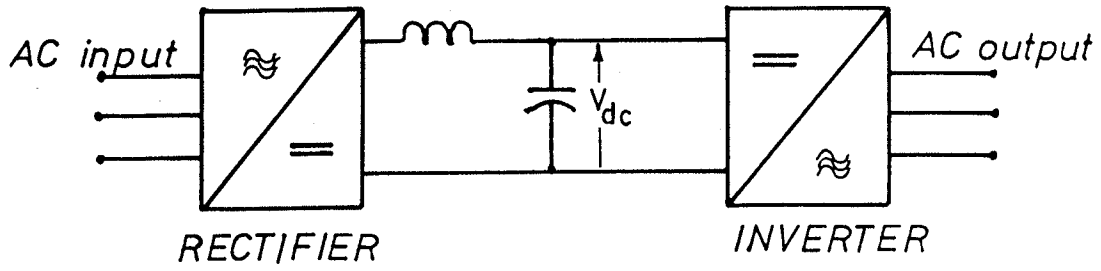

Figure 1.4: Elements of dc-Link Inverter ac Drive Unit

A good review of several types of PWM inverter systems is covered in references [6] and [7]. Voltage source PWM inverters for ac motor variable speed drives have conventionally employed sinusoidal PWM[8-19], optimum PWM[20-25] strategies or a current controller.[8,26-36] Each of these three methods has its advantages and limitations.[6,7,41,42] Sinusoidal PWM is best at low frequencies. Optimum PWM is difficult to implement and it is not as applicable at low frequencies as sinusoidal PWM. The current controller is still under investigation. It is therefore of interest to compare the different modulation techniques available and to introduce another technique that may combine the advantages of existing techniques. The sinusoidal PWM of

Schonung and Stemmler,[8] the optimum minimization techniques of Buja and Figalli[23,24] as well as the current controller strategy[30-34] will be discussed in Chapters 3 and 4 and compared in Chapters 5 and 6. These three strategies are not the only existing strategies, however, they are the only three techniques compared in the Thesis. The other techniques which may be included in a more general and comprehensive comparison are:

1. The other improved sinusoidal PWM techniques[9-19]
2. The delta modulation technique[37]
3. The duty ratio and the periodic modulation techniques[38,39]
4. The principle of circular rotating magnetic field[40]

A brief abstract will be given about each of these in the following:

Other improved sinusoidal PWM techniques recommended since first introduced by Stemmler[8]. Mokrytzki[6] reviewed the use of pulse width modulation and pointed out that before PWM can be easily applied to ac drives, the problems of complex control circuitry and relatively high motor losses must be solved. Zubec, Abbondanti and Nordby[9] discussed the performance of the inverter drives with the sinusoidal PWM technique, and indicated that the performance is critically influenced by the choice of the modulation policy . They proposed a transition between unsynchronized and synchronized PWM modes which allowed the extension of the practical speed range as the frequency is increased. Bowes[10] introduced a new sinusoidal PWM which uses ordered, uniform or regular sampling rather than natural sampling. The new uniform sampling

technique results in a symmetrical modulation, defines the pulse configuration more precisely and produces explicit expressions for the switching angles. Nayak and Hoft[11] predicted the efficiency for various carrier frequencies using Stemmler[8] and Pollac[12] techniques. They concluded that Stemmler's modulation approach, with a carrier frequency of 900 Hz, is found to be optimum as it results in a low filter rating and an efficient inverter. Barton[13] introduced the bessel approximation which shows high accuracy and gives good analytical insight into the waveform structure. Kliman and Plunkett[14] developed a method of analysis to predict the performance of an induction motor in response to inverter waveforms. They suggested a PWM method that allows the transitioning from sine wave shaping to square wave output voltage at the high frequencies before dropping pulses. Grant and Barton[15] reported also that, there are three distinct modes of operations, the pure PWM at the lower speeds, pure six step at the higher speeds, and quasi-PWM at the intermediate speeds. In the quasi-PWM mode they recommended that a modulation ratio be an odd multiple of three. Grant[16] discussed the traditional overmodulation method of pulse dropping and its practical limitations, (pulse of finite width must be dropped abruptly to obtain square wave). He also suggested a new method which produces smaller step changes in the output voltage. Green [17] discussed a new method for obtaining an optimal PWM sequence by considering the crest factor of the current waveform as a performance index. Ohnishi and Okitsu[18] introduced a novel PWM technique in which, the switching timing is obtained from the intersection of a triangular carrier waveform with control signals produced from the three phase desired voltages by removing the

largest one of them. They have shown, this new technique has some advantages over the natural PWM. Azusawa and Shiraishi[19] introduced a novel subharmonic method in which the carrier wave signal is sinusoidal rather than being the usual triangular sawtooth. The phase of the carrier changes abruptly by a factor of M (modulation ratio) when the phase of the modulating signal changes abruptly.

The delta modulation which was proposed by Ziogas[37] requires a simple circuit implementation, provides a smooth transition between PWM and single pulse (square wave) modes of operation. This technique has shown to be advantageous in static PWM inverter applications and can be used with ac drives.

The variable ratio and periodic modulation techniques. Adams and Fox[38] introduced an adaptive ratio modulation scheme, which combines the good features of the fixed and variable modulation techniques. The adaptive ratio modulation makes the necessary compromise to optimize the operating characteristics of a modulated six-step inverter. Sen and Premchandran[39] developed a novel PWM strategy based on the duty ratio and periodic modulation principles. They compared the new method with sinusoidal PWM and found that the new method produces acceptable motor current waveforms while keeping a low number of commutations per cycle.

The principle of circular rotating magnetic field. Murai and Tsunehiro[40] introduced an improved principle for obtaining a better PWM pattern for the three phase bridge inverter. The new method is based on the principle that, when a circular rotating magnetic field is formed at the air gap of the motor, the most desirable performance can be achieved.

1.3 SPEED CONTROL OF INDUCTION MOTORS

It is a common practice that, almost all the PWM strategies discussed in the previous section and even the variable voltage dc-link inverter (6-pulse inverter) should be equipped with some sort of volts/hertz control to be adequate and suitable for the application of interest. Feedback controls may also be used to enhance the operation of the drive , and therefore, three practical control methods for induction motors will be reviewed.[41-43]

Scheme No.1 discusses the variable voltage dc-link inverter in Figure 1.5. The part of the diagram inside the dotted line represents the simplest form of the drive without the feedback loop for slip regulation.[44,45] Scheme No.2 discusses the PWM inverter with a current controller.[26-36] A feedback control is added for the flux regulation, and torque regulation. Scheme No.3 discusses the field oriented control,[46,47] which is the most sophisticated existing type of control. It is very expensive and needs an on-line computer for processing. The field oriented control could be used with any PWM strategy. A phase locked loop for speed regulation could also be added to this scheme for obtaining a highly precise adjustable speed drive.

1.3.1 Scheme No. 1:

A block diagram of the speed control system with constant volts/hertz and controlled slip operation is shown in Figure 1.5. The slip frequency, ω_{sl}, which is proportional to torque is regulated by the speed loop errors. The ω_{sl} signal is added with speed signal ω_r to generate the inverter frequency ω_e^*. The voltage control signal V_e^* is generated from

ω_e^* through a function generator so as to maintain the air-gap flux approximately constant. The drive system accelerates with the clamped value of slip which may correspond to maximum torque, and then settles down to a value in steady state as dictated by the load torque. It should be noticed that in this scheme the waveform of the inverter output voltage is always square, (which means an appreciable amount of harmonics in the stator phase current), and that a tachometer is needed for the accomplishment of the feedback control.

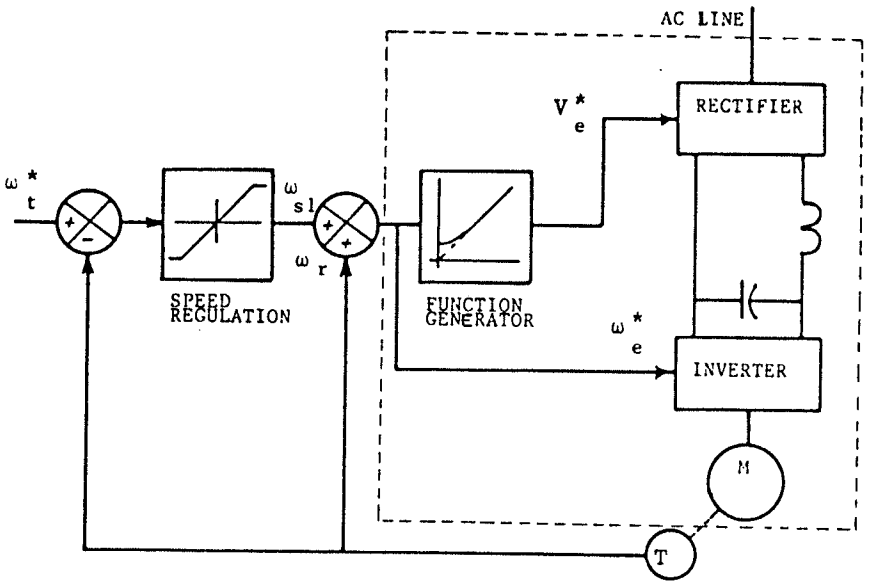

T= tachometer
M= squirrel cage induction motor

Figure 1.5: Scheme No. 1

1.3.2 Scheme No. 2:

A very improved control system can be designed where the flux and torque are close-loop controlled as shown in Figure 1.6. The torque loop error generates the slip command which is added with the speed to generate the frequency command. The air gap flux ψ_g may be either maintained constant as in a dc shunt motor or programmed as a function of torque for steady state efficiency improvement. The flux loop error generates the armature current command I_s^*, and the machine is operated continuously in current control mode. A set of three phase sinusoidal reference current waves is generated and the inverter switching devices are controlled such that the actual current profile remains within a hysteresis band (bang-bang control). Such a PWM control scheme tightly controls the ripple in the machine current wave. The feedback air gap flux and torque signals can be estimated from the machine terminal voltages and currents. The accuracy of estimation determines the precision within which the parameters can be controlled. The air gap flux can also be measured by inserting flux coils in the machine air gap.

The current control mode is in fact the heart of this thesis, and therefore it will be discussed separately in Chapter 4. For pump and fan drives, a very precise adjustable speed is not required, and therefore the feedback torque-frequency loop will be omitted from Figure 1.6 in our adapted model. The extremely steep characteristic of the stable part of the slip torque characteristic when the motor operates with a constant input current[26,27,34], (approximation of the current control mode of operation), justifies the neglect of this feedback loop. It will be shown later in Chapter 7 that, a programmed function between the

flux level at the air gap of the motor and the input frequency is needed to compensate for the omission of the torque-frequency loop.

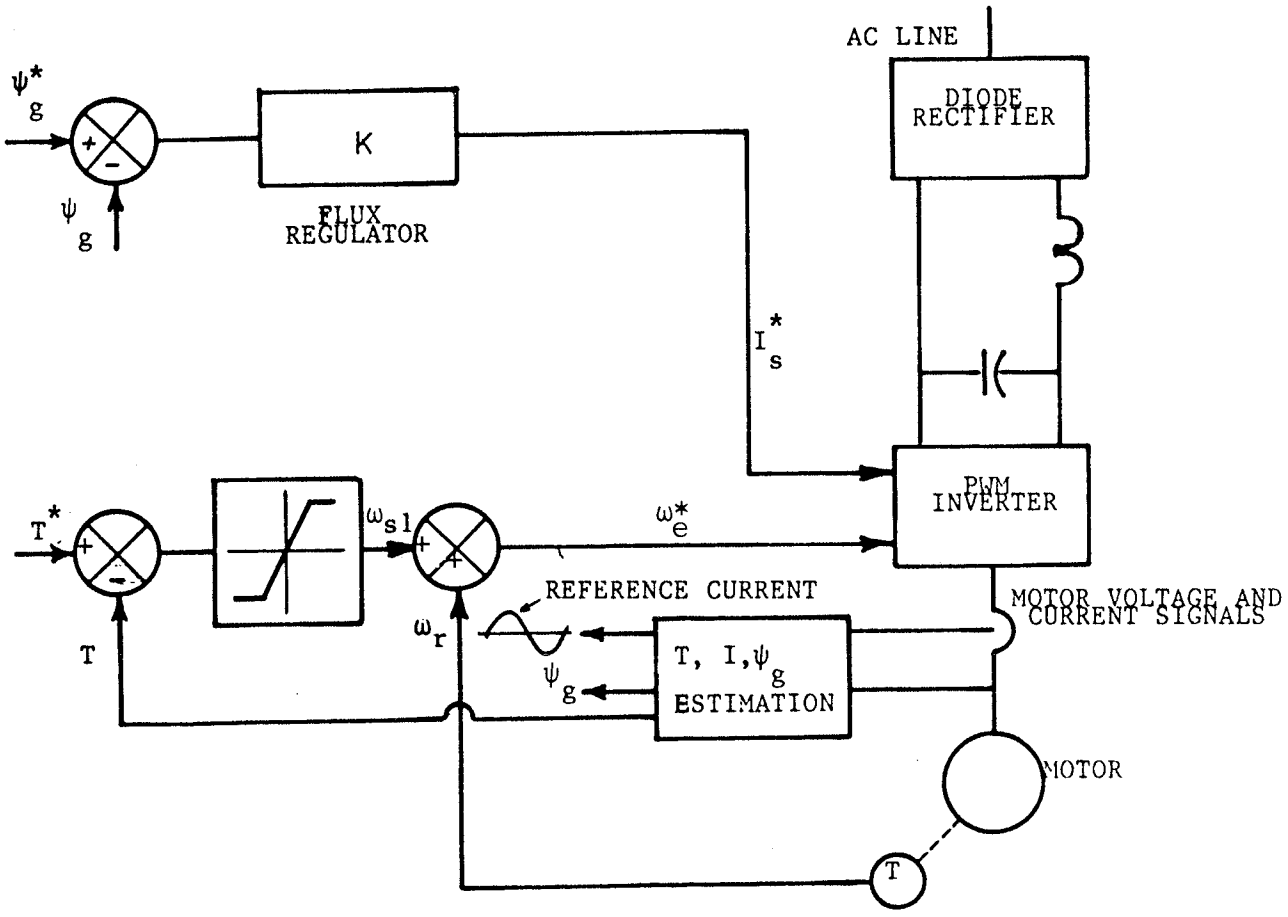

Figure 1.6: Scheme No. 2

1.3.3 Scheme No. 3:

Recently the concept of field oriented control which was introduced by the Siemens Company several years ago, is receiving wide attention. In field-oriented control, the induction machine is controlled like a dc machine and the principle can be explained as follows. In a dc machine, if armature reaction and saturation effects are neglected the developed torque is given by $T=K_t.I_f.I_a$, where I_f is the field current, and I_a is

the armature or torque producing component of current. The parameters I_f and I_a are mutually decoupled and best transient torque response can be obtained by controlling I_a with the rated value of I_f. In an induction motor the active and reactive power at the machine terminal correspond to the armature and field power, respectively, and these can be translated into the corresponding torque component and field component of current at a given frequency. This is explained in Figure 1.7 with the help of phasor diagrams in the d-q rotating reference frame. For simplicity the effect of rotor leakage flux is neglected. The developed torque across the air-gap is given by $T=K_t.\psi_g.i_{qs}$, where $i_{qs}=I_s.\sin\theta$, as shown in the figure. The air gap flux ψ_g is contributed by the component $i_{ds}=I_s.\cos\theta$. Therefore, the torque can be expressed as $T=k_t.i_{ds}.i_{qs}$, where i_{ds} is the field component of current and i_{qs} is the torque component of current. The torque equation is analogous to that of a dc machine. The parameters i_{ds} and i_{qs} are mutually decoupled and can be independently varied, by changing the torque and/or the flux commands.

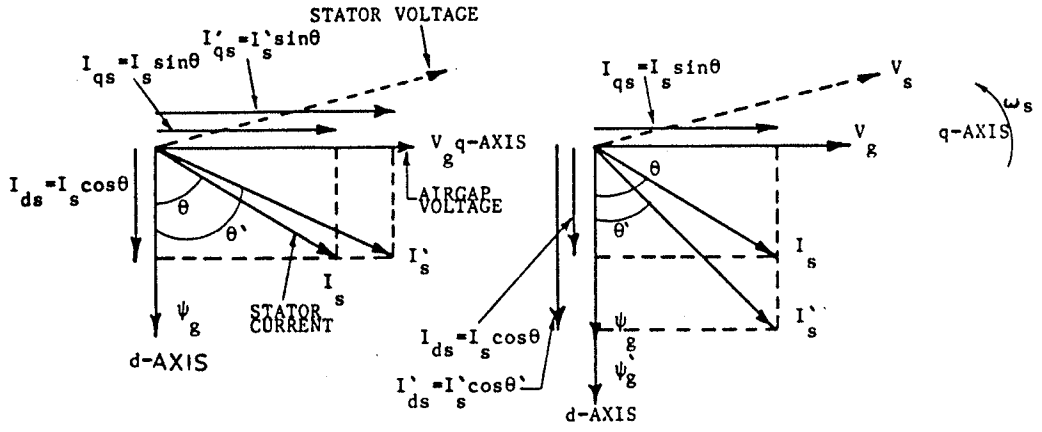

Figure 1.7: Scheme No. 3

1.4 OUTLINE OF THESIS

If the motor is to be operated under conditions in which fluxes vary widely, as for example when the stator voltage or frequency are changed, the effects of saturation changes on the parameters are not trivial and must be taken into account. The deep bar squirrel cage rotor has the desirable features of high effective resistance and correspondingly large torque at starting and low effective resistance and hence low losses at operating speed. Therefore, simulation of the induction motor should include the effects of saturation on the mutual and leakage inductances and the deep bar effect. This complete model is developed in Chapter 2 so as to be used afterwards in the comparative study of the different PWM strategies. The obtained simulation results compare well with that of test.

The time domain analysis technique is introduced in Chapter 3 and is compared to the frequency domain analysis previously widely used[48-50].

The design and operation of the reference current controller is introduced in Chapter 4. This type of control proved to be superior to the other PWM strategies in some parts of the frequency range and gives almost the same results in the other ranges. It is compared to the better technique throughout the complete frequency range.

The results of the comparative study are included in Chapter 5 as well as the applicability of the proposed drive to frequency or load changes.

The complete time domain model developed in Chapter 2 which include the simulation of the saturation and deep bar effects is used in Chapter 6 to compare the motor efficiency from different nonsinusoidal supplies, at 60 Hz. In order to obtain better values of the reference current with respect to, efficiency improvement, extensive calculations are made over 100 sample cycles.

A flux linkage controller that maintains constant flux linkage at the terminals of the motor (approximately constant air gap flux) is added to the reference current controller in Chapter 7. The features of this modification are demonstrated, during sudden and high load changes and during speed changes.

The conclusions and future recommendations are included in Chapter 8.

Chapter II

SIMULATION OF SATURATION AND EDDY CURRENTS EFFECTS

2.1 THE EFFECT OF SATURATION

In the linear model of induction motor used for simulation, it is assumed that the flux in the magnetic circuit can be divided into a relatively small number of components (main or mutual and leakage) and that no currents flow in the magnetic material. However, the assumption of ideal magnetic material in the generalized theory of induction machines is not valid over the whole range of operation. Different effective constant parameters applicable to the particular problem may be used. If the machine is to be operated under conditions in which fluxes vary widely, as for example when the stator voltage or frequency are changed, or in dc dynamic braking, the effects of saturation changes on the parameters are not trivial and have to be taken into account[51]. Also the effect of saturation of both magnetizing and leakage reactances is essential for more accurate calculations of the inrush current and accelerating time of induction motors[52].

When the ampere-turns consumed in the iron portions of the magnetic circuit become large with respect to the air gap ampere-turns, the value of inductances will consequently vary with current, depending on the flux density in the iron. There are four definitions of the inductance of a saturated magnetic circuit. The choice of inductance definition de-

pends on the purpose in view. These definitions will be included here for reference only.

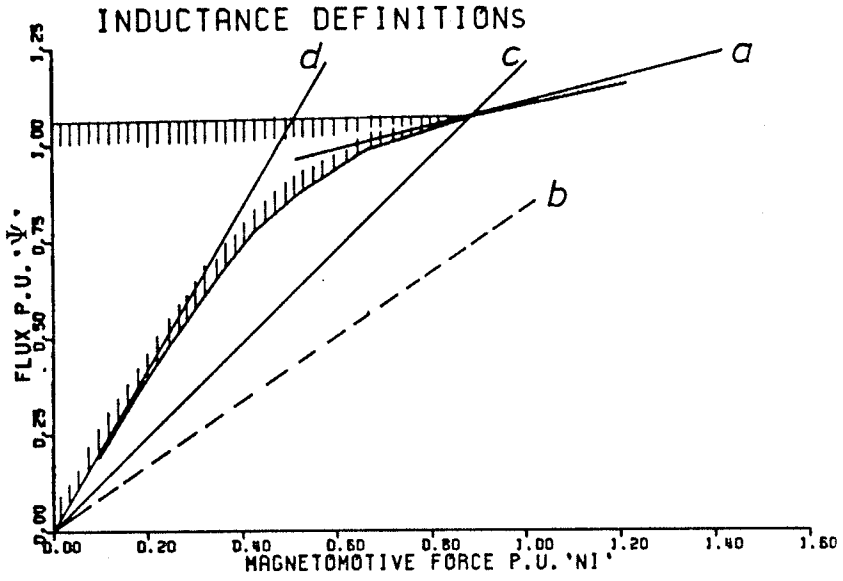

a) incremental b) effective

c) apparent d) air gap

Figure 2.1: Inductances of a Saturated Circuit.

Figure 2.1 indicates four alternative definitions of inductances:

a) The lowest value is the incremental inductance or,

$$L = (N \Delta \Psi)/\Delta I,$$

$$S = \Delta \Psi/(N \Delta I)$$

where;

S: slope

N: number of turns per phase

Ψ: flux

I: current

ω: angular frequency, f: frequency

b) The next lowest is the effective inductance, which is calculated from the energy stored in the inductance,

$$L = (2.0/I^2) \int ei \, dt$$

but,

$$e = -N(d\Psi/dt)$$

therefore,

$$L = (2.0/I^2) \int Ni \, d\Psi = (2.0 \times \text{shaded area})/I^2$$

and the effective slope,

$$S = (2.0 \times \text{shaded area})/(N^2 \times I^2)$$

c) The apparent inductance, defined by the final values of flux and current is,

$$L = (N \times \Psi)/I$$

d) The unsaturated inductance is defined by the air gap line of magnetization curve.

The reactance calculations in electrical rotating machines are derived as $\omega L = 2\pi f (N\Psi/I)$ values, on the apparent inductance basis, (line C in Figure 2.1). Due to the fact that, nearly all the flux paths have series air gaps, the saturation effects can usually be allowed for by simple corrections to the apparent inductance values. Therefore, these values will be used to take into account the effect of saturation in the induction motor model.

It is well known that the leakage reactance of an induction motor during starting at full voltage is appreciably less than during normal running. Since the main and leakage fluxes use the same iron, the effective magnetizing inductance is greatly reduced when the armature current and hence the armature leakage flux increases to a high value. Thus, a direct attack on the problem of saturation using the circuit equations is not feasible. Nevertheless, often useful results can be obtained by minor modifications of the linear theory which, although not rigorously valid, can at least give a result better than that obtained from linear equations.

2.1.1 The Equivalent Circuit

The equivalent circuit of a single cage induction motor with the saturation of mutual and leakage reactances being allowed for are shown in Figure 2.2.

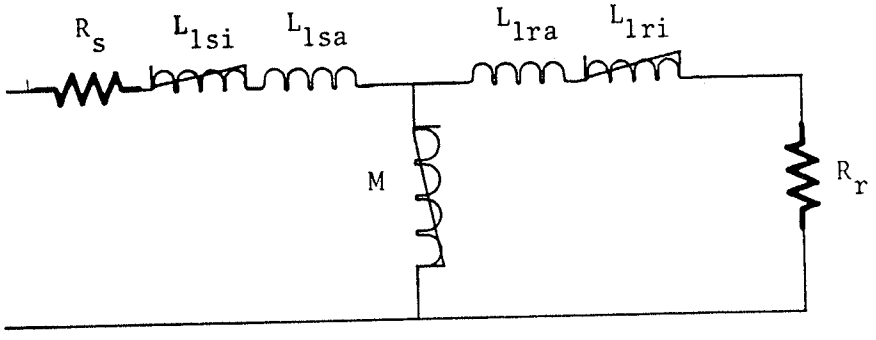

Figure 2.2: Equivalent Circuit (Leakage and Mutual Saturation)

Relatively little has been published on the prediction of saturation factors. One of the latest studies on this subject is the one made by Chalmers and Dodgson[53]. In this study the only components of leakage flux which are assumed not to saturate are the end-winding and slot-body leakage fluxes. This is due to the fact that these fluxes cross wide air gaps, so they have the same permeance at all currents, but those that cross short air gaps reach magnetic saturation at high currents, giving reduced permeance. Therefore, the total leakage reactance may be presented by the expression[54].

$$X = A + B\ (\ I'/I\ ) \qquad \text{approximately} \qquad (2.1)$$

where A is the reactance of the coil ends and the wide portions of the slots (slot-body), and B is the reactance of the tooth tips, zigzag, and skew leakage. I'/I is the ratio of the current at which saturation occurs to the actual current. This ratio is taken as unity for all values of current less than I'. The current at which saturation occurs is different for each leakage path, hence, the B term in equation (2.1) consists of three or more distinct terms with different values of I'. In medium size cage induction motors, the usual locked rotor current is about six times full-load current, and the values of I' may be any where from two to five times full load current, or even lower for fully closed rotor slots. There will be a problem, therefore, in calculating the values of I' at which the magnetic saturation occurs for stator and rotor tooth tips, for the zigzag leakage flux and for the skew leakage, respectively. Practically, it is only feasible to obtain a saturation factor for the whole leakage reactance as a function of the line current

as shown in Figure 2.6 from a locked rotor test.* It was recommended by Lipo and Consoli[52], that, the relative values of the end winding leakage inductances and the air dependent portions of the slot leakages (slot-body) is difficult to determine, unless special facilities are provided. They also added that, practically, the solution of the machine equations is effectively independent of the choice so long as the sum of the air dependent and iron dependent leakage inductances is always made equal to the measured total leakage inductance for any operating condition.

Consequently, the total stator and rotor leakage inductances may be given by,

$$L_{ls} = L_{lsa} + L_{lsi} \tag{2.2}$$

and,

$$L_{lr} = L_{lra} + L_{lri} \tag{2.3}$$

The terms L_{lsi} and L_{lri} correspond to the sum of the iron dependent slot, zigzag, belt and skew leakage inductances for the stator and rotor respectively, and are assumed to saturate. The terms L_{lsa} and L_{lra} correspond essentially to slot body and end winding leakage inductances and are assumed constant.

---

* With the help of a digital storage oscilloscope and a point on wave switch, it is possible to pass as large as 6 p.u. short circuit current for about 30-60 cycles, and, then record one cycle of voltage and current. Hence, V_{sc}, I_{sc}, and the phase angle between them are measured.

2.1.2 The Leakage Inductance Treatment

Although the previous analysis explains quite well what is going on inside the induction motor during saturation, it was found that quite reasonable results (as will be demonstrated later) may be obtained with induction motor parameters of stator and rotor leakages separated properly and by putting

$$L_{lsa} = L_{lra} = 0.0 \tag{2.4}$$

in equations (2.2&2.3) then,

$$L_{lsi} = L_{ls} \tag{2.5}$$

and,

$$L_{lri} = L_{lr} \tag{2.6}$$

In other words the constant air dependent component of the leakage inductance in equations (2.5&6) will be defined by the flat part of the saturation curve. The saturation factor used is that obtained from the saturation locked rotor test explained before (Figure 2.6). One should expect such a result because the leakage reactance obtained from the locked rotor test is the augmented total leakage which contains in it both the constant and iron dependent terms and the saturation factor there by obtained will produce the effect of both simultaneously.

2.2 THE EFFECT OF EDDY CURRENTS

There are two types of eddy currents which occur in electrical machines:

a) Those in the magnetic material.

b) Those in the electrical conductors.

The calculation of the losses due to the eddy currents in the magnetic material is to a great extent empirical since they include not only the losses in the laminated material due to the main flux, but also losses due to high frequency pulsations at the air gap surface and stray fluxes linking the structural material of the machine. The total loss when the machine is excited but carries no load current is known as the core loss. It is a small proportion of the rated output but it has an important effect on the efficiency and the heating of the machine. The core loss is an unavoidable defect of the machine and the design is carried out so as to make it as small as possible.

During load; the core loss is increased by an amount called the load loss, which depends approximately on the square of the load current. This loss is allowed for by deducting a separate value of the loss from the output. The effect may be important for motor starting, during which the loss is appreciable because of the high current.

In the linear model of induction motor it is assumed that the current density is uniform. Eddy currents effects occur in electrical conductors if the dimension in the radial direction is appreciable. Consider the rotor bar in Figure 2.3. Assume it to consist of an infinite number of layers of differential depth; one at the bottom and one at the top are indicated cross-hatched. The leakage inductance of the bottom layer is greater than that of the top layer, because the top layer is linked by less leakage flux. However, all the layers are electrically in parallel.

1 links 'x'
1,2,3,4 link 'y'

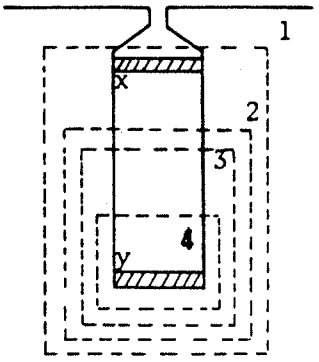

Figure 2.3: Deep Bar and Rotor Slot Leakage Flux.

Consequently, with alternating current, the current in the low reactance upper layers will be greater than that in the high-reactance lower layers; the current will be forced toward the top of the slot, and the current in the upper layers will lead the current in the lower ones. The nonuniform current distribution results in an increase in the effective resistance and a smaller decrease in the effective leakage inductance of the bar. Since the distortion in current distribution depends on an inductive effect, the effective resistance is a function of the frequency. Consequently, the deep bar rotor, in which the depth of the slots is purposely exaggerated, provides the desirable features of high effective resistance and correspondingly large torque at starting, while under running conditions its resistance is low so that speed regulation and efficiency are not impaired.

The double cage induction motor, which has two separate cages at different radial distances from the air gap, may be used for taking the deep bar effects into account. The double cage motor has the following steady state equations and equivalent circuit as shown in Figure 2.4.

$$V = V_m + (R_s + jX_s)\, I_s \tag{2.7}$$

$$0 = V_m + (R_{r1} + jsX_{r1})I_{r1} + jsX_{mr}(I_{r1} + I_{r2}) \tag{2.8}$$

$$0 = V_m + (R_{r2} + jsX_{r2})I_{r2} + jsX_{mr}(I_{r1} + I_{r2}) \tag{2.9}$$

$$I_m = I_s + I_{r1} + I_{r2} \tag{2.10}$$

$$V_m = jX_m I_m \tag{2.11}$$

The suffixes s and r indicate stator and rotor respectively, R_{r2} and jX_{r2} represents the second cage and X_{mr} is the reactance corresponding to the leakage flux which links the two rotor windings but not the stator.

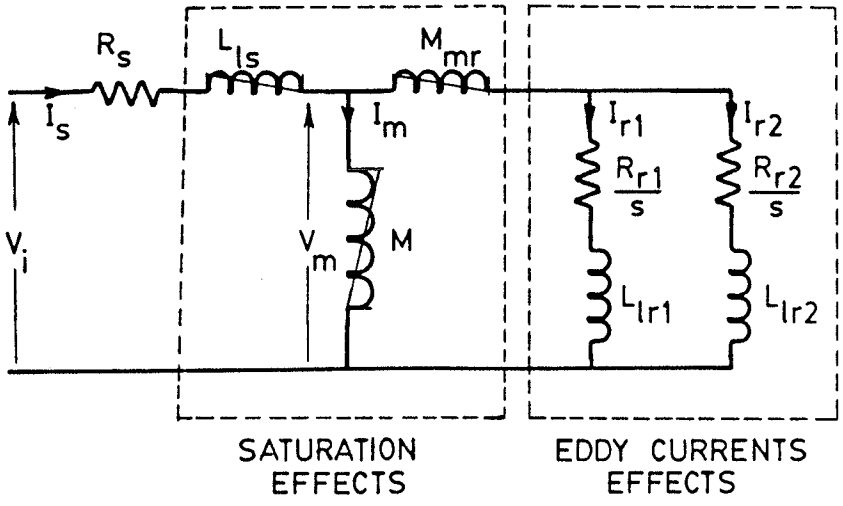

Figure 2.4: The Equivalent Circuit of the Double Cage Induction Motor

2.3 THE TRANSIENT SIMULATION OF THE COMPLETE MODEL

The dynamic performance of an induction motor is quite complex because of the coupling effect between the stator and rotor phases, where the coupling coefficients vary with rotor position and saturation, consequently the d-q axis model is used. In this method the complexity can be reduced and the variables and parameters be expressed in decoupled direct-and quadrature- axes.

2.3.1 Modelling of the Deep Bar Effects

The double cage induction motor was used for the simulation of these deep bar effects. The equivalence between the double cage and deep bar rotors is well established by the analysis made by Alger[55]. With the deep bar simulation different equations are needed for the different shapes of the deep bars. On the other hand, using the double cage technique, the same equations apply with only different parameter values. A practical method for measuring the double cage parameters is outlined in Appendix A. The equations for the direct and quadrature voltages in the stator and the two rotor windings are derived from those given by Adkins[56]. All the parameters are defined, with a step by step analysis in Appendix B. The final result is given by the following:-

$$\begin{bmatrix} v_{D1} \\ v_{Q1} \\ v_{D2} \\ v_{Q2} \\ v_d \\ v_q \end{bmatrix} = \begin{bmatrix} R_{r1}+L_{r1}p & 0 & M_r p & 0 & Mp & 0 \\ 0 & R_{r1}+L_{r1}p & 0 & M_r p & 0 & Mp \\ M_r p & 0 & R_{r2}+L_{r2}p & 0 & Mp & 0 \\ 0 & M_r p & 0 & R_{r2}+L_{r2}p & 0 & Mp \\ Mp & M\,Nu & Mp & M\,Nu & R_s+L_{ss}p & L_{ss}\,Nu \\ -M\,Nu & Mp & -M\,Nu & Mp & -L_{ss}\,Nu & R_s+L_{ss}p \end{bmatrix} \begin{bmatrix} i_{D1} \\ i_{Q1} \\ i_{D2} \\ i_{Q2} \\ i_d \\ i_q \end{bmatrix} \tag{2.12}$$

2.3.2 Modelling of Saturation

The saturation of the magnetizing reactance M is represented by a curve of reactance versus the magnetizing current I_m (Figure 2.5), following the technique introduced by de Mello[57]. The magnetizing current in the two cage simulation is given by;

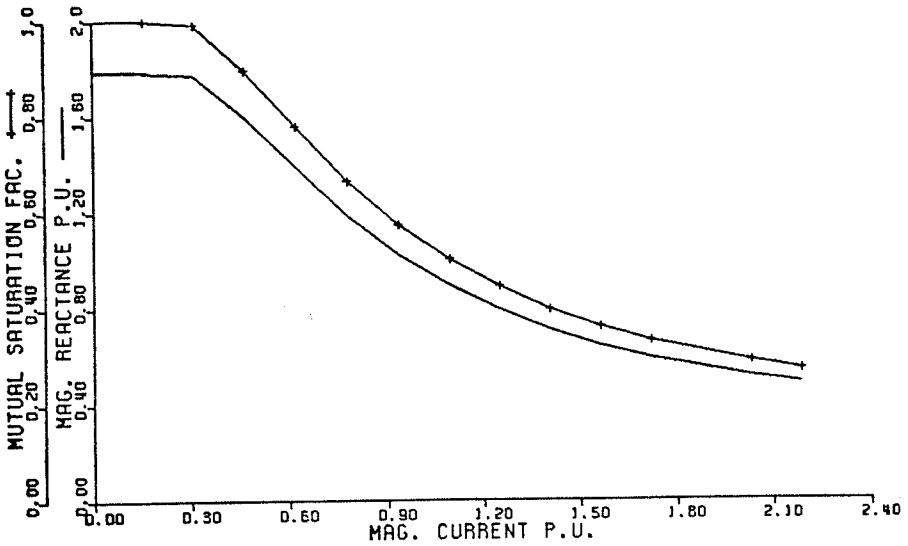

Figure 2.5: The Mutual Saturation Factor

$$I_m = \sqrt{(i_q+i_{Q1}+i_{Q2})^2+(i_d+i_{D1}+i_{D2})^2} \tag{2.13}$$

The simulation of the leakage reactances is allowed for by following the technique of Lipo[52] in which a locked rotor test is performed for acquiring the leakage saturation factor as a function of the line current (Figure 2.6). Depending on whether the leakage reactance is in the stator or the rotor circuit the respective current is substituted for the value of the line current versus the leakage saturation factor. In the simulated model, saturation is assumed to happen in the rotor mutual inductance and the stator leakage only. No saturation takes place in the leakage inductances of the two cages since, they are considered to be responsible for the simulation of the deep bar effect, Figure 2.4.

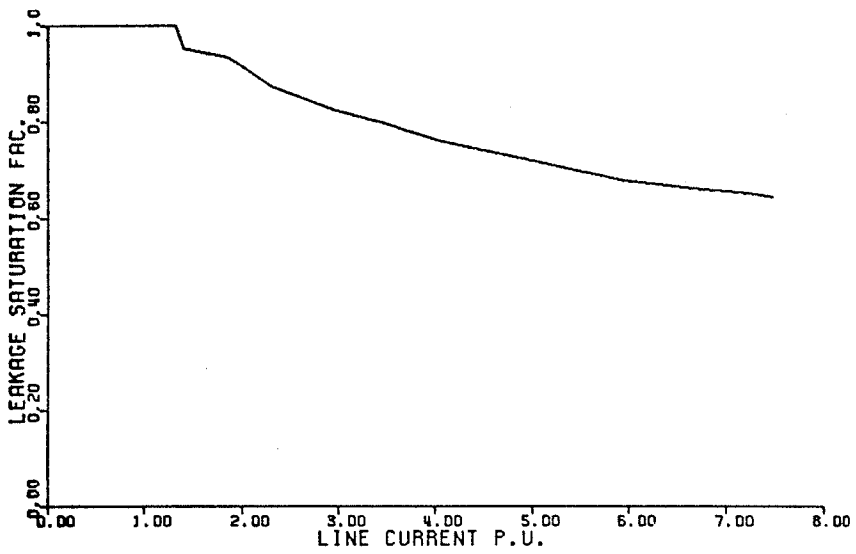

Figure 2.6: The Leakage Saturation Factor

The rest of the various resistive and reactive parameters in this study are assumed to have constant values for all conditions and are measured by conventional no-load and locked rotor tests (Appendix C). The double cage parameters are separated using the analysis made in Appendix A.

2.3.3 Transformation Equations

The d-q stator voltages are obtained from the standard transformation equations, with the stationary frame of reference fixed to the rotor (Appendix B).

$$v_d = 2/3[v_a \text{Cos } \theta + v_b \text{Cos } \theta_2 + v_c \text{Cos } \theta_3]$$

$$v_q = 2/3[v_a \text{Sin } \theta + v_b \text{Sin } \theta_2 + v_c \text{Sin } \theta_3] \qquad (2.14)$$

where, θ is the angle between phase 'a' and the direct axis.

$$\theta_2 = \theta - 120.0^\circ$$

$$\theta_3 = \theta + 120.0^{\circ}$$

2.3.4 Torque Equations

The instantaneous electromagnetic torque, T, in terms of the d-q axis quantities is:

$$T = M[(i_{Q1}+i_{Q2})i_d-(i_{D1}+i_{D2})i_q] \tag{2.15}$$

and the complete torque equation is:

$$J\ddot{\theta} + f_c\dot{\theta} = T - T_L \tag{2.16}$$

where;

J is the inertia ; f_c is the friction coefficient

T_L is the load torque

2.3.5 Numerical Technique

The machine equations (2.12-16) are solved numerically on a digital computer using the self starting modified Euler (predictor-corrector) method for integration. This method has comparable accuracy with respect to the more complex methods of Runge-Kutta as well as being more efficient with respect to computing time[58].

To obtain the solution with the desired degree of accuracy, separate solutions were run each with different step size and solutions obtained were then compared, decreasing the step size at each run until two consecutive solutions are in good agreement. Therefore, during starting transients, the time increment, H is selected to be 0.015625. If H is selected to be a fraction equal to the inverse of 2 raised to any power n i.e; $(1/2^n)$, this will eliminate the truncation errors likely to occur during successive computations extending over many cy-

cles of the input voltage, and this is equivalent to 0.9 of a degree at the 60 Hz (one per unit) frequency. The results of the simulation program have been verified by laboratory tests of starting the motor from rest under no-load conditions, where the comparison of the transient stator current, shaft torque and rotor speed will be demonstrated next.

2.4 PRACTICAL VERIFICATION OF THE SIMULATION

2.4.1 During Starting

Figures 2.7,2.8,2.9 show the stator phase current, the shaft torque and the rotor speed during starting. To demonstrate the effect of saturation of mutual and leakage, four different studies were performed. The first with both constant nominal mutual and leakage inductances. The second with saturation of both these inductances. The third with saturation of mutual inductance only. The fourth with saturation of the mutual inductance and constant saturated value of leakage inductance (taken as one half of the unsaturated leakage inductance). Hence, in this last run the assumed inrush values of the leakage inductances are used. Finally, a laboratory oscillograph for the machine during starting under the same loading conditions, as the simulation, is included in each Figure.

It can be noticed from these Figures that, when the mutual saturation alone, is active i.e; Figures 2.7,2.8,2.9 (c) the result is almost the same as that obtained from the linear model Figures 2.7,2.8,2.9 (a). This should be expected due to the fact that the magnetizing branch does not saturate heavily during starting, since it is shorted during starting by the small impedance of the cage rotor. The run-up time is about

160 p.u., and it is quite a bit larger than that obtained in the laboratory, Figures 2.7,2.8,2.9 (e).

Now, consider Figures 2.7,2.8,2.9 (b), on which the saturation of both mutual and leakage are active, together with Figures 2.7,2.8, 2.9 (e) from the laboratory test. It is clear that they agree very closely with each other except that, the first inrush values of the simulated current (5.0 p.u.) is little less than that obtained from test (5.6 p.u.). This error is due in part to the current probe indicator (3% sensitivity error in the current probe and 3% error in the attenuator accuracy of the current probe amplifier)[59,60], with which the current was measured. The error may also, be due to the fact that the iron losses are neglected in the simulation model during these runs. These iron losses are increased considerably during starting, since high currents add large stray load losses. Therefore the inrush current from test is expected to be higher than that from the simulation to cater for the neglected iron losses and stray load losses. The run up time from simulation (130 p.u.) is in good agreement with that of test (127 p.u.). The maximum torque is also close.

Finally, consider Figures 2.7,2.8,2.9 (d) in which one half the values of the normal leakage reactances are used. It can be seen that the machine starts very fast with larger transients in the currents and torque, which again does not compare to the laboratory tests.

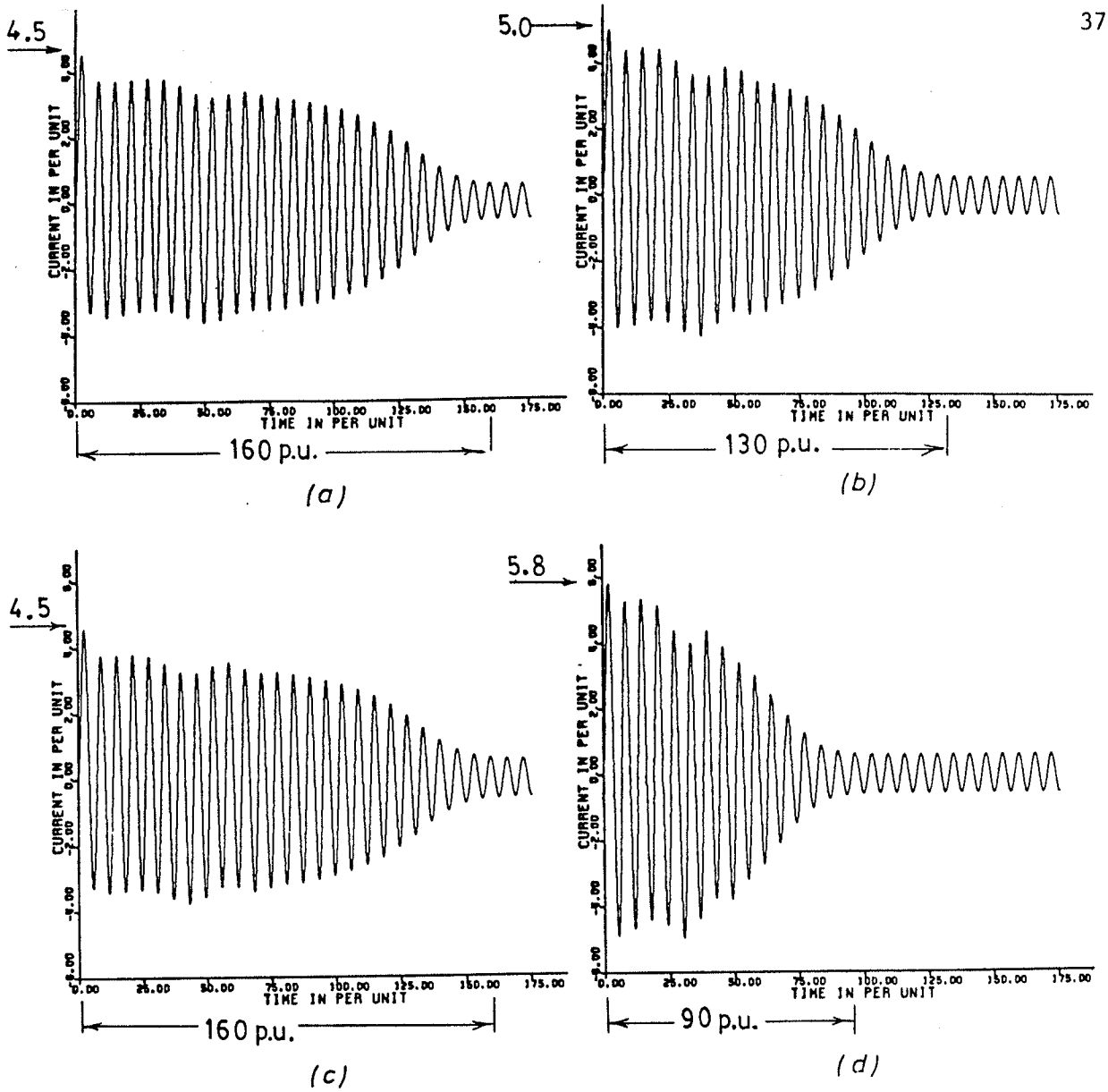

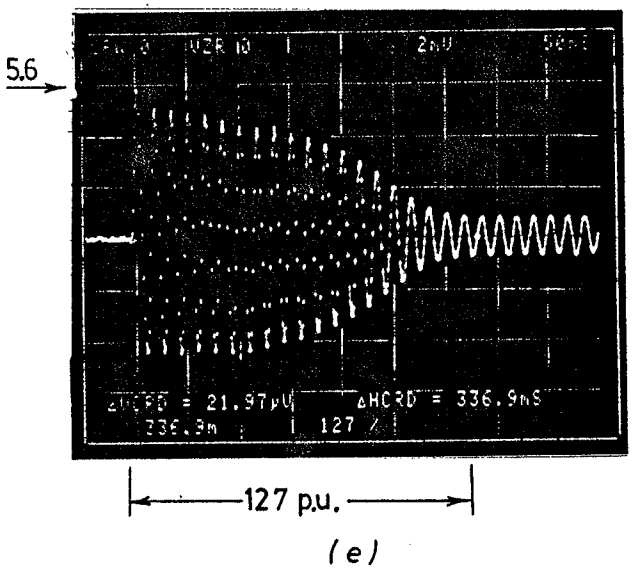

Fig. 2.7 The stator phase current of a 3-phase star connected induction motor during starting from different simulation routines and from a laboratory test of the machine being simulated.

(a) Linear model "no saturation".

(b) Magnetic and leakage saturation are simulated.

(c) Only magnetic saturation is simulated with full value of leakage reactance.

(d) Only magnetic saturation is simulated with half value of leakage reactance "inrush value".

(e) Laboratory.

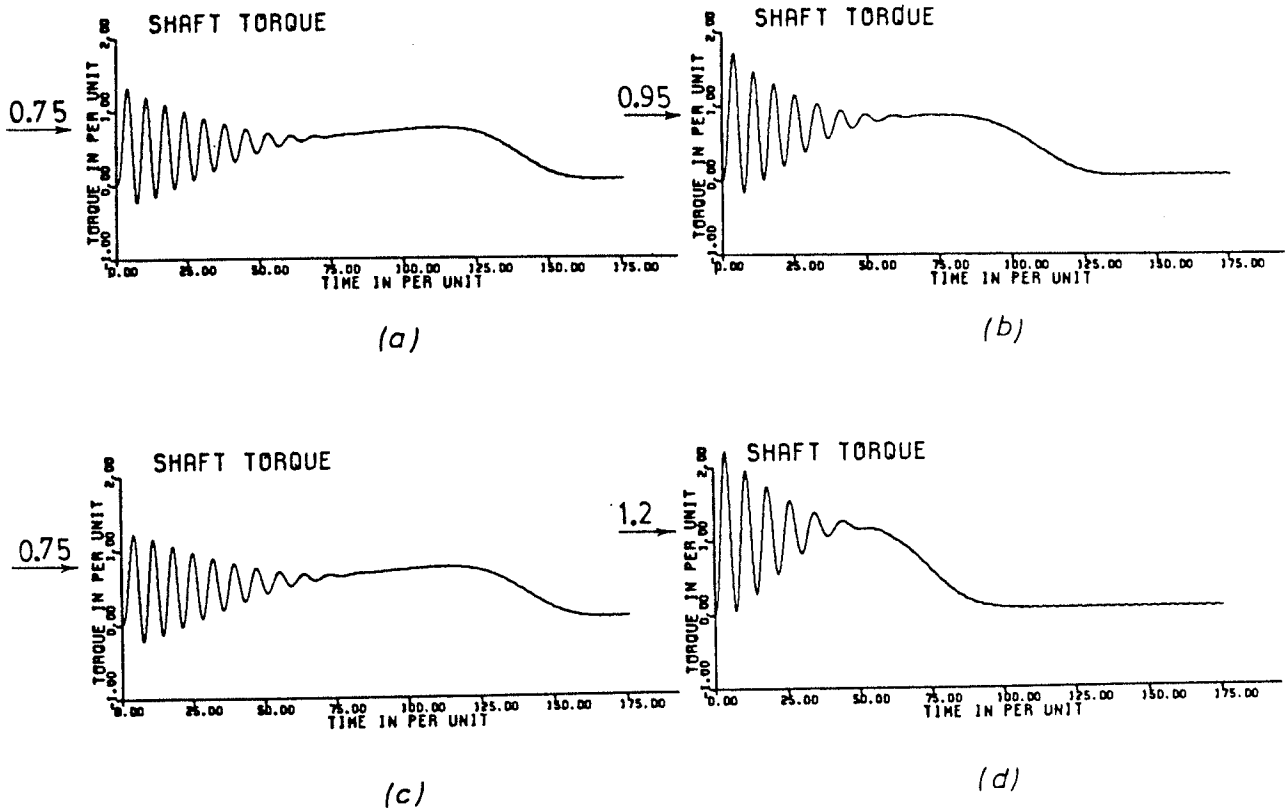

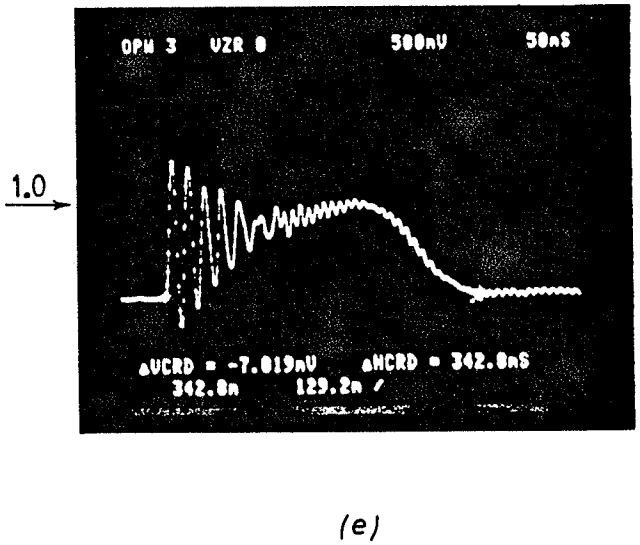

Fig. 2.8 The shaft torque of a 3-phase star connected induction motor during starting from different simulation routines and from a laboratory test of the machine being simulated.

(a) Linear model "no saturation".

(b) Magnetic and leakage saturation are simulated.

(c) Only magnetic saturation is simulated with full value of leakage reactance.

(d) Only magnetic saturation is simulated with half value of leakage reactance "inrush value".

(e) Laboratory.

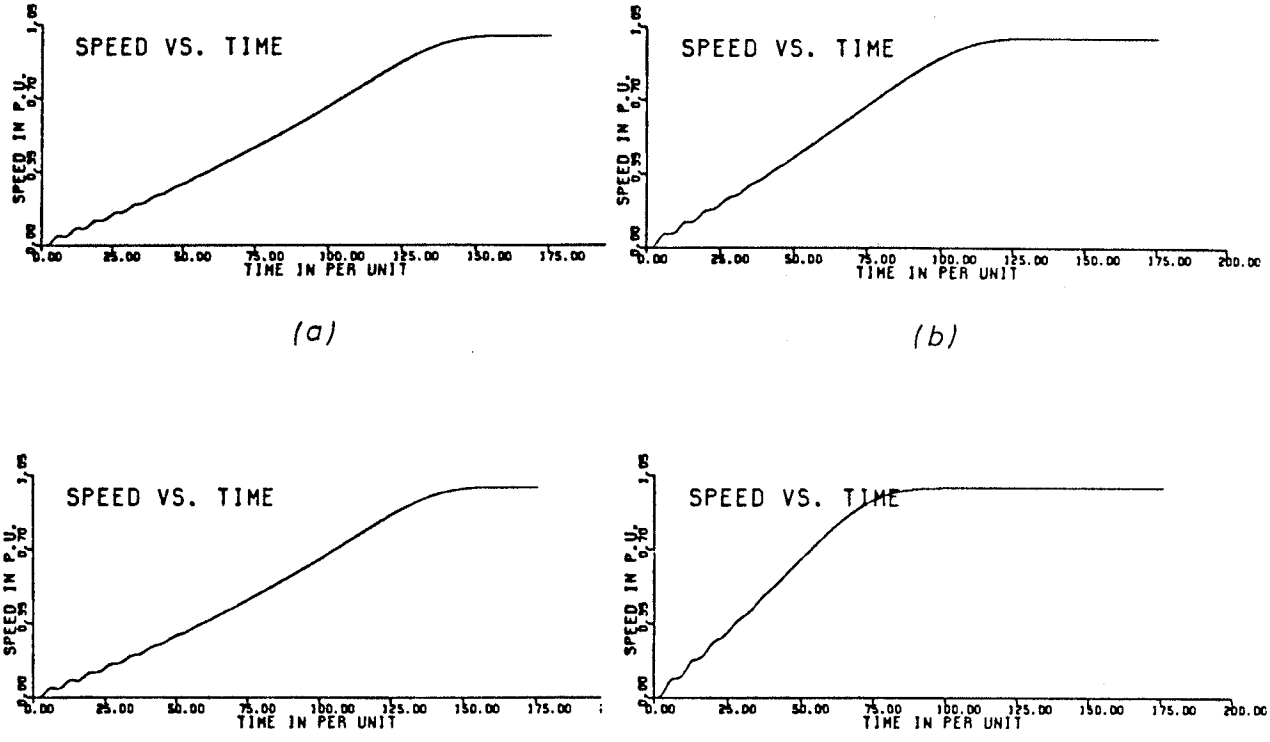

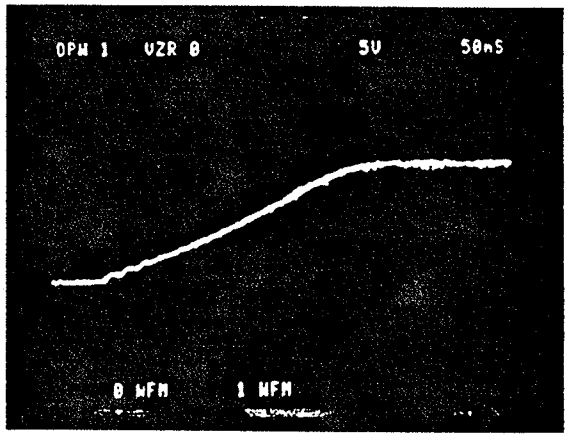

(e)

Fig.2.9 The rotor speed of 3-phase star connected induction motor during starting from different simulation routines and from a laboratory test of the machine being simulated.

(a) Linear model "no saturation".

(b) Magnetic and leakage saturation are simulated.

(c) Only magnetic saturation is simulated with full value of leakage reactance.

(d) Only magnetic saturation is simulated with half value of leakage reactance "inrush value".

(e) Laboratory.

2.4.2 During Loading Operation

The same motor used in the starting study will now be used for the verification of the motor model during load operation at two representative frequencies (60 and 30 Hz). A constant volts/cycle square wave inverter is used for testing the motor at load when fed from a square wave supply as well as sinusoidal supply (by driving a two synchronous machine set, at different speeds, to obtain variable voltage and variable frequency sinusoidal supply). The available inverter produces 120 volts at 60 Hz. However, since the motor under test is rated 208 volts at 60 Hz, the inverter volts/cycle was adjusted to a maximum of 160 volts at 60 Hz. Therefore, the motor has to be supplied a voltage lower than its rating (motor ratings and base values are given in Appendix C, Motor #2). The idea of using a step up transformer was given a trial, but it has been noticed that the square wave is smoothed slightly by the transformer leakage inductance. Therefore, during the study the motor was derated to about 160 & 80 volts at 60 & 30 hz respectively. The same shaft torque and the same root mean square input voltage were maintained from the two waveform supplies during the test. Afterwards the test operating point load torque is fed to the simulation program. In addition, the same per unit test values of the input frequency and voltage are also used in the simulation. The above should furnish a valid basis for comparing the test and the simulation results.

In Table 2.1 the frequency, f, was measured by a sample-hold digital frequency meter. The fundamental of the input voltage as well as the input current from the two supplies are also included in the table. During the test the torque was measured by a calibrated torque transduc-

er amplifier and the speed was measured by a tachometer calibrated by a stroboscope at the power frequency. It should be noticed that, the output power and the motor speed obtained from test and simulation are almost the same at each frequency, which implies that the comparison is made at almost one operating point throughout. The simulation calculates the motor losses and efficiency in the time domain using the snapshot and the sample cycle technique (explained in Chapter 3).

At 60 Hz the total motor losses (TML) as well as the motor efficiency (η) from simulation match quite closely with those from test. However the efficiency from both is low because the motor is derated. On the other hand at 30 Hz, the above indices from simulation are a bit far from those of test. The author attributes that to imbalance in the measured input voltages and currents which was not simulated, as well as to noticeable mechanical vibrations of the bench on which the tested induction motor-dc generator set was mounted, at 30 Hz. The phenomena of reduced speed oscillations or the lightly damped operation of the induction motor was noticed and studied before by Nelson, Lipo and Krause at the low frequencies[61]. In addition to that, there is the friction coefficient which is a mechanical nonlinear factor and could be the reason behind the decreased test efficiency, because due to the mechanical vibrations the motor shaft should be suffering from some sticking effort (torque). Hence, the friction coefficient should be effectively increased. On the other hand, only one value for the friction coefficient was used at both frequencies in the simulation.

Nevertheless, in order to judge the accuracy of the proposed model on a fair basis, let us consider the losses difference (LD) as well as the efficiency difference (ED) between the two waveform supplies. In fact the accuracy of the model should be determined by matching these differences in test and in simulation rather than by matching the total losses and or the efficiency. In conclusion, at both frequencies, the differences from simulation are a bit lower than those of test, which indicates that the model is slightly optimistic.

TABLE 2.1

MOTOR LOSSES AND EFFICIENCY CORRELATION

	60 Hz				30 Hz			
	TEST		SIMULATION		TEST		SIMULATION	
SUPPLY	SINE	SQUARE	SINE	SQUARE	SINE	SQUARE	SINE	SQUARE
f	1.00476	1.00733	1.00476	1.00733	0.50333	0.50333	0.50333	0.50333
V_1	0.74040	0.71619	0.74040	0.71474	0.38580	0.36912	0.38580	0.36881
I_s	0.95000	0.96355	0.96513	1.01997	0.56094	0.56823	0.55321	0.57512
P_{out}	0.43792	0.43636	0.43976	0.43744	0.10900	0.10851	0.10958	0.10867
Nu	0.92620	0.92293	0.92872	0.92270	0.47065	0.46846	0.47256	0.46932
TML	0.12590	0.13266	0.12678	0.13209	0.04193	0.04361	0.03510	0.03625
η	0.77670	0.76686	0.77622	0.76806	0.72230	0.71330	0.75741	0.74985
LD	6.76×10^{-3}		5.31×10^{-3}		1.68×10^{-3}		1.15×10^{-3}	
ED	9.84×10^{-3}		8.16×10^{-3}		9.00×10^{-3}		7.56×10^{-3}	

where:

ED	is the difference in motor efficiency
f	is the frequency in per unit
I_s	is the root mean square stator current
LD	is the difference in total motor losses (TML)
η	is the motor efficiency
P_{out}	is the shaft output power
TML	is the total motor losses
V_1	is the fundamental of the supply voltage

2.5 SUMMARY

The double cage simulation of the deep bar induction motors is simple and practical for solving the induction motor operation during transients. Consideration of the saturation of the mutual and leakage inductances is necessary for an accurate representation during starting. A practical method for finding the double cage parameters is outlined and the results obtained were used in the program. Excellent agreement between the simulated and test results of the starting transients at no-load was achieved, which indicates that the suggested model is accurate. The accuracy of the model was also confirmed during load operation at two representative frequencies. The model is suitable for time domain performance studies of the induction motor when fed from variable frequency nonsinusoidal supplies, since it takes into account the deep bar and the saturation effects.

Chapter III

THE PERFORMANCE OF INDUCTION MOTOR SUBJECT TO PWM WAVEFORMS

The digital simulation discussed in the second Chapter is used with a single cage linear model, (Motor #1 in Appendix C), of the induction motor for the determination of the performance when PWM strategies are applied to it. It is the purpose of this Chapter to demonstrate the simulation of these different PWM strategies and the performance of the motor subjected to them. Regarding performance, our objective is to calculate the harmonic contents of a stator phase current, the electromagnetic harmonic pulsating torques, the efficiency of the motor and the over-all efficiency of the inverter-induction motor system. The linear model is used for the prediction of the stator current harmonic contents and the electromagnetic harmonic torques. The efficiency is calculated with deep-bar and saturation effects being included, (Motor #2 in Appendix C).

3.1 AN ENERGY EFFICIENT PWM DRIVE

For obtaining an energy efficient PWM drive system, three main parts should be investigated as shown in the schematic of Figure 3.1.

It can be detected that, the logical beginning in such a scheme is to start by evaluating the induction motor performance subject to different PWM waveforms. Comparing these different strategies will cer-

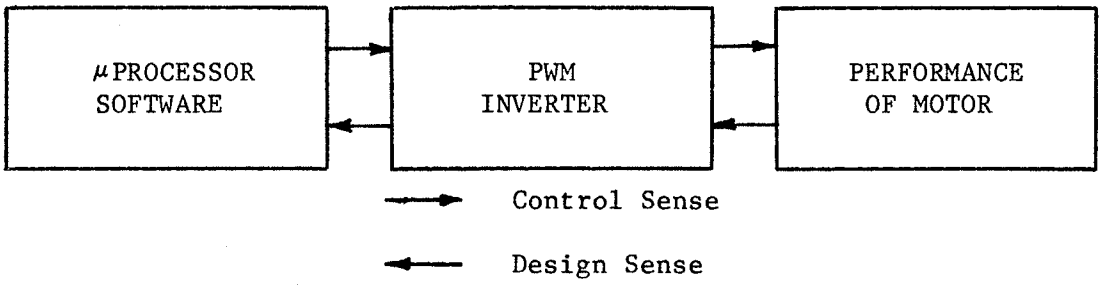

Figure 3.1: Steps Required for Obtaining an Efficient PWM

tainly be essential for the determination of the most efficient and/or the most suitable strategy for the purpose under consideration. Knowning the required strategy is the key for the selection and design of the inverter, and will guide the development of the microprocessor control program.

Hence, the objective now is to obtain a model for the calculation of the performance of the induction motor when fed from nonsinusoidal or especially PWM waveforms. The following PWM strategies are the most used techniques today.

* The sub-harmonic or sinusoidal PWM technique [8-19].
* The harmonic elimination PWM technique [20-22].
* The minimum distortion or optimal PWM technique [23-25].
* The reference current controller or Bang-bang technique [30-36].

3.2 REVIEW OF EXISTING PWM TECHNIQUES

The subharmonic method[8] requires many commutations per cycle of the output waveform, but, it proves to be superior to the other PWM techniques at low frequencies, where a high number of commutations per cycle is feasible to use.

In the harmonic elimination technique[20-22], optimal switching patterns are developed to eliminate a fixed number of harmonics. To vary the fundamental of the output voltage, a phase shifting technique between the poles of the full wave bridge is used.

The study made by Buja[23] on the minimum distortion technique leads to significant results even with small number of commutations per cycle, which implies in turn low commutation losses in the inverter. The comparison study, using Fourier analysis or frequency domain analysis, made by Murphy, and Egan[62,63] on the usual types of PWM strategies, with regard to the additional harmonic losses in the motor and the pulsating torques confirmed the above statement and added the following information. The selection of a large number of switching angles for the optimum PWM is very tedious and hard to implement, but, the optimum PWM strategy is superior to the sinusoidal PWM at high speeds, in respect to efficiency and amplitude of peak current.

According to the calculations made by De Buck[64] the reduction in the harmonic content by increasing the pulse number does not necessarily offer a substantial improvement.

3.3 THE FREQUENCY DOMAIN ANALYSIS

To illustrate the advantages of the time domain technique for the calculations of the steady state performance of the induction motor when subject to nonsinusoidal waveforms, let us try to evaluate the previous work using the frequency domain technique[48-50].

3.3.1 The Saturation Problem

To be able to include saturation in frequency domain calculations the fundamental frequency equivalent circuit shown in Figure 3.2 should be used together with a semi-empirical formula for the calculations of L_m

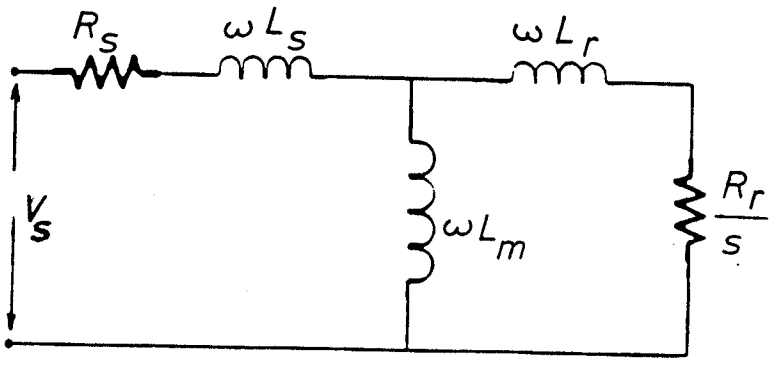

Figure 3.2: The Equivalent Circuit of Fundamental

(saturated). With a no-load saturation curve of sinusoidal excitation, being previously fed to the computer, the no-load current is calculated from the empirically found equivalent no-load voltage and substituted versus the curve to find the saturated value of L_m. In addition to that, the leakage inductances are also influenced by the harmonic current peaks, which are to be found later. Therefore, it is necessary to use leakage inductances of somewhat less than the full load values in

motor performance calculations. A 15-20 percent reduction was proposed to be satisfactory for the motors and waveforms discussed in this previous work. However, this assumed reduction in the leakage reactance due to saturation is very approximate.

3.3.2 The Applicability of Superposition

Despite this weak approach of taking the effects of saturation into account, the frequency domain method is based on the application of the superposition theorem. Consequently, there stems the question posed previously by Abrams[65] which is;

> How then, does the use of the superposition theorem be justified in the presence of the magnetic saturation which is certainly a nonlinear effect?

Actually, there was no justifying answer to this question. This indicates the need for a somewhat better approach to the problem of saturation.

3.3.3 The Accuracy of Harmonic Circuits

It should also be pointed out that, the harmonic circuits are all essentially locked rotor equivalent circuits, i.e, the slip equals approximatly 1.0 for all higher harmonics. This causes discrepancies between the calculated and measured harmonic currents. Also, neglecting magnetizing inductance in computing these currents introduces some error.

3.3.4 In Conclusion

All the above may give clear and justifying reasons, why the time domain analysis for the calculations of the induction motor performance subject to nonsinusoidal or especially PWM waveforms should be introduced.

3.4 THE TIME DOMAIN ANALYSIS

The study of the induction motor performance subject to nonsinusoidal waveforms and especially PWM ones is based primarily on the d-q axis simulation described in Chapter 2. In this study, a simulation of different PWM strategies is programmed and tested on the digital computer, together with the well known sinusoidal and six step quasi-square type of waveforms. Although the simulation of the sinusoidal voltages, square wave voltages and the subharmonic PWM strategies are very straight forward, this is not the case with the harmonic elimination technique or the harmonic minimization technique, in which a predetermined vector of angles is used and switchings will be encountered according to these angles. Three vectors of angles for each of the three phases should be supplied or calculated by the computer. A brief description of each of the simulated input voltages will be given for reference and completeness.

3.5 THE SIMULATED INPUT VOLTAGES

All the possible input voltages are included in one subroutine and it responds with the required input voltage according to the identification of the MODE parameter:-

MODE#1 is assigned to pure-sinusoidal voltages.

MODE#2 is assigned to 6-pulse quasi-square voltages.

MODE#3 is assigned to the sinusoidal PWM technique.

MODE#4 is assigned to the optimal PWM technique.

MODE#5 is assigned to the reference current controller technique.

3.5.1 MODE#1 Pure Sinusoidal Voltages

This is introduced to provide a basis of comparison with the other modes and to check the simulation. The three phase voltages are given by:

$$\begin{aligned} v_{as} &= V_{pu}\ \mathrm{Sin}(\omega t) \\ v_{bs} &= V_{pu}\ \mathrm{Sin}(\omega t - 2\pi/3) \\ v_{cs} &= V_{pu}\ \mathrm{Sin}(\omega t - 4\pi/3) \end{aligned} \qquad (3.1)$$

3.5.2 MODE#2 The Six Step Quasi-Square Waveform

If a two level half bridge inverter is considered, the voltages v_{ao}, v_{bo} and v_{co} between the three phases and the zero level (earth point or intermediate point of the battery supply) are shown in the inverter circuit diagram shown in Figure 3.3. These voltages, and those between the three phases and the neutral of the load are drawn versus time in Figure

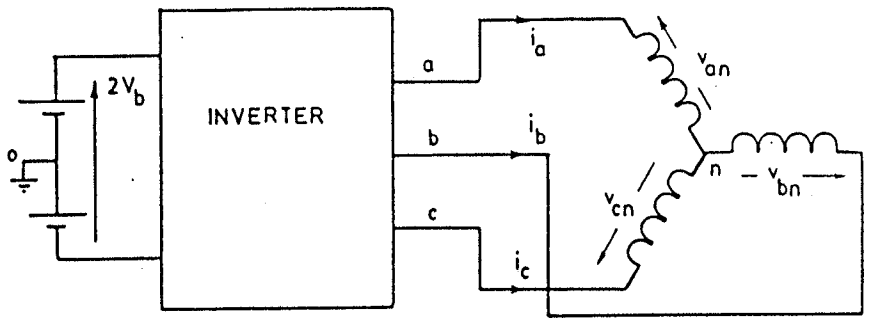

Figure 3.3: The Square Wave Inverter Scheme

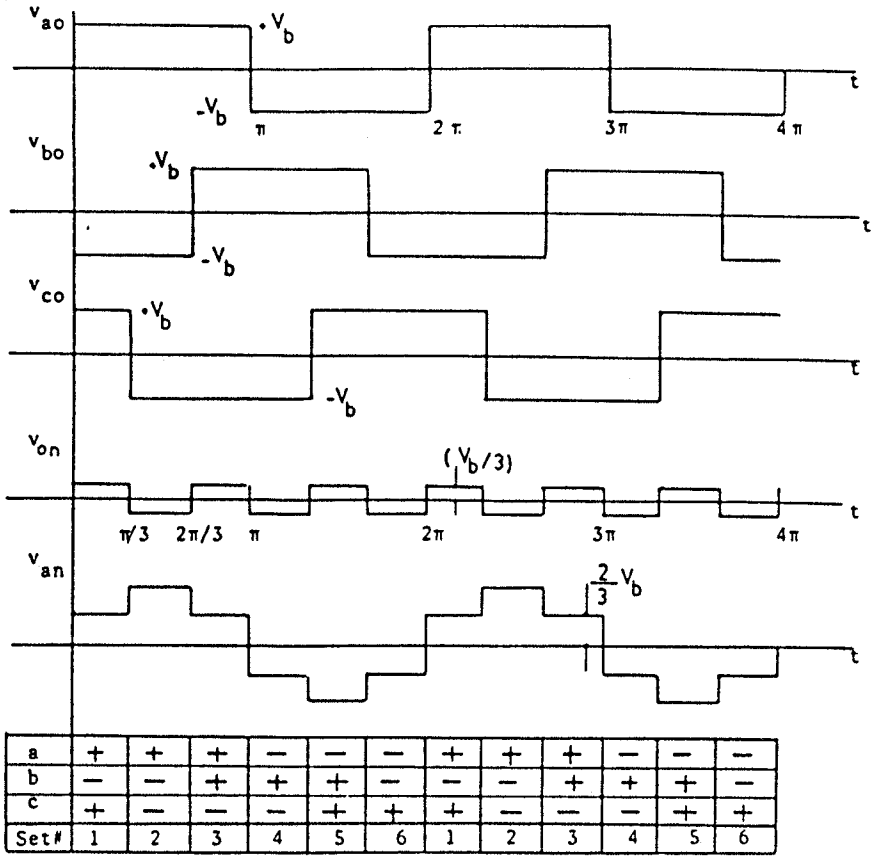

Figure 3.4: The Square-Wave Generation

3.4. The phase voltages (v_{an}, v_{bn} and v_{cn}) are derived from the fact that at any instant of time, any two of the three phase voltages (v_{ao},v_{bo} and v_{co}) are always equal and opposite, therefore, they cancel each other leaving the third to be divided by 3.

Now,

$$v_{on} = \frac{v_{ao}+v_{bo}+v_{co}}{3} = \pm \frac{V_b}{3} \qquad (3.2)$$

and hence,

$$\begin{aligned} v_{an} &= v_{ao} - v_{on} \\ v_{bn} &= v_{bo} - v_{on} \\ v_{cn} &= v_{co} - v_{on} \end{aligned} \qquad (3.3)$$

In fact, the above result can be verified, more rigorously, by evaluating the sum of the Fourier series of the three phase voltages. Although the performance of the induction motor subject to square wave voltage is not the aim of this study, it was simulated because, its output current waveform at steady state has a very salient and well known feature, shown in Figure 3.5. Therefore the square wave may be used to check the simulation, as well as, it represents the case with minimum number of commutations (only two) per cycle in any PWM strategy. It has been also used for checking the harmonic analysis routines as shown in Figure 3.5, since the harmonic content of the square wave is also typical and can be found analytically.

Referring, to Figure 3.4 it can be seen that, only one of the three phase voltages changes its sign after ($\pi/3$) radians or 60 degrees. Hence, to achieve a frequency output of ω rad/s, the first set of voltages is applied for $\pi/3$, and then a switching to the set #2 is affected at $t > \pi/3$, and to set #3 at $t > 2\pi/3$ ..... and so on, until one complete cycle is elapsed. By this instant, the counter which defines the numbering of sets will be reset to one again. Let us recall here again that, the time increment, H, is equal to 0.01625 p.u. (less

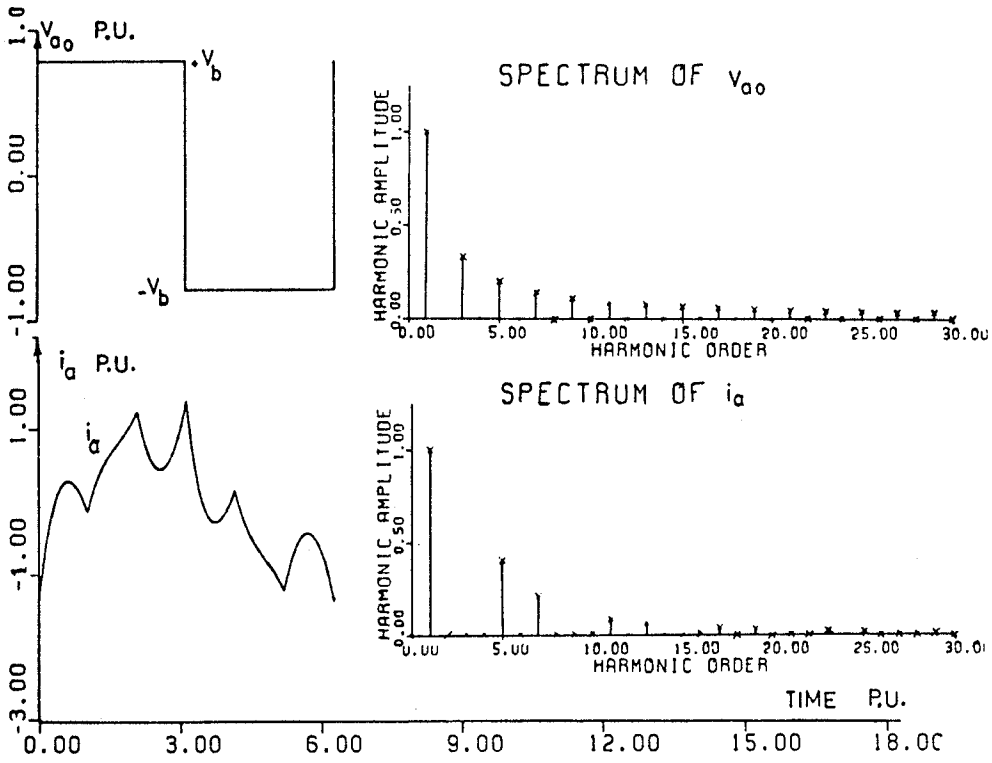

Figure 3.5: The Current Waveform of a Square Voltage

than one degree at the highest frequency). The resolution may be increased by dividing, H, by ,2 , raised to any power ,n , and this is done when a steady state sample is required for the harmonic analysis of the stator phase current and steady state electromagnetic torque.

3.5.3 MODE#3 The Sinusoidal PWM Technique

Consider that the high frequency voltage shown in Figure. 3.6 is applied to one winding of a three phase induction motor. The widths of the pulses are made to change in a predetermined way so that, this high frequency voltage has certain shape of average or mean voltage. If the voltage-time areas of the supply voltage are made sufficiently small at a definite amplitude, the flux produced in the winding will only vary according to the mean value of the alternating voltage. It should be noticed also that, the mean value of this applied voltage is a subharmonic of the high frequency voltage. The amplitude and frequency of the sinusoidal voltage may be varied independently of each other. This is the idea of the subharmonic method first introduced by Stemmler[8]. Being now required to select a sinusoidal PWM method, it should be pointed out that, two level subharmonic inverters are less expensive to built and they give a reduction in the harmonic content as good as three-level inverters. To produce the subharmonic three-phase supply voltages, four methods were suggested. The method which uses an in phase isosceles triangular carrier, intersected by the three phase reference sinewave voltages, gives the best results in respect to harmonic contents[8]. Hence, this method is the only method simulated to be compared with the other PWM strategies in this study.

As shown in Figure 3.7, an isosceles triangular carrier wave is compared with a sinewave reference signal. The frequency of the reference determines the operating frequency supplied to the motor. The points of intersection between the carrier and the reference waveform, determine the points of commutation. The ratio of the frequency of the

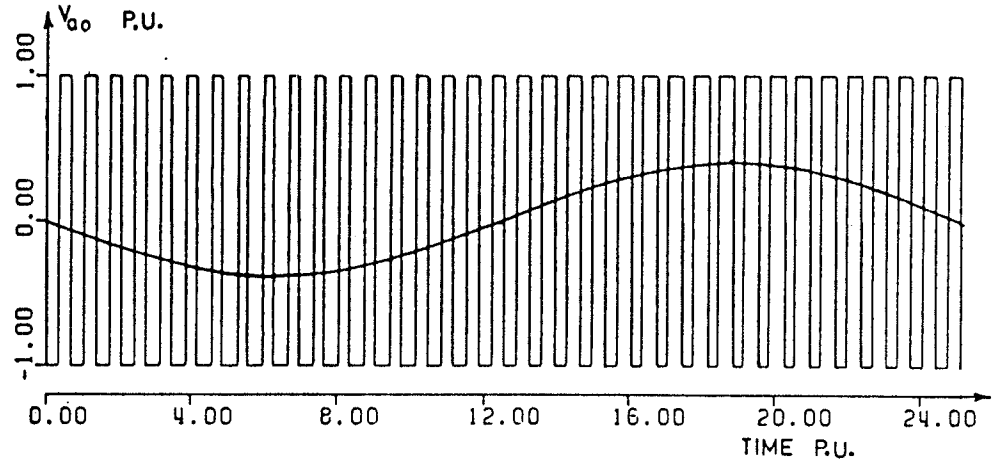

Figure 3.6: The Subharmonic Principle

carrier to the frequency of the reference is defined as the modulation ratio, M_r. Except, at very low frequencies, the carrier is synchronized with the reference, and even integral (multiple) of three ratio is maintained to minimize the harmonic contents.[10] The ratio between the amplitude of the reference to the amplitude of the carrier is defined as the modulation index, M_i. The fundamental output voltage can be changed by the variation of the modulation index. It can be shown that, if the modulation index is less than unity, only carrier frequency harmonics with fundamental frequency related side-bands may appear at the output.[10] This mode produces good results only if there are many commutations per cycle and hence, it will be considered at lower frequencies only.

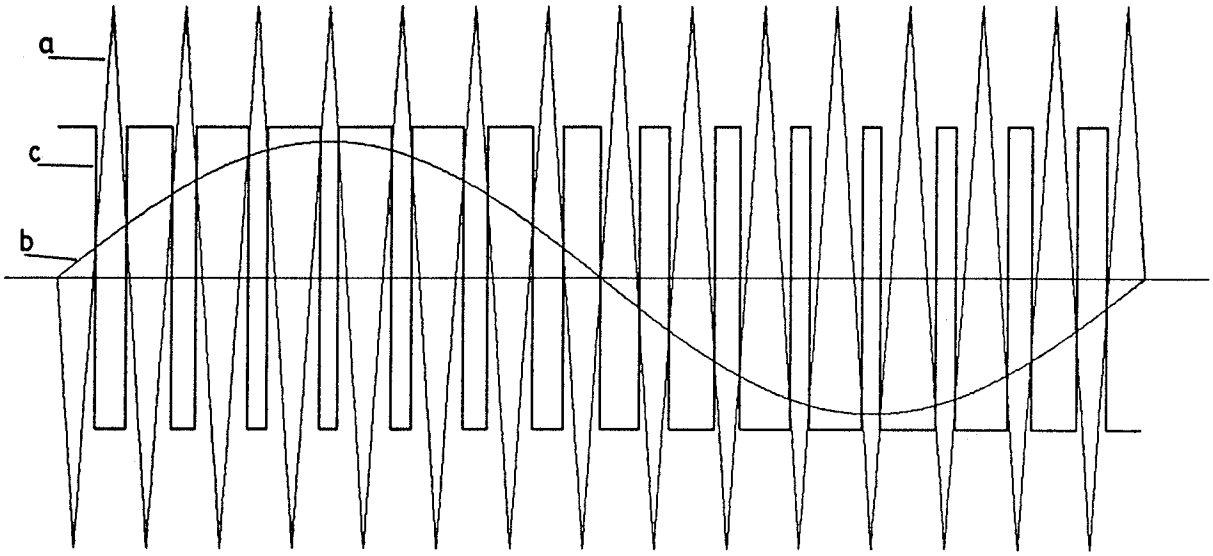

a) Carrier b) Reference c) PWM Voltage

Figure 3.7: The Sinusoidal PWM Technique

3.5.4 MODE#4 The Optimum PWM Techniques

It is only as a result of the recent developments in the microprocessor technology that the feasibility of implementing optimized PWM strategies has become a real possibility[7]. A general PWM waveform in terms of a set of switching angles is defined and optimized with respect to a particular performance criteria such as; the elimination of low frequency harmonics, or the minimization of the harmonic current distortion or peak current. Using performance criteria of this kind results in a set of nonlinear equations in terms of the unknown commutation angles. These equations are solved using a numerical minimization techniques. Once these angles are obtained the PWM waveforms can be simulated on the digital computer by feeding to it three vectors of angles each for a certain phase of the three phase system as shown in Figure 3.8. Actual-

ly it is possible to manipulate the angles of one phase to obtain the other two vectors of angles. The program afterwards is used to synthesize the required optimized PWM voltage and apply it to the simulation of the induction motor.

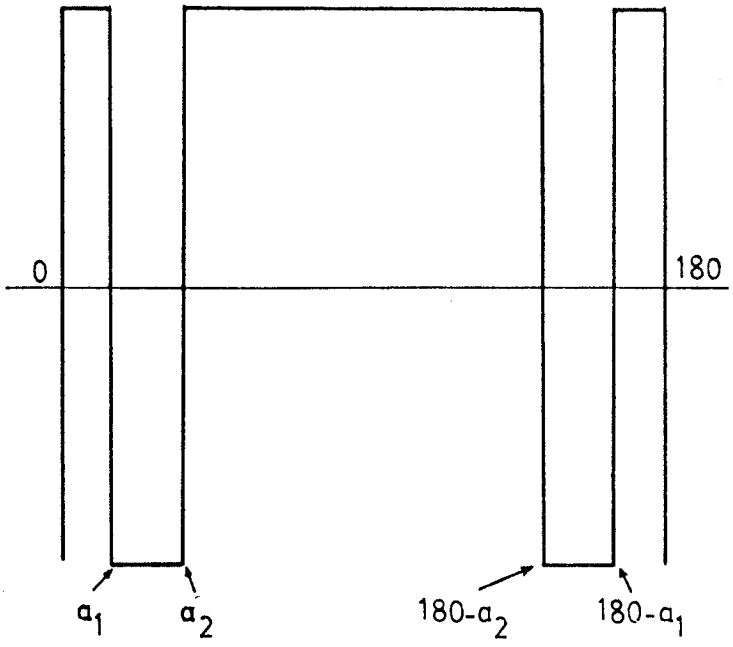

Figure 3.8: The Optimum PWM

The subroutine three-phase is devised to generate the angles of the other two phases from the angles of the first phase, and a flowchart of it is shown in Figure 3.9.

Some precautions or additional logic should be programmed to include the odd and even modulation. The initial setting of the three-phases in MODE#4 is very critical to choose and, if it is not selected properly the three-phases generated will not produce a revolving magnet-

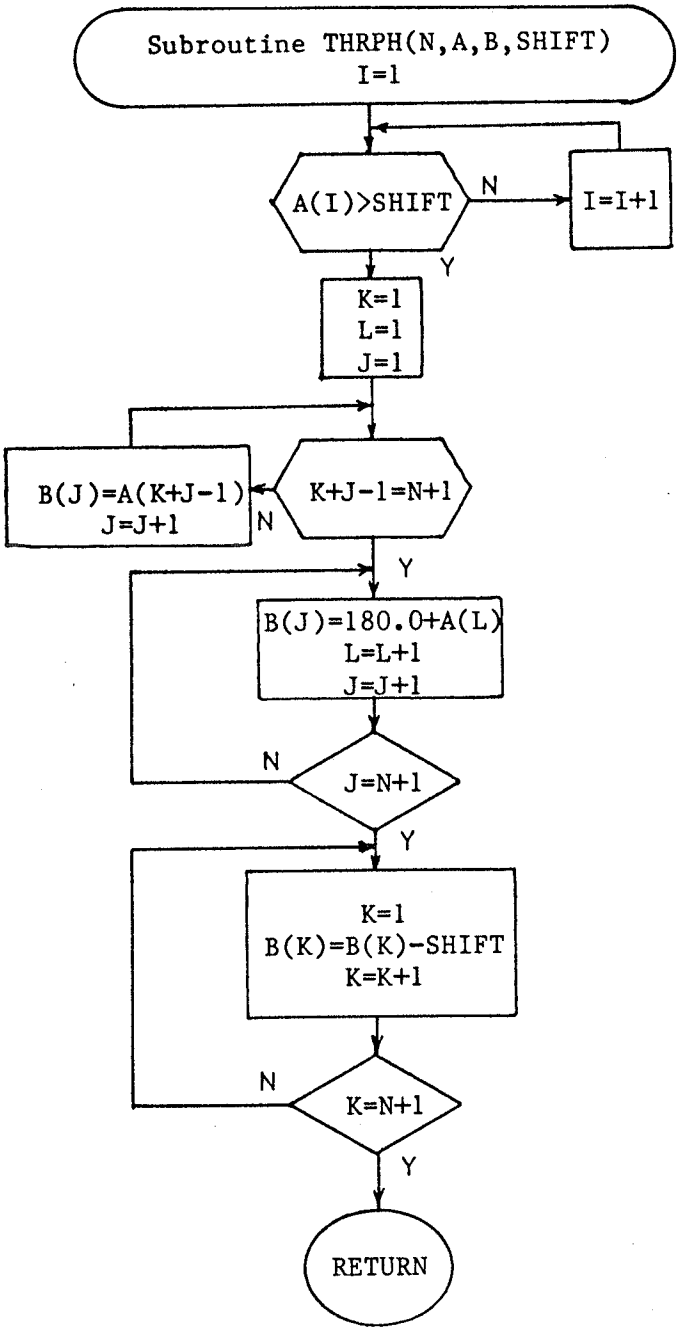

N :number of commutation angles per half cycle.
A :array of angles of given phase.
B :array of angles of required phase.
SHIFT:suitable shift for, phase B=60 and, phase C=120.

Figure 3.9: The Angles of the Other Two Phases From the First

ic field, in the positive sequence as is required. The following rule

should be applied for obtaining a positive sequence revolving magnetic field, depending on the number of additional commutations per quarter cycle '$N_{quarter}$':- if $N_{quarter}$ is even and the number of commutation angles, which are greater than the phase belt shift, N_{gts}, between the three phases (i.e.;60 degrees) is even then, the initial setting should be, (+,-,+), otherwise, if N_{gts} is odd the setting should be (+,+,-).

If $N_{quarter}$ is odd then the settings are (+,+,-) and (+,-,+) depending on N_{gts}, being even or odd respectively. The optimum angles for 45 and 60 Hz are obtained from the minimum distortion index curves of Buja[23]. Those for 30 Hz are obtained from Bellini and Figalli curves[24]. The optimum angles used at the various frequencies in the comparative study are: 9.4488° and 14.1752° at 60 Hz; 6.0° ,10.0° ,74.5° and 82.0° at 45 Hz; 18.564°, 28.562°, 32.573°, 57.463°, 59.416°, 77.063° and 81.360° at 30 Hz.

The last technique which is MODE#5 will be introduced and analyzed in Chapter 4.

3.6 THE STEADY STATE PERFORMANCE

As mentioned before at the beginning of this chapter, performance means the calculations of the motor current harmonics when subject to different PWM waveforms, and the calculations of the harmonic pulsating torques as well as the efficiency of the motor. This is done by taking a sample of one cycle from the spectrum of the current and the electromagnetic torque, when the machine is running at steady state. The calculation of the efficiency is done in a similar fashion by calculating

the input and output power during one cycle. The input power will be considered as equal to the output power + losses. A detailed study of the motor and inverter losses will be given in Sections 3.7 and 3.8 respectively.

The computer acquires one cycle, after there is a guaranteed indication that the steady state has been reached, through the calculation of the average speed in two consecutive cycles. If the difference between these two averages is less than a prescribed value, EPS, (taken as 0.005), the motor is considered to be in the steady state and the acquiring of the cycle is started. For increasing the accuracy of the calculations, a smaller time step is used for the acquisition of the sample cycle.

3.6.1 The Snapshot Technique

For obtaining the required performance, and minimizing the computing time the snapshot technique is used. In this technique all the state variables and time as well as all the pertinent parameters of the mode of operation under consideration are saved in a data set so that they may be read from it in a subsequent run for some other extention of time to calculate the performance at some other speed or load. Therefore, this technique saves computing time and is useful in starting different studies from any desired moment during transients. This method shows that it is possible to proceed from a certain snapshot of state variables on to another very smoothly without any undesirable transients if and only if the snapshot state variables and the special parameters of each mode are selected properly.

3.6.2 The Harmonic Analysis

The maximum number of harmonics that can be calculated in the program is one hundred (100). However, the larger the number of harmonics to be calculated the larger the computing time. Hence, the number of harmonics is set to 30.

The Fourier analysis, the harmonic contents, the harmonic loss factor, H_c, and the distortion index, DI, of stator phase current are given by the following equations:

$$i_a(n)=(1.0/m)[i_{a1}+i_{am}\text{Cos }\theta] + (2.0/m)\sum_{k=2}^{m-1} i_{ak}\ \text{Cos}[n(k-1)\Delta\omega t] \tag{3.4}$$

$$i_b(n)=(1.0/m)[i_{am}\text{Sin }\theta] + (2.0/m)\sum_{k=2}^{m-1} i_{bk}\ \text{Sin}[n(k-1)\Delta\omega t] \tag{3.5}$$

$$\text{where, } \theta=n(m-1)\Delta\omega t \tag{3.6}$$

$$i_c(n)=\sqrt{i_a(n)^2+ i_b(n)^2} \tag{3.7}$$

$$H_c = \sqrt{\sum_{n=2}^{N} i_c(n)^2} \tag{3.8}$$

$$DI = \sqrt{\sum_{n=2}^{N} [i_c(n)/i_c(1)]^2} \tag{3.9}$$

where:

n is the harmonic order;

m is the number of points in one cycle; and

N is the maximum number of harmonics.

3.7 THE INDUCTION MOTOR LOSSES

The five induction motor power loss components are the following [66]:

a) Stator copper loss P_{cs}.

b) Stator iron loss P_{e+h}, depends on the supply voltage and frequency.

c) Rotor copper loss P_{cr}.

d) Friction and windage loss P_m, is a function of speed.

e) Stray load loss $P_{s\text{-}loss}$.

The stator and rotor copper losses are normally dependent on the currents in the stator and rotor respectively and therefore, they are functions of the load torque and temperature. If a nonsinusoidal variable voltage and frequency is applied to the motor,then these losses will be increased due to the time harmonic components in the stator and the rotor currents. In this case the copper losses become dependent on the voltage and frequency of the supply as well.

The stray load loss is any additional losses in the core or the conductors of the motor, and may be divided into two groups of components. One group depends on the current time harmonics, while the other does not.

3.7.1 The Stator Copper Loss P_{cs}

$$P_{cs}=\frac{R_s}{T}\int_0^T i_s^2(t)\,dt = \frac{R_s}{m}\left[\sum_{k=1}^{m} i_s^2(k)\right] \qquad (3.10)$$

where:

T is the period

H is the integration time increment;

R_s is the stator resistance per phase; and

m is the number of points in one cycle, therefore T=H x m.

As $i_s(t)$ is the actual stator phase current obtained from the simulation program, the losses calculated will be due to both the fundamental and all harmonic currents.

3.7.2 The Stator Iron Losses P_{e+h}

The following approach can be used for the calculation of the stator iron losses, when the induction motor is fed from PWM supplies.

$$P_{e+h} = \frac{0.5}{T\,R_{e+h}} \int_0^T V_m^2(t)\,dt = \frac{0.5}{m\,R_{e+h}} \left[\sum_{k=1}^{m} V_m^2(k) \right] \qquad (3.11)$$

where:

V_m is the voltage across the magnetizing reactance; and

R_{e+h} is the no-load stator iron loss resistance.

If saturation is to be taken into account then, R_{e+h} has to be fed to the computer as it varies with V_m and treated in the same way as X_m during saturation.

For the magnetic materials employed in the construction of electric machines, the power dissipated in hysteresis loss is given by;

$$P_h = K_h\, f\, (\hat{B})^n \qquad W/m^3 \qquad 1.5 \leqslant n \leqslant 2.5 \qquad (3.12)$$

and the power dissipated in eddy current loss is given by;

$$P_e = K_e\, (\hat{B} f d)^2 \qquad W/m^3 \qquad (3.13)$$

where: K_h and K_e are constants determined by the nature of the ferromagnetic material and the dimensions of the machine[67];

f is the supply frequency;

d is the lamination thickness; and

$\hat{B}$ is the maximum flux density per pole.

The hysteresis loss (3.12) and the eddy currents loss (3.13) are lumped together, as the core losses of the machine. These losses are measured for given values of lamination thickness, frequency, and peak value of flux density. Equations (3.12) and (3.13) give no indication of the relative magnitudes between P_h and P_e. Therefore, for a certain machine and material, let us assume approximately that the following relation holds for the core loss of the motor.

$$P_{e+h} = K\, f^x\, (V_m)^n \qquad W/m^3 \qquad \text{for} \quad 1.0 \leqslant x \leqslant 2.0 \tag{3.14}$$

The effect of variable frequency operations on the measured value of the core loss resistance R_{e+h} may be taken into account as follows. The core loss power is known at 1.0 p.u. frequency, therefore;

$$P_{e+h|1} = K\, (1.0)^x\, (V_m)^n \qquad W/m^3 \tag{3.15}$$

The core loss resistance at any frequency, f, may be shown to be equal to;

$$R_{e+h|f} = R_{e+h|1}\, (1.0/f)^x \text{ p.u.} \qquad \text{for} \quad 1.0 \leqslant x \leqslant 2.0 \tag{3.16}$$

This value should be used in equation (3.11) for the value of R_{e+h}.

As a check the stator iron losses were also calculated using the fourier analysis of the phase, a, air gap voltage V_{am} as:

$$P_{e+h} = (0.5/R_{e+h}) \sum_{n=1}^{N} (n)^x\, V_{am}^2(n) \tag{3.11a}$$

where:

n is the harmonic order ; and

N is the total number of harmonics.

The same results,in per unit , as those calculated from equation (3.11) were obtained. This emphasize the validity of using the magnetizing voltage directly evaluated from the d-q parameters for the calculation of the stator iron losses.

3.7.3 The Rotor Copper Loss P_{cr}

The deep bar effect is taken into account through the double cage simulation. The rotor copper power loss is the sum of the copper losses in the two cages of the rotor simulation.

$$P_{cr1} = \frac{R_{r1}}{T}\int_0^T i_{r1}^2(t)\,dt = \frac{R_{r1}}{m}\left[\sum_{k=1}^{m} i_{r1}^2(k)\right] \tag{3.17}$$

$$P_{cr2} = \frac{R_{r2}}{T}\int_0^T i_{r2}^2(t)\,dt = \frac{R_{r2}}{m}\left[\sum_{k=1}^{m} i_{r2}^2(k)\right] \tag{3.18}$$

$$P_{cr} = P_{cr1} + P_{cr2} \tag{3.19}$$

where:

R_{r1} is the locked rotor resistance per phase, for the first cage.

i_{r1} is the actual rotor phase current for the first cage.

R_{r2} is the locked rotor resistance per phase, for the second cage.

i_{r2} is the actual rotor phase current for the second cage.

3.7.4 The Friction and Windage Loss P_{f+w}

$$P_{f+w} = \frac{f_c}{T}\int_0^T Nu^2(t)\,dt = \frac{f_c}{m}\left[\sum_{k=1}^{m} Nu^2(k)\right] \tag{3.20}$$

where: f_c is the friction coefficient; and

Nu is the speed of the rotor.

3.7.5 The Stray Load Losses $P_{s\text{-}loss}$

The results obtained by Alger in 1960 [68], on the stray load losses measured and calculated for several wide ranges and types of motors are summarized in Figure 3.10. These losses may be divided into two main parts and they constitute two terms on the graph of Figure 3.10. The losses of the first term are constant while, the losses in the second term depend on the current time harmonics.

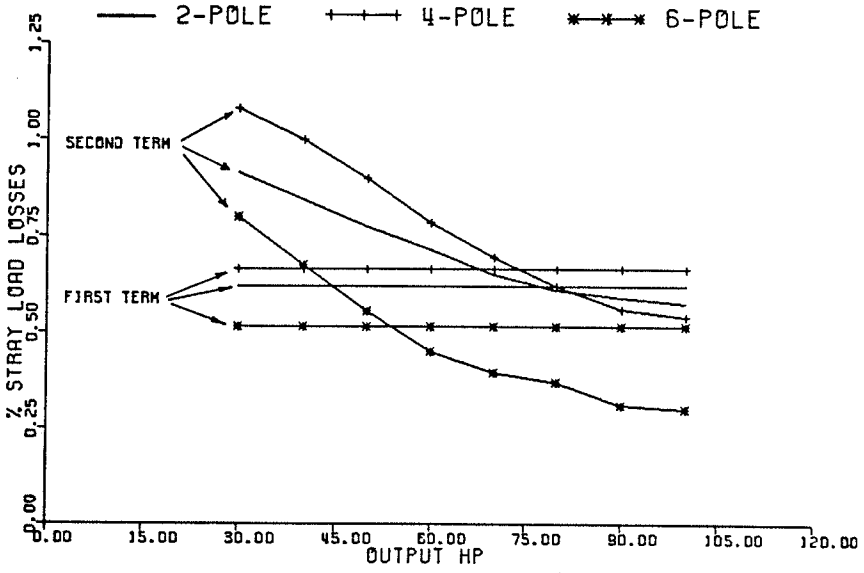

Figure 3.10: Approximate Alger Results

3.7.5.1 The First Term

The losses of the 'first term' are the skew loss, W_k, the belt loss, W_B, and the surface losses of the stator and rotor, W_{sL1} and W_{sL2}. Both the skew and the surface losses depend on current ratios and therefore, they will not increase as a result of the voltage time harmonics. The belt

loss depends on the space harmonics and the fundamental therefore , this loss will not be affected by the voltage time harmonics as well. Consequently all these terms will be treated as independent of the current harmonics and are represented by the 'first term' in equation (3.21). From Alger's values it was found that the sum of these losses varied up and down for the same number of poles and different outputs. Therefore, in Figure 3.10 an average value of these variations is given.

3.7.5.2 The Second Term

The losses of the 'second Term' are the zigzag loss, W_Z, and the end loss, W_E. These two components do depend on the current and therefore they will be assumed to vary with the harmonic current content of the stator phase current, when the motor is fed from nonsinusoidal voltage supply [48-50].

$$P_{s-loss}=['first\ term'+'second\ term'(1.0+DI)]\ P_{out} \qquad (3.21)$$

where:

DI is the distortion index. It is a normalized value of the harmonic loss factor given by equation (3.8); and

P_{out} is the average output power over one cycle acquired from the simulation.

Although the second term losses are functions of the square of the current they are given in Figure(3.10) as a percentage of the total output power which is proportional to the current rather than the current squared. Therefore, the value of the distortion index rather than the distortion index squared is used in equation (3.21).

The first and second terms in equation (3.21) may be found from Figure 3.10 according to the motor ratings and its number of poles. In Figure 3.10 both terms are given in percent values of the output power.

3.8 THE INVERTER LOSSES

3.8.1 Power Dissipated in Thyristors

Thyristor devices have the necessity of heat dissipation. A low temperature limit may be required to limit the thermal stress in the silicon crystal to safe values. This type of stress is due to the difference in the thermal coefficients of expansion of the materials used in fabricating the cell assembly. The power generated in the junction in typical thyristor operation consists of the following five components of dissipation; the turn on switching loss, the conduction loss, the commutation loss, the blocking loss and the triggering loss.

The reverse blocking losses and the gate triggering losses are negligible. The turn on switching losses will be taken into account as a part of the commutation losses on the assumption that the quality factor of the inverter circuit will include the effects of the resistive components of the circuit inductances as well as the forward resistance drop of the semi-conductors. Therefore, we end up with two types of losses to be considered only, namely the on-state losses and the turn off losses.[69,70]

3.8.2 The On-state Conduction Loss $P_{on\text{-}loss}$

The on-state power dissipation is equivalent to a forward voltage drop of ΔV in series with each phase. ΔV is assumed to be 1.0 volt for the two thyristors conducting in series or for one thyristor and one diode, in series. Therefore, the effective r.m.s. value of the stator phase current may be considered for the evaluation of the total conduction on-state loss of the whole inverter. Hence;

$$P_{on\text{-}loss} = \Delta V \cdot \frac{1}{T} \int_0^T i_s^2(t)\, dt$$

$$= \Delta V \cdot \frac{1}{m} \left[\sum_{k=1}^{m} i_s^2(k) \right] \qquad (3.22)$$

3.8.3 The Turn-off Commutation Loss $P_{off\text{-}loss}$

Let us select the General Electric "C140" thyristor for our inverter to evaluate the turn-off commutation losses. The turn-off time t_q of this thyristor is, 15 μs. The total per unit loss per commutation may be found from Figure 3.11 calculated by Bhagwat and Stefanovic [70]. For our specific problem;

ν is the ratio between the maximum load current and the ideal value of the peak commutation current (0.66);

E is the line to line bus voltage (π /2.0 p.u.);

t_q = 15 μs. (5.66×10^{-3} p.u.); and

I_L is the maximum load current to be commutated (1.0 p.u.).

Therefore, $E\, I_L\, t_q = (\pi/2)(1.0)(5.66 \times 10^{-3}) = 8.891 \times 10^{-3}$ p.u. and for an assumed quality factor Q=15 for our inverter circuit, (this is a

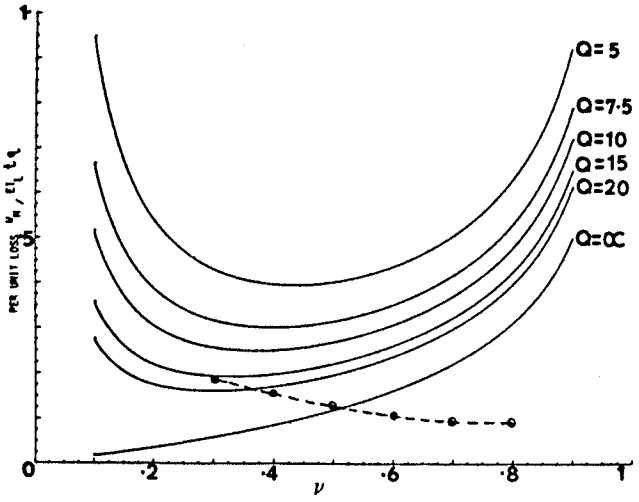

Figure 3.11: The Power Loss per Commutation Taken From Reference [70]

low value, a well designed inverter may have a higher Q value) then, the energy loss per commutation, W_E, from Figure 3.11 may be given by:

$$W_E = 0.24 \times E\ I_L\ t_q$$
$$= 0.24 \times 8.891 \times 10^{-3} = 2.134 \times 10^{-3} \text{ p.u.}$$

The energy loss per cycle = $W_E\ N_c$

Where, N_c is number of commutations per cycle.

The turn-off commutation power loss is the energy per second, or per unit time. At 60 Hz the period of one cycle is equal to the time base but this is not the case, with other frequencies, so in general;

$$P_{\text{off-loss}} = W_E\ N_c\ f \qquad (3.23)$$

Where; f is the frequency in per unit.

3.9 COMMENTS AND PROSPECTIVES

The time domain method is quite straight forward and when the snapshot technique is used the computing time is reasonable. The number of harmonics needed in the time domain analysis depends on how far it is required to investigate the harmonic contents of the already existing waveforms of voltage, current and electromagnetic torque. On the other hand the accuracy of the frequency domain analysis depends primarily on the number of harmonics involved in the calculations and therefore this number should be larger in this case. Hence, using time domain methods, and taking into account the effect of starting the run from a snapshot, computing time can be reduced.

The comparison of the different PWM techniques simulated will be delayed until Chapter 5 after the introduction of the Bang-Bang reference current controller which will be included in Chapter 4.

Chapter IV

THE BANG-BANG REFERENCE CURRENT CONTROLLER

The subharmonic method is simple to implement, but is best at low frequencies when the number of commutations per cycle is large. The optimum PWM technique is more difficult to implement. Hence, a simple and cheap control strategy is needed especially for pump and fan drives.

Almost all of the PWM methods which could be used have in common two implementation disadvantages[31]. The first is that these methods are voltage control systems which are susceptible to imbalance and dc offset problems. This imposes a requirement for a high degree of precision on the waveform generation. The second disadvantage occurs at high voltages when synchronized transitions with different modulation ratios and/or pulse dropping techniques are required to achieve the output voltage. For maximum output voltage, the inverter must operate in the square wave mode without notches in the output waveform.[9,13-17]

The Bang-Bang reference current controller strategy has been investigated and studied to eliminate these two problems. Brod and Novotny[36] have made an overview of several current controllers. They developed a switching diagram which reveals some of the operating characteristics of the hysteresis controllers. They also stated that, in the case of a hysteresis controller, the stator voltage vector can assume only one of eight states at any instant of time.

Three phase reference current sinewaves of appropriate magnitude and frequency are generated for each phase. These reference currents are compared to the actual motor phase currents and a switching takes place from the positive to the negative dc bus when the actual current exceeds, the reference current by a fixed amount. Another switching from the negative to positive dc potential occurs when the actual current is less than the reference current by the fixed amount.[30-36]

This, produces a PWM waveform which is dependent on the motor current and hence the load. Clearly, this PWM strategy requires feedback, nevertheless, it is within the inverter module itself, no feedback from the motor is required. Some obvious advantages of such a strategy are that; the motor is over-load protected;[28] the motor currents are constrained about the rated value. Secondly, because the motor current is monitored, redundant commutations can be suppressed in suitably designed inverters[70]. Lastly, the number of commutations per cycle changes automatically with frequency without having to decide optimum ranges and/or encounter transitions for each frequency.

4.1 APPROXIMATE ANALYSIS OF THE REFERENCE CURRENT CONTROLLER

As the proposed PWM technique will control and maintain the current almost constant and confined within a hysteresis band of width $2\,\Delta I$, it can be instructive to examine the operation of the induction motor on a constant current supply.

A simplified analysis using the equivalent circuit shown in Figure 4.1 will be used[67]. The no-load losses will be taken into account as a constant term or as a term proportional to the square of the speed dur-

ing the calculations of the performance curves of the motor. The saturation of the magnetizing reactance X_m will be taken into account as well. For comparison purposes the familiar equations of constant voltage operation will be given by the (b) equations, which will be derived

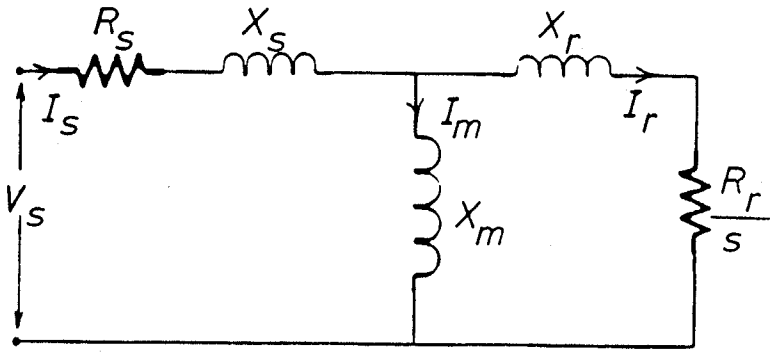

Figure 4.1: Exact Equivalent Circuit

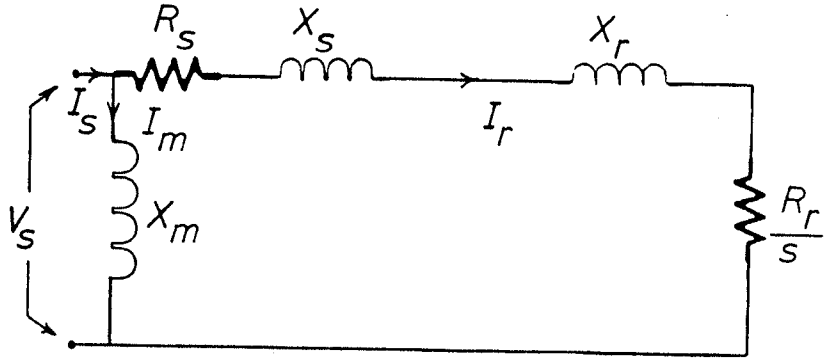

Figure 4.2: Approximate Equivalent Circuit

from the approximate equivalent circuit in Figure 4.2.

For constant current operation the stator current, I_s, is known, hence,

$$I_r = \frac{jX_m I_s}{R_r/s + j(X_m + X_r)} \qquad \text{(A)} \qquad (4.1a)$$

$$\text{c.f.} \quad I_r = \frac{V_s}{(R_s + R_r/s) + j(X_s + X_r)} \qquad \text{(A)} \qquad (4.1b)$$

$$T = \frac{3}{\omega_s} \frac{X_m^2 \, |I_s|^2}{(R_r/s)^2 + (X_m + X_r)^2} \frac{R_r}{s} \qquad \text{(N.m)} \qquad (4.2a)$$

$$\text{c.f.} \quad T = \frac{3}{\omega_s} \frac{|V_s|^2}{(R_s + R_r/s)^2 + (x_s + x_r)^2} \frac{R_r}{s} \qquad \text{(N.m)} \qquad (4.2b)$$

$$\text{and} \quad V_s = \left[R_s + jX_s + \frac{jX_m (R_r/s + j X_r)}{R_r/s + j(X_m + X_r)} \right] I_s \qquad \text{(v)} \qquad (4.3a)$$

$$\text{c.f.} \quad I_s = V_s \left[\frac{1.0}{R_s + R_r/s + j(X_s + X_r)} + \frac{1.0}{jX_m} \right] \qquad \text{(A)} \qquad (4.3b)$$

The suffixes s and r stand for the stator and rotor quantities respectively. The suffix m is for the magnetizing branch. The torque and voltage for constant current operation as they vary with speed are shown in Figure 4.3. The torque and current for constant voltage operation as they vary with speed are shown in Figure 4.4. For starting when the slip has a value approximately one, the torque equations (4.2a), (4.2b) may be simplified by assuming;

$$X_m \gg X_r \gg R_r/s \approx R_s$$

so that,

$$T = \frac{3}{\omega_s} \frac{X_m^2 \, |I_s|^2}{(X_m + X_r)^2} \frac{R_r}{s} \qquad s \approx 1.0 \qquad (4.4a)$$

$$\text{c.f.}\quad T = \frac{3}{\omega_s}\ \frac{|V_s|^2}{(X_s+X_r)^2}\ \frac{R_r}{s} \qquad s \approx 1.0 \qquad (4.4b)$$

In the above equations if $|V_s|$ is considered approximately equal to $|I_s\ X_m|$ then, the torque produced by constant current operation at starting will be related to that of the constant voltage operation by the ratio;

$$\frac{T_{\text{constant current}}}{T_{\text{constant voltage}}} = \left[\frac{X_s + X_r}{X_m + X_r}\right]^2 \qquad (4.5)$$

This is again shown in Figures 4.3 and 4.4. This low starting torque of the motor may be a problem, but it can be alleviated by ramping up the frequency and/or increasing the reference current during acceleration.

At low values of slip;

$$R_r/s >> X_m >> X_r+X_s >> R_s$$

therefore,

$$T = \frac{3}{\omega_s}\ \frac{X_m^2\ |I_s|^2}{R_r}\ s \qquad s_{Tmax} \geqslant s \geqslant 0.0 \qquad (4.6a)$$

$$\text{c.f.}\quad T = \frac{3}{\omega_s}\ \frac{|V_s|^2}{R_r}\ s \qquad s_{Tmax} \geqslant s \geqslant 0.0 \qquad (4.6b)$$

Again if we consider that $V_s = X_m I_s$ it can be seen that the motor torque is the same in both cases. Actually, not all of the current I_s passes through X_m, but this is nearly true in the case of very small values of slip. Equation (4.2) may be differentiated with respect to slip to yield a maximum torque of,

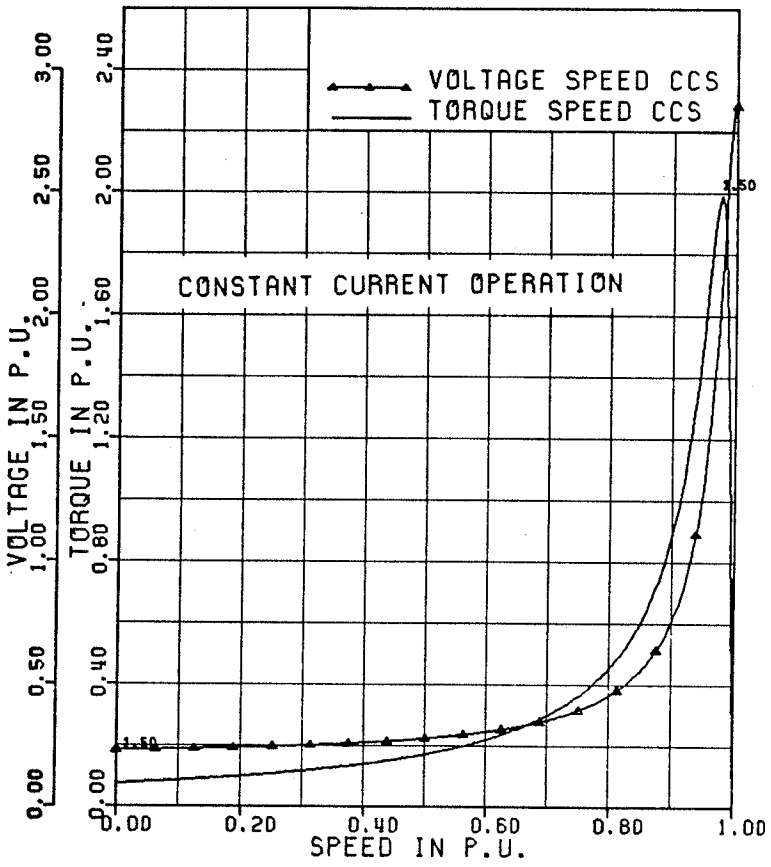

Figure 4.3: Torque and Voltage vs. Speed (Constant Current) for I_s=1.5 p.u.

$$T_{max} = \frac{3}{\omega_s} \frac{X_m^2 |I_s|^2}{2 (X_m+X_r)} \qquad (4.7a)$$

at a slip of; $s_{Tmax}=R_r/(X_m+X_r)$

c.f. $$T_{max} = \frac{3}{\omega_s} \frac{|V_s|^2}{2 (X_s+X_r)} \qquad (4.7b)$$

at a slip of; $s_{Tmax}= R_r/(X_s+X_r)$

By inspecting equations (4.7 a and b); it can be seen that both the maximum torque and the slip at which maximum torque occurs are reduced by a factor of approximately $2X_r/X_m$ for the constant current drive.

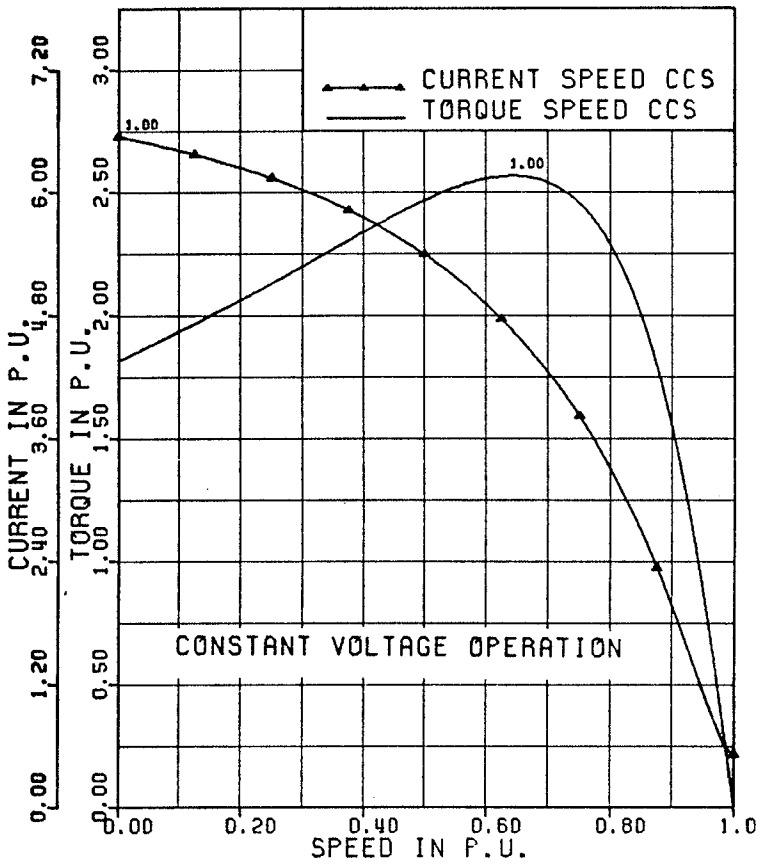

Figure 4.4: Torque and Current vs. Speed (Constant Voltage) for V_s=1.0 p.u.

But, it should be noticed also that the constant current that produces that torque is 1.5 p.u. as shown in Figure 4.3, while the corresponding current at maximum torque during constant voltage operation is about 4.6 p.u.. Of course, a higher value of torque should be obtained with a higher value of current. If the motor is operated with a low value of reference current i.e in the range between 1.0-1.5 p.u., in order to limit the stator and rotor copper losses, then, the margin between the rated torque to the maximum torque may be critical. As a result of a small margin ,the motor may encounter stability problems. As the load increases the motor impedance decreases which results in a reduced input

voltage and consequently a reduced voltampere input to the motor. Figures 4.5 and 4.6 show the efficiency and power factor versus load for the motor with constant current and constant voltage respectively. As can be seen the constant current drive has poorer efficiency and power factor at lower loads , but approaches the performance of the constant voltage drive at full load. However , it should be remembered that this analysis deals with sinusoidal supplies and that the results with PWM supplies may be considerably different.

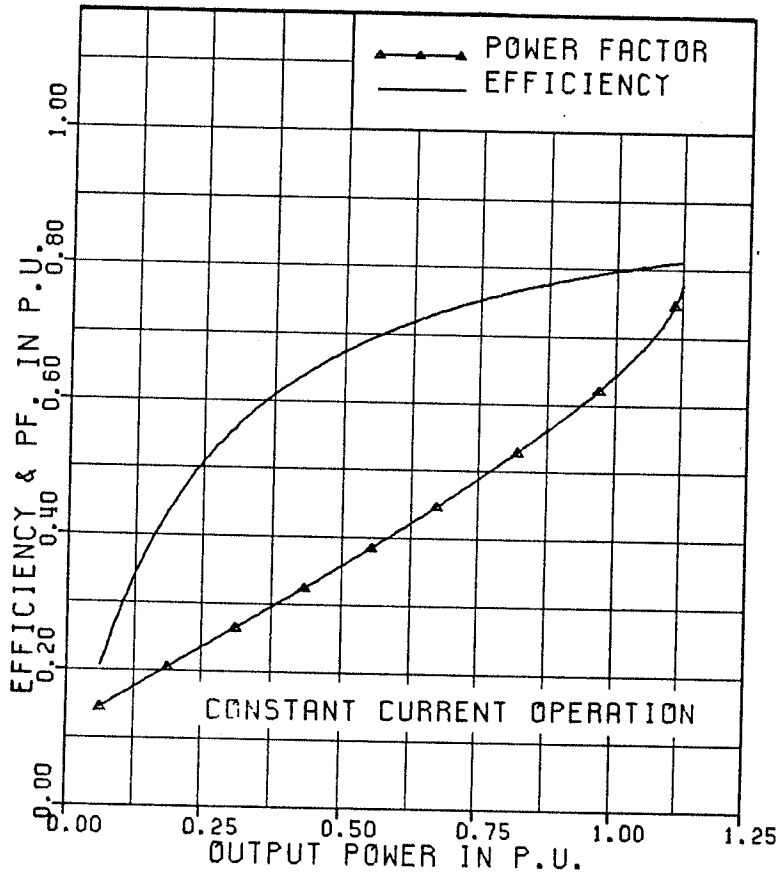

Figure 4.5: Efficiency and P.F vs. Load (constant current)

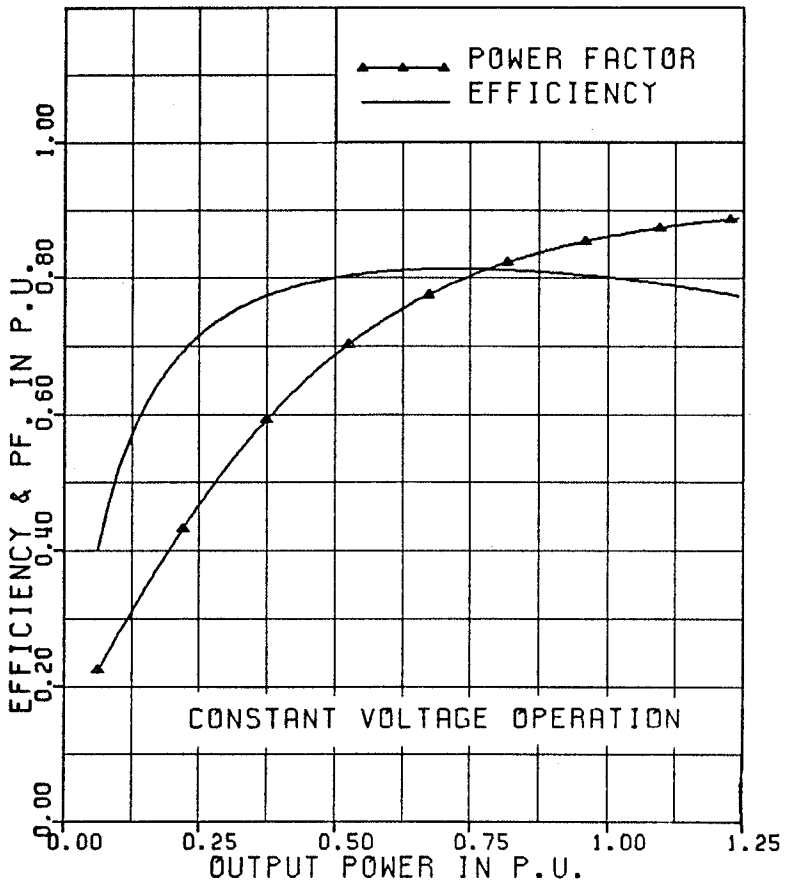

Figure 4.6: Efficiency and P.F vs. Load (constant voltage)

4.2 THE BANG-BANG REFERENCE CURRENT CONTROLLER

A set of three-phase reference current waveforms is generated and the inverter switching devices are controlled such that the actual current profile remains confined within a hysteresis band. That is, within the inverter controls the actual output currents of all three phases are monitored and compared to the reference current generated for that particular speed. In the actual implementation only two currents need be monitored, the third can be calculated for three wire supplies . If a phase current is greater (or less) than its reference current by a small prescribed value, ΔI, the applied voltage is switched to the negative (or positive) voltage bus, respectively, leading to a Bang-Bang type of

feedback control on the current. This type of control may be expressed mathematically as:

$$\begin{aligned} v_n &= -V_{bus} \quad \text{for} \quad i_n \geqslant I_R + \Delta I \\ v_n &= +V_{bus} \quad \text{for} \quad i_n \leqslant I_R - \Delta I \end{aligned} \tag{4.8}$$

where, $n = a, b, c$ for the three phases.

v_n is the phase voltage.

V_{bus} is the dc bus voltage to neutral

I_R is the reference current

i_n is the actual phase current.

ΔI is a small prescribed current deviation from the reference current.

Waveforms of the reference current and actual output voltage and current are shown in Figure 4.7. It should be noted that, the actual current waveform does not remain within the channel of width $2\Delta I$ about the reference current as switchings in the other phases will affect the current waveform as well. It should also be noted that the fundamental component of the actual current is considerably smaller in magnitude than the actual reference current, especially when there are few commutations per cycle.

There are three main control parameters for the Bang-Bang controller; the dc bus voltage, V_{bus}, the reference current amplitude, I_R, and the current deviation setting ΔI. All these parameters have an effect on the operation of the induction motor. The number of commutations per cycle, the fundamental voltage and current, the harmonic currents and torques are all functions of these parameters.

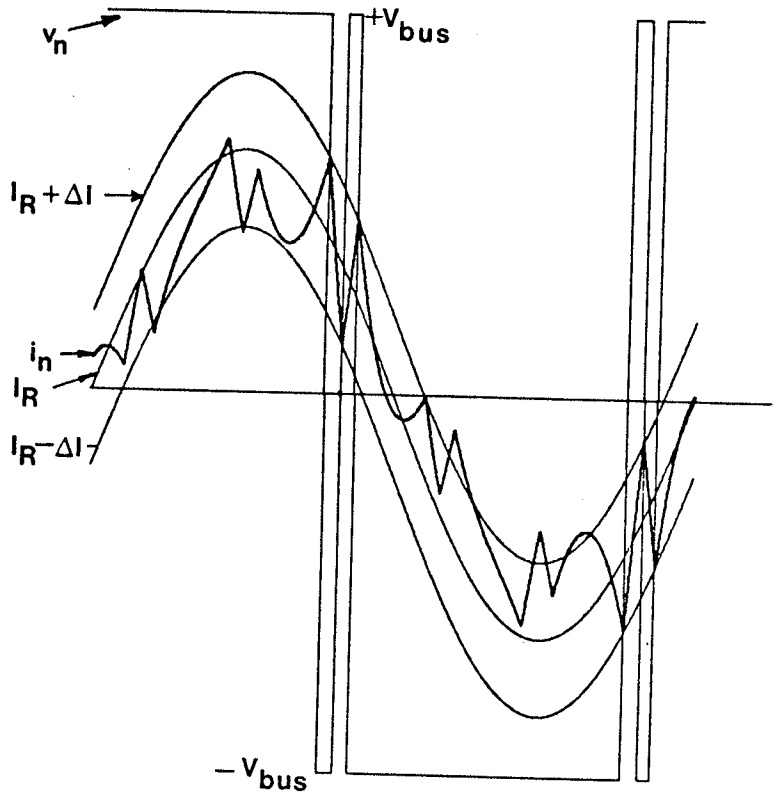

Figure 4.7: The Reference Current Controller

4.2.1 dc Bus Voltage

The dc bus voltage was set at $\pi/4$ per unit for the Bang-Bang and optimal PWM methods and at one per unit for the sinusoidal PWM method. The value of $\pi/4$ per unit for the dc bus voltage produces a one per unit fundamental output voltage for rectangular waveform operation (obtained with only two commutations per cycle) and the output voltage was only slightly reduced for two additional commutations per quarter cycle. As shown in reference [23], this will yield close to minimum losses for the optimal PWM technique.

4.2.2 The Reference Current Setting

The reference current, I_R, has two settings; the frequency setting which determines the operating frequency of the inverter and the magnitude which can be set to maintain a given motor voltage, or a given ratio of maximum torque to load torque. A valid basis for comparing the harmonic loss factors and harmonic torques is required . Therefore, the reference current was set to yield approximately the same fundamental current at each frequency as produced by the other methods. This was achieved by one of the following two approaches and according to the loading conditions. In the first approach, the reference current is given by:

$$I_R = \sqrt{\frac{2\,(L_m + L_r)}{L_m^2}\,.R\,.T_L} \qquad \text{(p.u.)} \qquad (4.9)$$

which is deduced from equation (4.7a). Equation (4.9) gives reasonable values for the reference current if the motor is at least half loaded. However, if the motor is less loaded, the calculated reference current value will not be enough for establishing a one per unit excitation level in the air gap of the motor, as will be shown later. The ratio R of the maximum torque to the load torque T_L at any particular operating point is set equal to 1.5 so as to provide an adequate steady state stability margin. The values of the reference currents calculated by equation (4.9) for Motor #1 in Appendix C are shown in Table 4.1.

As a check on the values of the reference current calculated by equation (4.9) and included in Table 4.1 for a ratio R=1.5, a steady state simulation program for the constant current operation is prepared. The function of this program is to find the point of intersection be-

TABLE 4.1

I_R FROM EQUATION (4.9)

	FAN TYPE LOAD TORQUE		CONSTANT LOAD TORQUE	
f	T_L	I_R	T_L	I_R
1.0	0.7400	1.1489	0.7400	1.1499
0.75	0.4350	0.8817	0.7150	1.1304
0.50	0.2100	0.6126	0.6900	1.1045
0.25	0.0650	0.3408	0.6650	1.0900

tween the load torque (fan type or constant torque), and the motor torque characteristic using a value of reference current according to equation (4.9) which is;

$$T_{max} = R\ T_L \tag{4.10}$$

Again R is set equal to 1.5 to provide adequate steady state stability margin, between the operating point and the maximum torque. The results obtained from the simulation program are provided in Table 4.2.

The difference between load torque settings in Tables 4.1 and 4.2 is due to the fact that, the load torque is a function of speed as indicated in Table 4.2 and it is determined by the operating point in the simulation. Actually, equation (4.9) gives only approximate value because it determines the load torque at the synchronous speed. However, the discrepancies in the computed values of I_R from both methods are very small. This emphasizes the validity of using equation (4.9) for

TABLE 4.2

I_R FROM SIMULATION PROGRAM

		FAN TYPE LOAD TORQUE $0.64(SPEED)^2+0.1(SPEED)$			CONSTANT LOAD TORQUE $0.64+0.1(SPEED)$		
f	s_{Tmax}	T_L	I_R	s_{ROOT}	T_L	I_R	s_{ROOT}
1.0	0.0252	0.7268	1.1379	0.0096	0.7390	1.1475	0.0096
0.75	0.0336	0.4248	0.8683	0.0129	0.7140	1.1282	0.0128
0.50	0.0503	0.2028	0.5987	0.0195	0.6890	1.1071	0.0193
0.25	0.1006	0.0612	0.3369	0.0365	0.6640	1.0878	0.0385

getting a close approximation to the desired value of reference current. As a matter of fact the most important feature that simulation adds, is the value of the slip at which the motor operates with this reference current value. The slip at the intersection point s_{ROOT} should be less than s_{Tmax} to ensure a stable operating point as shown in Table 4.2. This information can not be ascertained by just substituting the value of the load torque in equation (4.9). The value of s_{Tmax} in Table 4.2 is calculated from equation (4.7a) which when transferred to the p.u. system gives;

$$s_{Tmax} = \frac{R_r}{\omega L_m + \omega L_r} \qquad \text{(p.u.)} \qquad (4.11)$$

where ω is different at different frequencies but, L_m, L_r and R_r are constants at all frequencies.

Let us recall the fact that equation (4.9) is only valid if the motor is at least half loaded. Consider for example the value of the reference current that equation (4.9) gives at no load (friction and windage), it is almost zero and therefore questionable. Hence, in the following (second) approach, one per unit flux at the air gap of the motor will be maintained. The reference current should not therefore be less than the no load current. If a lower value is used the motor will be undermagnetized. Consequently the limiting value of the reference current may be derived from the equivalent circuit of Figure 4.1 as:

$$I_{Rmin} = I_m = \frac{1.0}{L_m + L_s} \qquad \text{(p.u.)} \qquad (4.12)$$

where: I_m is the magnetizing current and is the lower limit for the reference current I_{Rmin}. Again all the motor parameters are in Appendix C. This should explain the reason why the value of the reference current used for the fan type load torque at 15 Hz. in Table 5.1 is larger than that calculated in Table 4.1. Consequently let us look for another torque expression from which we can calculate the rotor current instead of the total stator phase current. From the expression of the power input to the rotor it can be shown that the maximum torque is given by,

$$T_{max} = \frac{I_r^2 \cdot R_r}{\omega_s \; s_{Tmax}} \qquad \text{(p.u.)} \qquad (4.13)$$

But, $(\omega_s \; s_{Tmax})$ is a constant for the motor at all the frequencies. Therefore substituting equation (4.10) and (4.11) in equation (4.13) gives:

$$I_r = \sqrt{\frac{1.0}{L_m + L_r} \cdot R \cdot T_L} \qquad \text{(p.u.)} \qquad (4.14)$$

Using phasor addition (Figure 4.8) then, the stator current or the estimated value of the reference current, is:

$$\dot{I}_R = \dot{I}_m + \dot{I}_r$$

hence, the reference current magnitude is:

$$I_R = \sqrt{I_m^2 + I_r^2 + 2 \, I_m \, I_r \, \text{Cos} \, [(\pi/2.) - \theta_1]} \qquad (4.15)$$

Thus assuming a linear torque slip characteristics the angle θ_1 may be calculated by;

$$\theta_1 = \tan^{-1} \left[\frac{1.0}{R} \cdot \frac{R_r}{L_m + L_r} \right] \qquad \text{(p.u.)} \qquad (4.16)$$

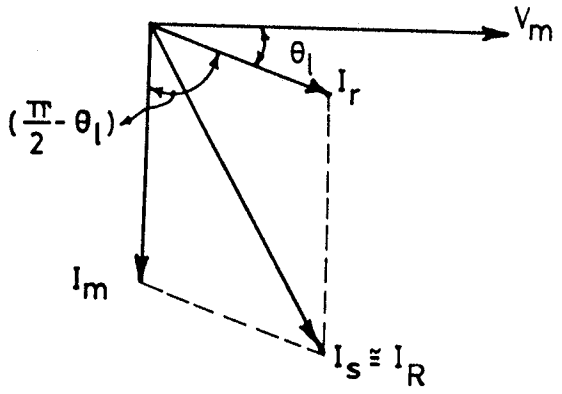

Figure 4.8: I_R from the Second Approach

where: θ_1 is the rotor impedance angle.

When the load torque T_L is equal to 0.325 p.u. (about half load), for Motor #1 in Appendix C, the value of I_R calculated from equations (4.9) and (4.15) is the same. For lower load torques equation (4.15) gives higher values for I_R and for higher load torques equation (4.9) gives higher values for I_R

For load torque values lower than 0.325 p.u., equation (4.15) should be used, since as the load torque decreases, the calculated value of I_R from equation (4.9) diminishes quickly and becomes almost zero at no load (friction and windage). Such values for the reference current cannot be accepted since it will not allow for enough current in the magnetizing branch. Besides, equation (4.15) is reasonably accurate at light loads, (T_L is less than 0.325 p.u.), because the loading effect of the rotor circuit can be neglected over this low load torque range.

For load torque values larger than 0.325 p.u. equation (4.9) becomes more accurate, since it takes into account the loading effect of the rotor circuit on the magnetizing impedance branch. In other words the reference current in equation (4.9) is determined by the equivalent input impedance of the equivalent circuit. However, on the other hand in equation (4.15) the magnetizing branch is not affected by the parallel rotor circuit, and therefore equation (4.15) becomes less accurate at high loads. Besides, the difference between the calculated values of I_R from both equations becomes more considerable as the torque is increased. Therefore, equation (4.9) should be used at load torques higher than 0.325 p.u. Computed results are given in Appendix D.

In summary equations (4.9) and (4.15) give the same value of I_R at about half load torque (T_L =0.325 p.u.). Equation (4.15) gives high I_R value at lower loads and equation (4.9) gives high I_R value at higher loads. Equation (4.9) should be used at the high load torque range ($T_L \geqslant 0.325$ p.u.) and equation (4.15) should be used at the lower load torque range ($T_L \leqslant 0.325$ p.u.).

4.2.3 The ΔI Setting

The actual current is restricted to flow within a channel of width $2\Delta I$ and has the shape of the reference current shown in Figure 4.7. The smaller the deviation current setting ΔI is, the larger the number of switchings per cycle.

Actually the ΔI setting is critical. If it is too large, only two commutations per cycle may be encountered and the inverter will operate in the quasi-square waveform mode, with the result that the current will not follow the shape of the sinusoidal reference current. On the other hand, If ΔI is too small many switchings per cycle will be encountered, with the result that, the inverter losses are increased, and thyristors with very small turn off time should be used.

The value of ΔI was selected to give a comparable number of commutations as the other methods, and was found that ΔI should be in the range 0.22 to 0.33 p.u. as the frequency decreases from 60 to 15 hertz respectively. This permits some degree of comparison between the Bang-Bang controller and the other PWM techniques.

Chapter V

COMPARISON RESULTS AND APPLICABILITY

This chapter will be concerned with the results of the comparative study and the applicability of the reference current controller to speed and load variations.

5.1 THE COMPARISON RESULTS

The criteria to be compared are, the stator harmonic current loss factor and the harmonic torque pulsations at different frequencies. These performance indices are to be compared at four operating frequencies, 60, 45, 30 and 15 Hz, which will give four distinct operating speeds for the motor. The reference current controller introduced in Chapter 4 will be compared to the sinusoidal PWM and/or the optimal PWM techniques.

The fact that the optimum techniques are superior to sinusoidal PWM above 0.6 per unit frequency, which were quoted before in Chapter 3 from the work done by Murphy and Egan[62,63], is also confirmed by our results. Therefore, all methods are compared at 0.5 and 0.75 per unit frequency. Only optimum PWM is compared above and sinusoidal PWM compared below these two frequencies. The reference current controller is compared with the better method throughout the whole frequency range.

The results are included in Table 5.1, for both an essentially constant load torque;

$$T_L = 0.1 \quad Nu + 0.64$$

and fan type load torque;

$$T_L = 0.64 \quad Nu^2 + 0.1 \quad Nu$$

Table 5.1 lists the pertinent parameters of each controller. The digital simulation calculated harmonic components of the stator current and harmonic pulsations in output torque. A harmonic loss factor, defined as the root sum of the squares of the current harmonics is used as the basis of comparison. The average torque, the sixth and the twelfth harmonic torques are listed in Table 5.1. The fundamental voltage and current are also listed. Although other indices of the induction motor could be used to determine the performance, Bellini and Figalli[24] have shown that minimizing the above index will also minimize most other performance criteria.

The general observation that can be drawn from Table 5.1 is that, the harmonic loss factor is of the same order or less for the reference current controller as compared to the other methods except at the lowest frequency where the sinusoidal PWM appears to be superior. The same observation can be made from a comparison of the harmonic torques. Sometimes the average electromagnetic torque is a little bit lower than the load torque, equal to or a little bit higher. This may be due to a subharmonic component of very low frequency being superimposed over the torque pulsations and cause a small degree of offset on the average torque value. Another possibility is that, the motor was considered to be running in the steady state, if the difference between the average rotor speeds acquired from two consecutive cycles is within a prescribed small value, EPS=0.005 p.u. It should be pointed out also that, the

TABLE 5.1

COMPARISON OF THE THREE STRATEGIES

FREQUENCY	Sinusoidal PWM									Optimum PWM								Reference Current Controller								
	M_1	M_r	T_{av}	T_6	T_{12}	N_c	V_1	I_1	H_c	T_{av}	T_6	T_{12}	N_c	V_1	I_1	H_c	I_R	ΔI	T_{av}	T_6	T_{12}	N_c	V_1	I_1	H_c
60										0.736	0.106	0.025	10	0.966	0.990	0.120	1.114	0.25	0.684	0.121	0.016	10	0.970	0.916	0.123
45	0.75	9	0.721	0.282	0.183	18	0.75	0.956	0.360	0.712	0.125	0.292	18	0.725	0.966	0.220	1.095	0.24	0.636	0.117	0.024	18	0.950	0.876	0.098
30	0.50	15	0.684	0.013	0.103	30	0.497	0.942	0.189	0.673	0.436	0.118	30	0.620	0.870	0.917	1.059	0.23	0.635	0.044	0.077	30	0.926	1.049	0.051
15	0.25	36	0.667	0.001	0.004	72	0.25	0.976	0.019								1.027	0.35	0.67	0.070	0.043	74	0.535	0.997	0.080
60										0.692	0.108	0.023	10	0.966	0.936	0.120	1.114	0.25	0.651	0.124	0.017	10	0.970	0.908	0.123
45	0.75	9	0.414	0.274	0.187	18	0.748	0.675	0.358	0.412	0.129	0.302	18	0.725	0.680	0.22	0.854	0.25	0.395	0.938	0.017	18	0.947	0.767	0.089
30	0.50	21	0.224	0.008	0.009	42	0.498	0.559	0.078	0.185	0.481	0.129	30	0.620	0.661	0.917	0.575	0.33	0.207	0.045	0.029	46	0.542	0.538	0.070
15	0.25	36	0.071	0.017	0.008	72	0.253	0.531	0.028								0.6	0.33	0.059	0.032	0.017	68	0.29	0.594	0.079

computed fundamental voltage applied to the motor when using the reference current controller is higher than that of the other techniques. Although this may indicate that the motor is operating under a higher value of magnetic loading i.e; (higher V/f ratio), the stator phase current cannot be excessive, because it is limited, within the defined hysteresis band around the reference current,(by the inherent characteristics of the controller).

Figures 5.1,5.2 and 5.3 show the stator phase currents for all the values indicated in Table 5.1,for the case of fan type load torque. These results indicate the effect of frequency on the harmonic content of the stator phase current I_A for the three techniques under consideration. Figure 5.1 for the sinusoidal PWM , shows that this technique is only good at the low frequencies (30 and 15 Hertz). At 45 Hertz this technique is still giving a harmonic loss factor (H_c = 0.36) less than that obtained from a pure square wave operation, (H_c = 0.406), nevertheless, the harmonic loss factor is quite high. Therefore, this technique is not recommended at such high frequencies. Of course at one per unit frequency the technique will give a harmonic loss factor higher than that encountered with the square wave operation. This is in good agreement with the fact that a transition to the square wave operation is always used at high frequencies. These transitions add complexity to the control logic used in practice with the sinusoidal PWM strategy. Figure 5.2 for the optimal PWM shows that this strategy is only good at high frequencies (60 and 45 Hertz). At 30 Hertz, the technique is no longer applicable because of the high harmonic current content. Therefore, the need for a technique that is good throughout a larger frequency range is

now clear. Figure 5.3 for the reference current controller indicates that the results of this technique are a compromise of the other two techniques. The controller is giving a harmonic current content equal to the optimum at the high frequencies (60 and 45 Hertz) and quite close results to the subharmonic method at the low frequencies (30 and 15 Hertz). Consequently this technique may be the solution to alleviate extensive transitions between the different modes of operations during the whole frequency range. These results indicate that, the reference current controller gives superior performance indices in the mid frequency range and very similar results to the optimum PWM technique at 1.0 per unit frequency.

Figures 5.4 and 5.5 show the voltages, currents and torque pulsations of the three techniques at 45 and 30 Hertz respectively. From a thorough investigation of Figure 5.4 and Table 5.1, it can be recognized that at 45 Hz, the number of commutations per cycle (18) is the same for all the techniques. The harmonic loss factor of the phase current and the torque pulsations for the reference current technique are far less than that experienced in the other two methods.

The harmonic contents of the three techniques at 45 HZ with fan load are also illustrated in Figures 5.6,5.7 and 5.8 respectively. These Figures emphasize the fact that, the waveform which looks closer to the pure sinusoidal waveform, (this is the basic idea behind the suggestion of using a reference current controller), is the one containing less harmonics.

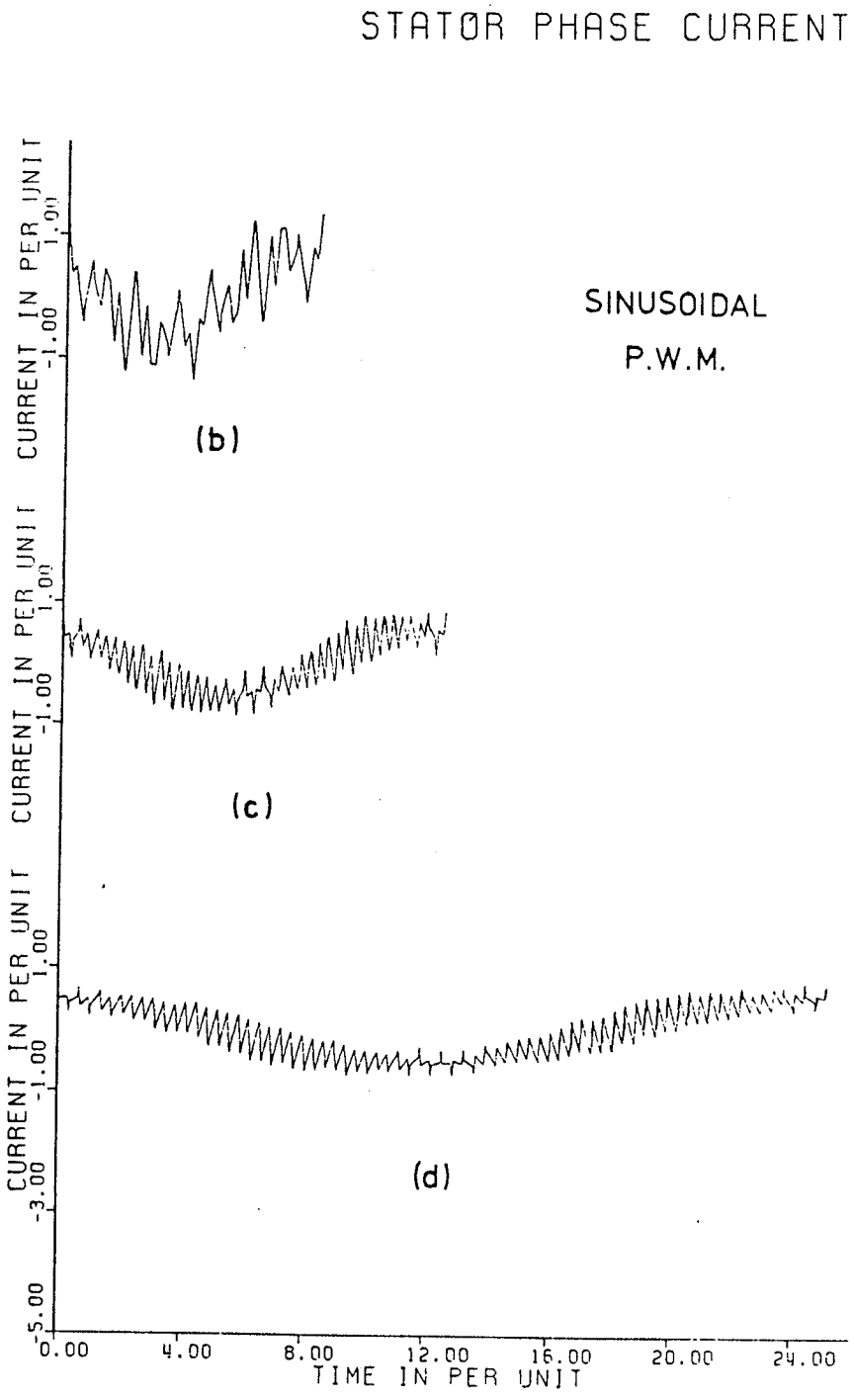

Figure 5.1: Effect of Frequency on Current, (a) f=60 Hz, (b) f=45 Hz, (c) f=30 Hz, (d) f=15 Hz

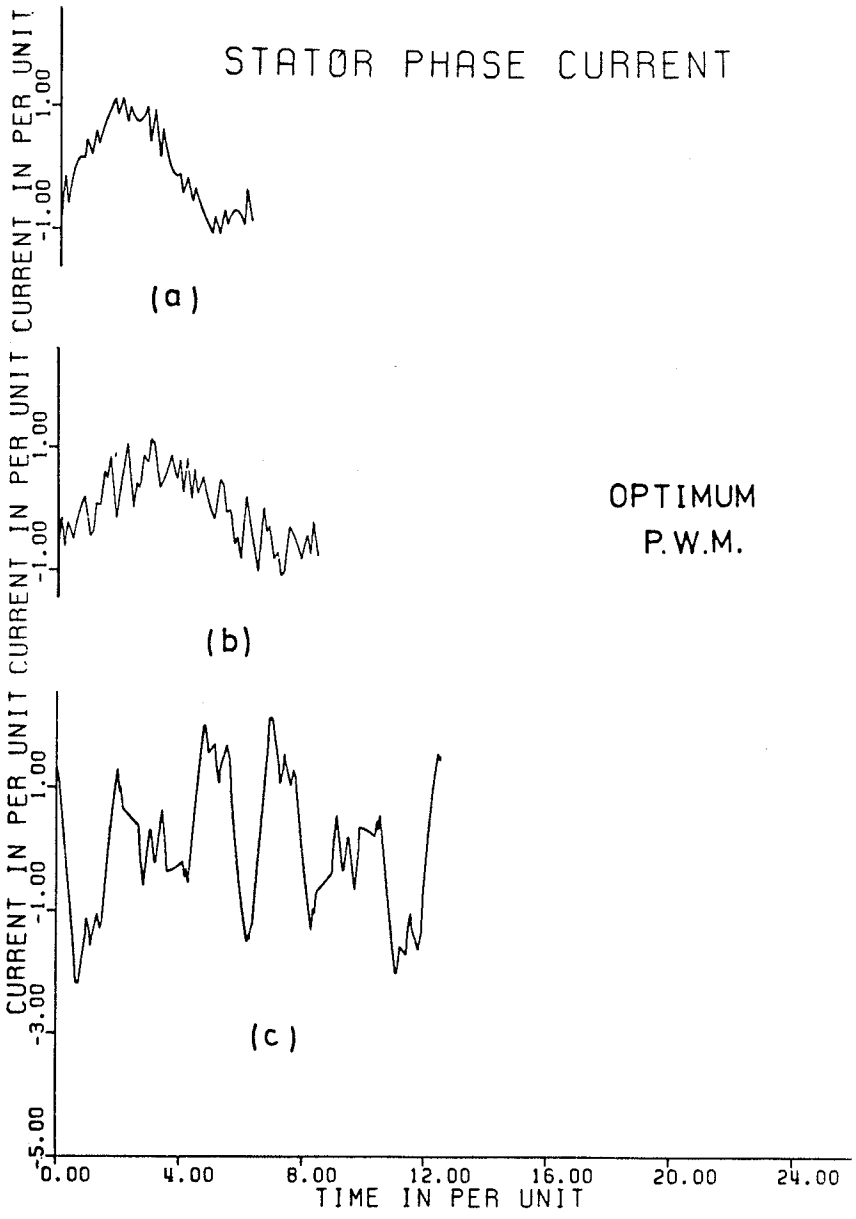

Figure 5.2: Effect of Frequency on Current, (a) f=60 Hz, (b) f=45 Hz, (c) f=30 Hz, (d) f=15 Hz

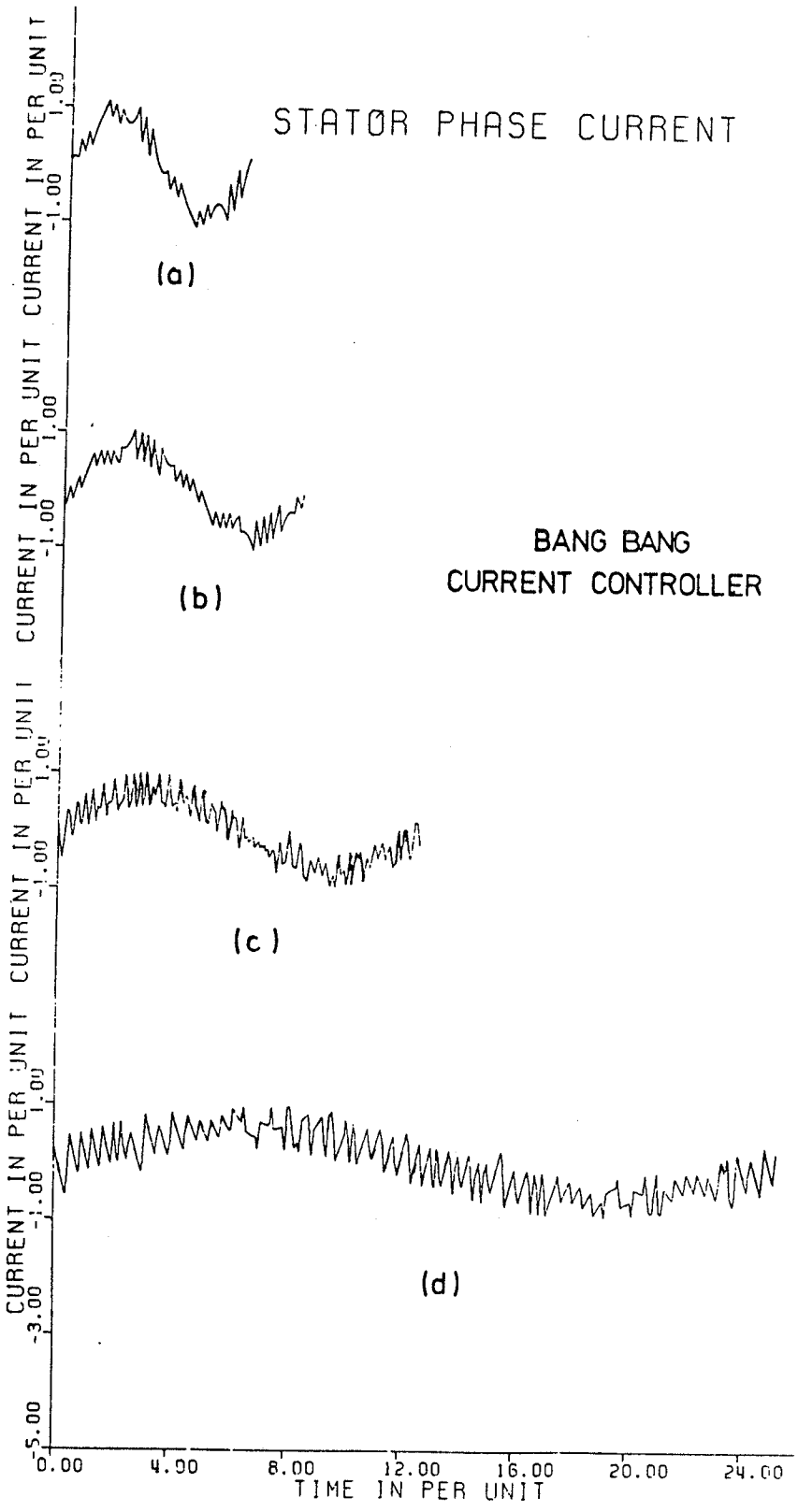

Figure 5.3: Effect of Frequency on Current, (a) f=60 Hz, (b) f=45 Hz, (c) f=30 Hz, (d) f=15 Hz

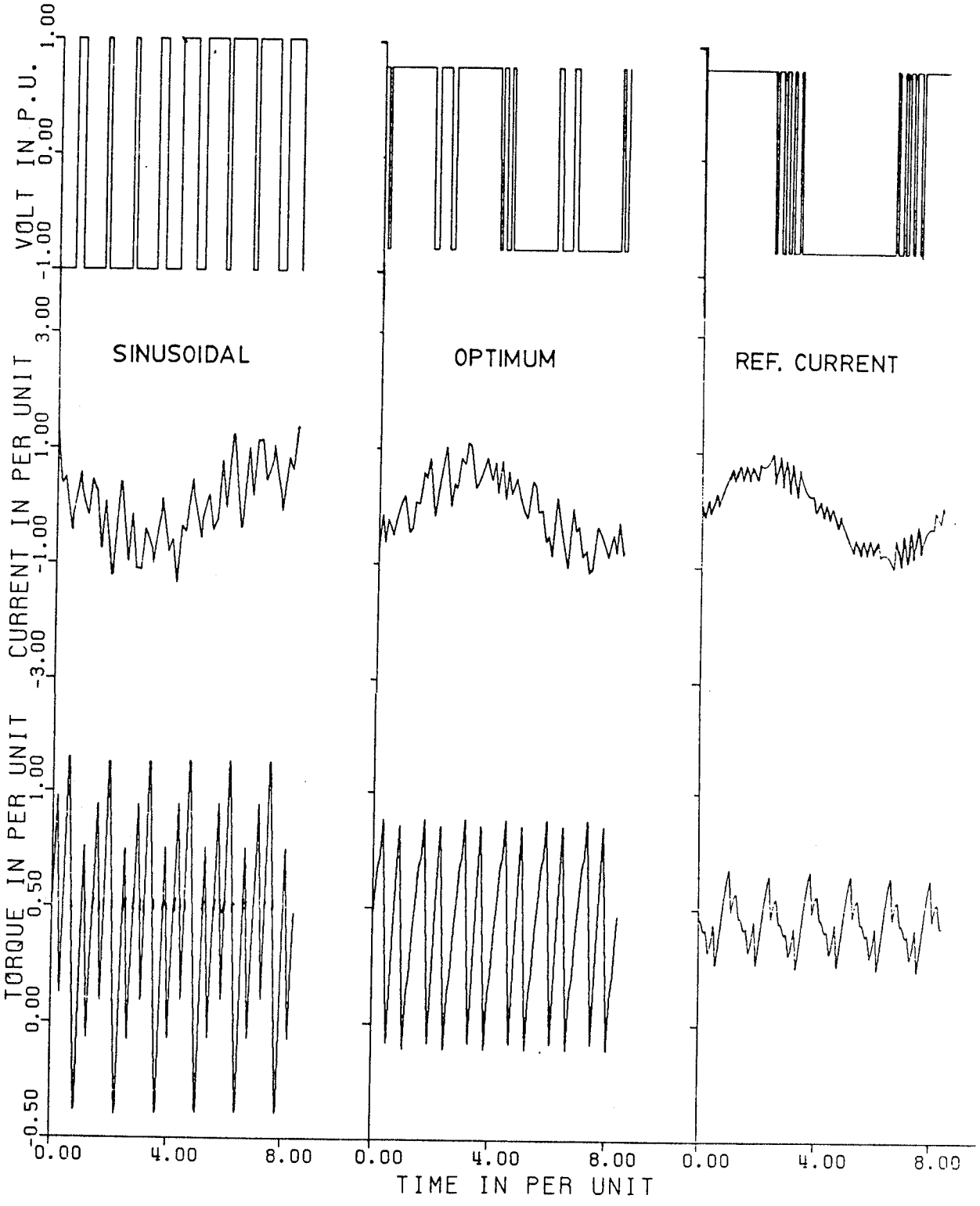

Figure 5.4: Voltages Currents and Torque Pulsations at 45 Hz

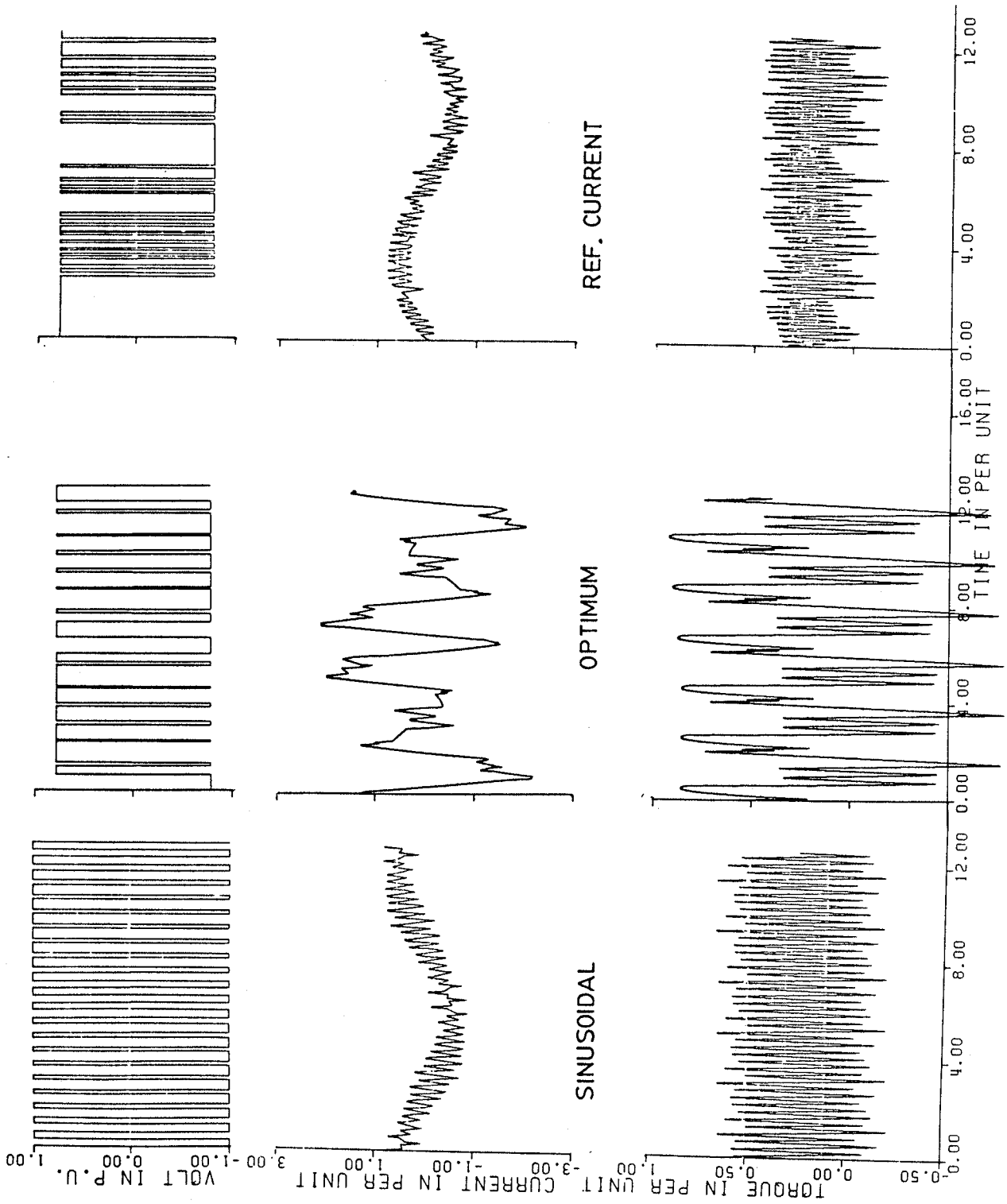

Figure 5.5: Voltages Currents and Torque Pulsations at 30 Hz

The question to be addressed now is, how can the reference current controller give better results than the optimum angle technique, at 45 Hz? This is due to the fact that, although the reference current method is obtained from constant dc bus voltage and it is a constant voltage source , however, it acts in another sense as a constant current source. The advantage of this controller is that, whatsoever, the fundamental of the output voltage at the inverter terminals may be the input current is constrained between a certain minimum and maximum about the reference current settings, with the result that a small deviation from the constant V/f ratio is feasible with such type of control, (this behaviour is given more explanation in Section 7.3). Within these allowances a higher fundamental input voltage at the desired frequency is feasible and at this voltage the desired optimum harmonic loss factor from Buja's curves themselves is less. This may explain why the reference current controller gave a lower harmonic content than the optimum PWM. If the V/f ratio was increased for the optimum PWM strategy, equivalent harmonic loss factor would result, but the fundamental current would be higher.

In addition to that, there is another important advantage, to the reference current controller. Considering that the controller acts approximately as a constant current of sinusoidal excitation, it can be easily shown that the slip at maximum torque is given by;

$$s_{Tmax} = \pm R_r/(X_r + X_m) \qquad \text{compared to}$$

$$s_{Tmax} = \pm R_r/(X_s + X_r) \qquad \text{for constant voltage}$$

and the ideal efficiency of the induction motor is also given by;

$$\eta_i = 1 - s$$

and therefore, the machine may be operated at higher speeds with constant current than with constant voltage and consequently at higher ideal efficiencies. Therefore an induction motor supplied from a reference current controlled inverter operates at a lower slip, with lower harmonic currents and torques and hence, a higher efficiency should be expected.

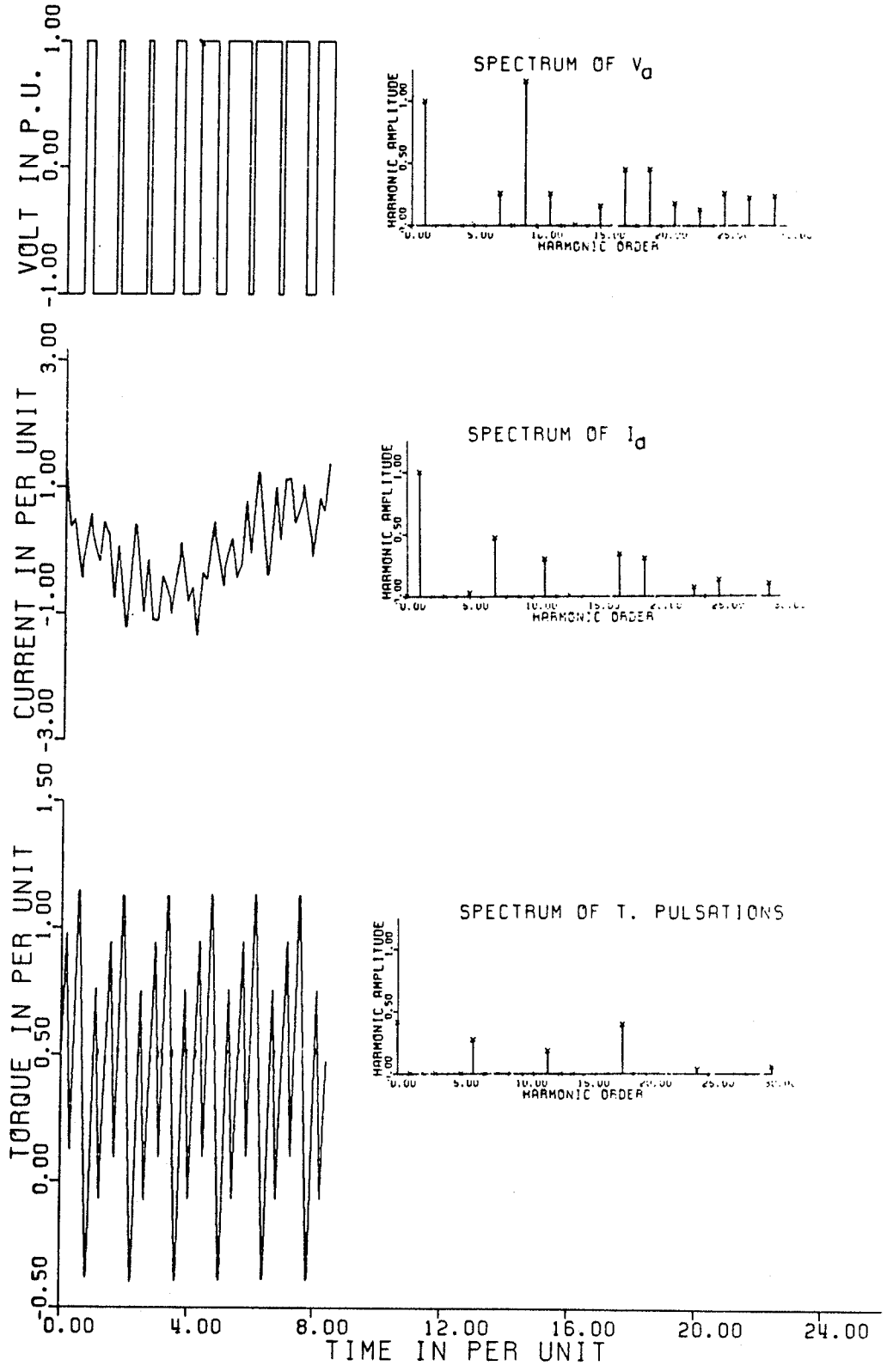

Figure 5.6: Harmonic Contents in Sinusoidal PWM at 45 Hz

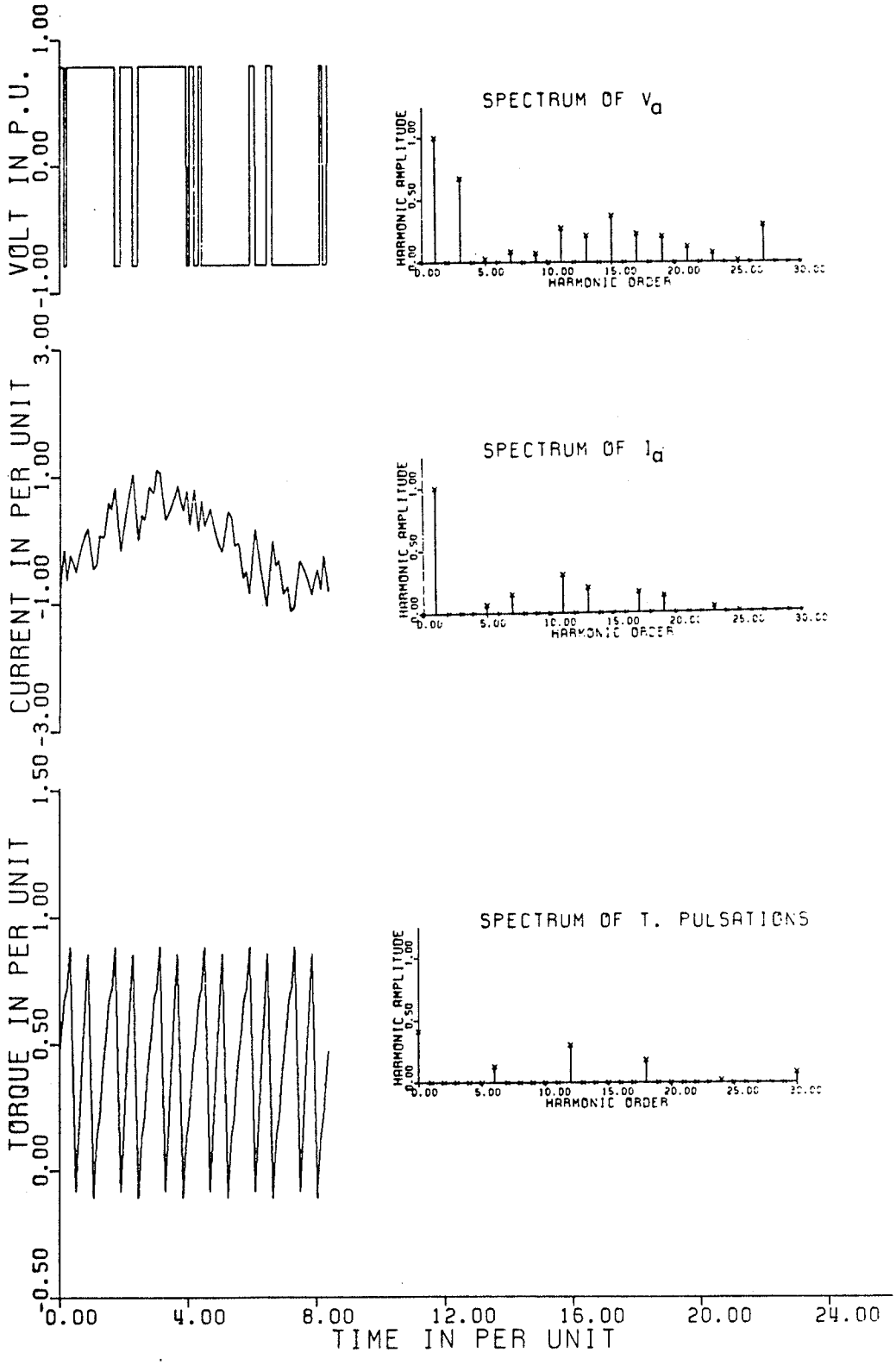

Figure 5.7: Harmonic Contents in Optimum PWM at 45 Hz

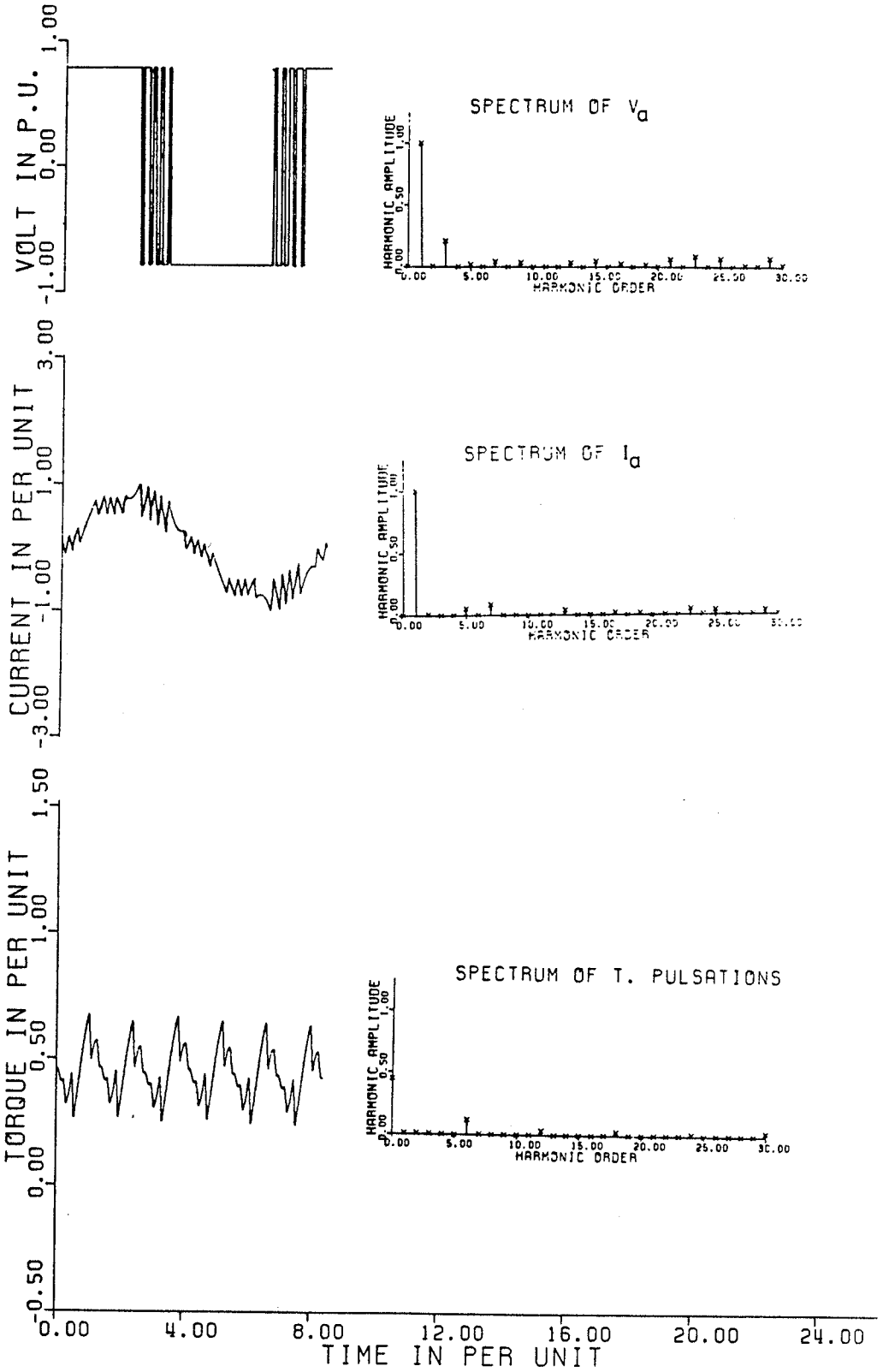

Figure 5.8: Harmonic Contents in Reference Current Controller at 45 Hz

5.2 THE ACCURACY OF THE SAMPLE CYCLE TECHNIQUE

During later research work in Chapters 6 and 7 the author found that some performance indices of the current controller such as the number of commutations per cycle and consequently the fundamental of the input voltage, vary considerably from cycle to cycle at 30 and 15 Hz. Therefore, the results of Table 5.1 will be checked over 12 consecutive cycles, (Table 5.2) in the case referred to by an arrow in Table 5.1. Since the harmonic loss factor is the most important index in Table 5.1, it is the only index checked for accuracy in Table 5.2.

In Table 5.2, $H_{c(ph-a)}$ is the harmonic loss factor calculated from a cycle of phase a, $H_{c(3ph)}$ is the average of three harmonic loss factors calculated from three cycles acquired from the three phases simultaneously. One of these cycles is that of phase a. $H_{c(12-av)}$ is the average value of the harmonic loss factor from the 12 cycles. σ_{n-1}, is the standard deviation and it is given by,

$$\sigma_{n-1} = \sqrt{[1/(n-1)] \sum_{j=1}^{n} (U_j - \bar{U})^2}$$

and defined as the square root of the sum of the squares of the deviations of the sample values from the mean $\bar{U}$, divided by (n-1), where n is the number of samples. The standard deviation is a measure of the spread or dispersion of the sample values from the mean.

Considering the $H_{c(ph-a)}$ row, in Table 5.2, the variance range $(\bar{U} - \sigma_{n-1})$ to $(\bar{U} + \sigma_{n-1})$ is 0.065 to 0.0816, and encompasses cycles # 1,2,3,4,5,6,8,9,11 and 12 (10 cycles). Therefore, the probability that the sample cycle will be close to the mean $\bar{U}$ within the calculated standard deviation range is

$$(10/12) .100 = 83 \%$$

The percentage error from the mean (correct) value within the variance range is 11.3 % .

It should be noticed also that, sampling three cycles from the three phases and averaging (corresponding probability=75 %, and percentage error=10.56 %, in a variance range from 0.067 to 0.083) did not give significant improvement, and that when the harmonic loss factor from phase a is high(low) the average of the three phase sample cycles is also high(low). Hence, considering one sample from one of the phases is of the same order of accuracy as considering the three phases.

In conclusion, a thorough investigation of the variations of all the performance indices of the induction motor, over a large number of cycles, is recommended in order to find the frequency distribution of the indices. The author has the intuition that such distributions may be normal Gaussian distributions or approximately normal or at leaset can be transformed into normal easily.

TABLE 5.2

ACCURACY OF H_c OVER 12 CYCLES

I_R=0.575 , ΔI=0.33 T_L=0.0 + 0.0921 Nu + 0.64 Nu^2 , Nu=0.48961

FAN TYPE LOAD TORQUE

Cycle #	1	2	3	4	5	6	7	8	9	10	11	12	$H_{c(12\text{-}av)}$	σ_{n-1}
$H_{c(ph\text{-}a)}$	0.0687	0.0655	0.0700	0.0672	0.0663	0.0667	0.0821	0.0790	0.0667	0.0912	0.0759	0.0807	0.0733	8.30 E-3
$H_{c(3ph)}$	0.0670	0.695	0.0684	0.0725	0.0676	0.0722	0.0874	0.0817	0.0660	0.0830	0.0865	0.0774	0.0749	7.91 E-3

5.3 APPLICABILITY OF THE DRIVE

As mentioned before in Chapter 4, the starting torque may be a problem with a constant current source feeding the induction motor and that this problem may be alleviated by ramping up the frequency during starting or changes of speed. Therefore in this section the effect of changes in speed or load will be studied[35]. A control strategy will be developed in Chapter 7, now simple methods are presented to examine these effects.

5.3.1 Change of Speed

Figure 5.9 shows the waveforms obtained from ramping the frequency linearly from 15 to 45 Hz at the rate of 140 Hz/s. The load torque is assumed to be a fan type load torque defined as $T_L=0.64\ Nu^2$ p.u.. The waveforms start with one cycle at 15 Hz with the reference current set to 1.0 per unit. During acceleration to 45 Hz the reference current is increased to 3 per unit to provide the torque required to accelerate the motor and load. Following the frequency change the reference current is returned to 1.0 per unit. It should be noted also that around 100 per unit time the applied voltage is not sufficient to maintain the phase current at 3.0 per unit, because of the increase in the back emf of the motor due to the increase in speed. This is indicated by the rectangular voltage waveform, which has maximum fundamental voltage, with only two commutations per cycle. By 200 per unit the motor speed has settled down to a value determined by the load and the applied voltage achieves a repeatable pattern again.

This indicates successful transition from one frequency to the other with this type of control. The successful transition depends on the

amplitude of the reference current during acceleration as well as on the rate of change of frequency.

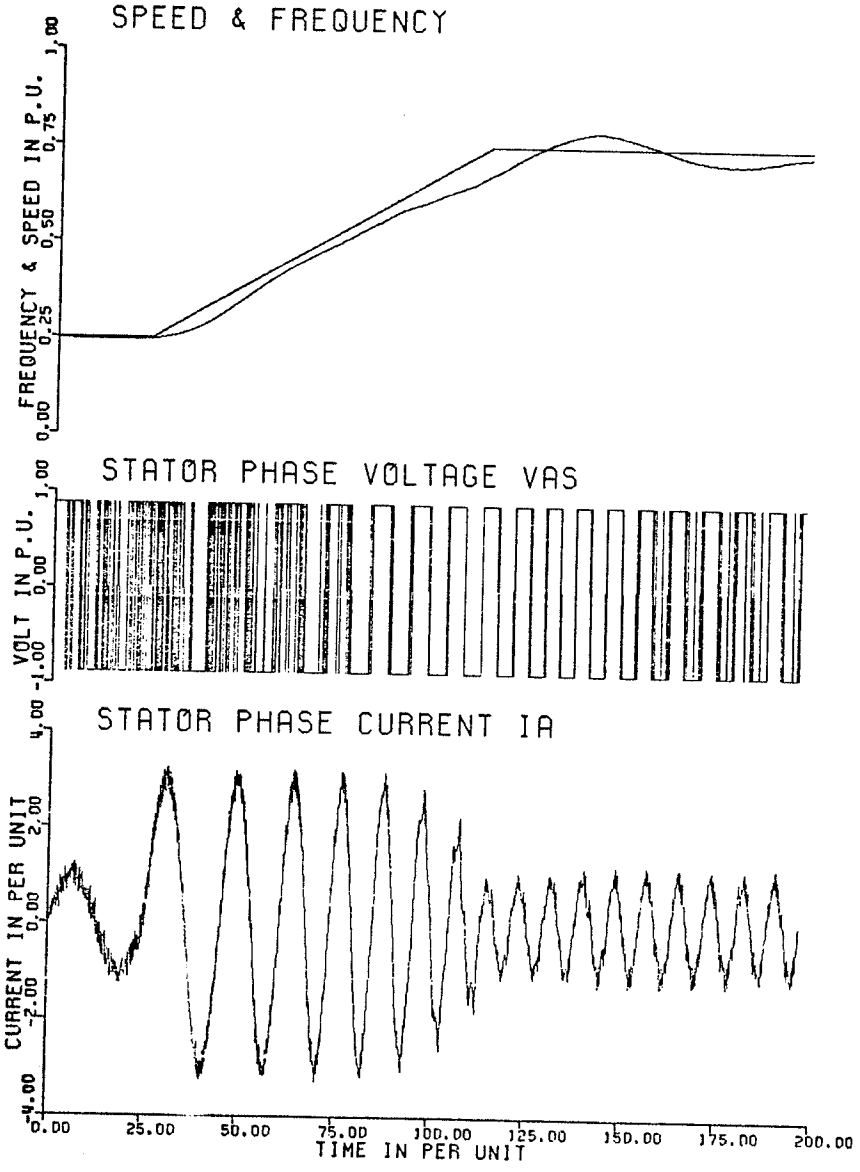

Figure 5.9: Variation in Frequency from 15 Hz to 45 Hz

5.3.2 Load Variations

The effect of load variations is shown in the waveforms of Figure 5.10. The motor is operating at rated torque until 35 per unit time when the load torque is instantaneously increased by 10%, At 70 per unit time the load torque is then reduced to 50% rated. The stator phase current remains uniform during the complete transient period. The voltage waveform remains constant except for additional commutations during the increase in the load torque. The transients in speed are low.

This indicates that the controller can provide a stable operation during small load variations. A higher load variation may be allowed for with higher values of reference currents. During the above small variations, the reference current was kept constant at 1.0 p.u.

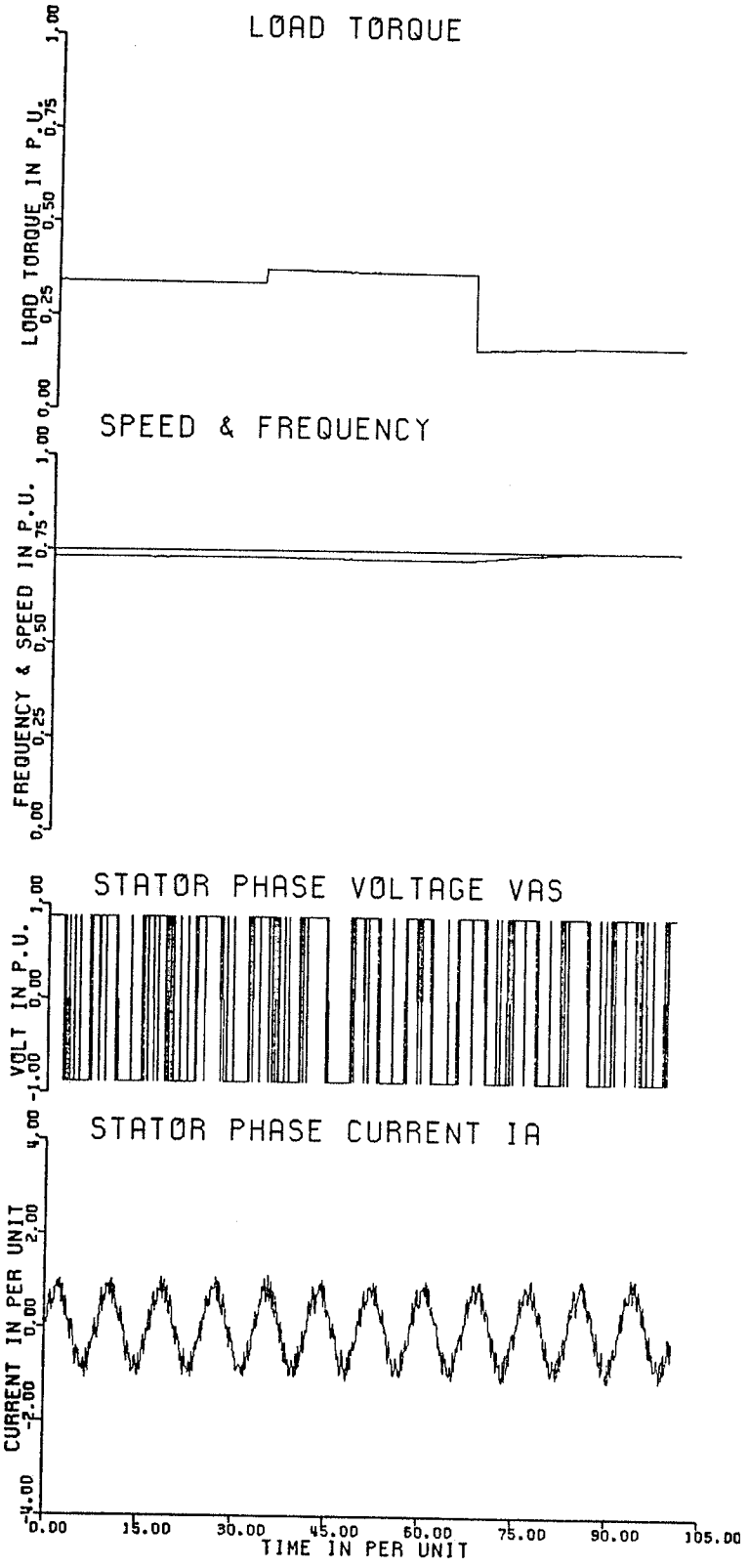

Figure 5.10: Variation in Fan Type Load Torque at 45 Hz

Chapter VI

EFFICIENCY COMPARISON AND BETTER PERFORMANCE

This chapter is divided into two sections. In the first section the method of calculating the motor losses (developed in Chapter 3) will be used in comparing different nonsinusoidal waveform supplies at 60 Hz. The induction motor model used takes into account the saturation in both the mutual and leakage inductances as well as the deep bar effects. In the second section, the same tools will be used extensively for obtaining better values for the reference current, in order to improve the efficiency, at four representative frequencies.

6.1 EFFICIENCY COMPARISON

6.1.1 The Strategies to be Compared

The time domain approach previously introduced, in Chapter 3, is now used for the evaluation of the given induction motor efficiency at 60 Hz under constant load torque when fed from six different voltage waveform supplies. These waveforms are; the pure sinusoidal voltage, the constant volts per hertz square wave voltage, the sinusoidal PWM voltage of Stemmler[8], the optimum PWM voltage for harmonic minimization of Buja[23], the harmonic elimination PWM voltage of Hoft[21,22] suppressing the fifth and seventh harmonics, and the reference current controller voltage[30-36]. The inverter bus voltage was set at, 0.7854 p.u., for the square wave and the current controlled supplies, since the fundamental

of the square will be, one per unit, and the current controller may produce only two commutations per cycle at 60 Hz. The bus voltage for the sinusoidal PWM was set at, 1.0 per unit with a modulation index of, 1.0, which will produce a fundamental of, one per unit as well. For the optimum PWM and the harmonic elimination PWM strategies, the bus voltage was set at, 0.8 and 0.9 p.u., respectively for the same reason. Hence, the comparison between all these voltage sources will be based on the fact that, they all produce the same fundamental voltage and almost the same output power and fundamental stator phase current, when the motor is operated under the same loading conditions from all the sources. The five induction motor loss components, the efficiency, the harmonic loss factor, the fundamental voltage, the fundamental stator current and the output power from all the six sources are included in Table 6.1.

6.1.2 Results and Discussions

The main objective of this study is to show the response of the time domain approach for the calculation of the induction motor losses to the existing harmonics in the different nonsinusoidal voltage waveforms. The harmonic loss factor, H_c, indicates the harmonic content in the stator phase current produced by the different voltage waveforms. It can be noticed that the eddy and hysteresis loss in the stator is not affected by the extra harmonics in the stator current and it primarily depends on the value of the fundamental of the input voltage, V_1. This is due to the inductive nature of the induction motor which prevents the drastic commutations in the nonsinusoidal input voltage from being transferred to the air gap voltage. On the contrary the stator copper

loss does depend on these harmonics and this fact is emphasized from a glance at the square wave voltage and the sinusoidal PWM voltage columns in Table 6.1. It should be noticed that although the fundamental current of the square wave is higher than that of the sinusoidal PWM wave, the stator copper loss of the sinusoidal PWM wave is higher, and this is due the fact that its harmonic loss factor is higher. The same observation is equally applicable between the sinusoidal PWM voltage and the optimum PWM voltage or the current controller voltage. The effect of harmonics is again emphasized in the values of the rotor copper loss, and generally high rotor copper loss occurs when the harmonic loss factor is high. The stray load loss is a function of the output power and the harmonic loss factor, and it can be noticed from Table 6.1 that when the output power is slightly lower and the harmonic loss factor is considerably higher, the stray loss is higher. This is true from a comparison between the optimum PWM voltage and the harmonic elimination voltage. The friction and windage loss is almost constant and this is due to the fact that the load torque was constant and the motor was running at almost the same speed from all the sources.

TABLE 6.1

THE TIME DOMAIN EFFICIENCY EVALUATION FROM THE SIX SOURCES

AT 60 Hz

VOLTAGE STRATEGY / INDEX	PURE SINUSOIDAL	SQUARE WAVE	SINUSOIDAL PWM[1]	OPTIMUM BUJA[2]	HARMONIC ELIMINATION[3]	CURRENT CONTROLLER[4]
P_{out}	0.70590	0.70538	0.70744	0.70720	0.70332	0.704495
V_1	0.99900	0.99900	1.00379	0.98360	0.96606	0.96611
I_1	1.11129	1.11205	1.11082	1.13187	1.16714	1.14755
H_c	0.00000	0.14699	0.29845	0.05250	0.16322	0.08814
P_{e+h}	0.02785	0.02797	0.02862	0.02654	0.02530	0.02531
P_{cs}	0.04357	0.04519	0.04998	0.04555	0.05014	0.04703
P_{cr}	0.02510	0.02660	0.03080	0.02748	0.02533	0.02716
P_{f+W}	0.04427	0.04432	0.04431	0.04406	0.04371	0.04373
P_{s-loss}	0.00991	0.01100	0.01219	0.01030	0.01103	0.01052
EFFICIENCY	0.82407	0.81978	0.81005	0.82126	0.81893	0.82087

H_c : is the harmonic loss factor

I_1: is the fundamental of input current

P_{out}: is the output power

V_1: is the fundamental of input voltage

1 is obtained with an in phase isosceles synchronized triangular carrier with a modulation ratio of, 6.
2 is obtained with the angles (9.44880^o, 14.17320^o, 165.82670^o, 170.55110^o, 180.00000^o)
3 is obtained with the angles (23.62000^o, 33.30000^o, 146.69990^o, 156.38000^o, 180.00000^o)
4 is obtained with a reference current of, 1.24 p.u., and a current deviation of, 0.24 p.u.

6.1.3 Conclusions

The response of the time domain snapshot and sample cycle technique to the existing harmonics in the different nonsinusoidal voltages was very sensitive and this verifies the validity and the accuracy of the approach. An interesting conclusion that came out from this study as well is that, the stator iron loss component does not depend on the stator current harmonics introduced by the nonsinusoidal voltage supplies. It only depends on the fundamental of the input voltage.

The common practice of making a transition from the sinusoidal PWM voltage to the square wave voltage at 60 Hz is confirmed by this study, since the efficiency and the harmonic loss factor are better with the square wave voltage. The order of preference of the studied voltage sources at 60 Hz from the efficiency point of view is as follows; the pure sinusoidal, the optimum PWM of Buja, the current controller, the square wave, the harmonic elimination and then the sinusoidal PWM. Finally the comparison made by this approach can be very easily extended over a wide frequency for the investigation of all the aforementioned strategies, in order to find the most suitable strategy for the application.

6.2 BETTER PERFORMANCE

Previous researchers have optimized certain performance indices and obtained optimum commutation angles for the PWM inverters.[20-25] However, the practical implementation of these predetermined vectors of angles is quite involved. Therefore, since the current controller strategy has the advantage of being very easily implemented it is at-

tractive to find out optimum values for the control parameters of such a strategy. However, the feasibility of optimizing the current controller parameters I_R and, ΔI, in the time domain, using nonlinear optimization techniques, has been discussed in a paper[71] and found questionable. Therefore, in this section better values of the reference current are to be found, in order to improve the efficiency. The current deviation, ΔI, will be given a constant value throughout the study at four different representative frequencies. The idea of improving the efficiency of the induction motor has been discussed in quite a few papers.[72-75] An attempt to select optimal stator voltage and frequency analytically in the frequency domain for a variable speed induction motor drive, has been done by Tsivitse and Klingshirn[74], but a large number of simplifying assumptions were used. Recently published results in a comparative study by Murphy and Egan[63], between different PWM strategies in the frequency domain as well have provided some information on the magnitudes of the additional harmonic losses due to the nonsinusoidal waveform supplies. However, the frequency domain analysis is not directly feasible for the investigation of the induction motor performance when controlled by the reference current controller strategy since it is an adaptive current source strategy.[30] Hence, the time domain snapshot and the sample cycle technique will be used for obtaining better reference current values.

6.2.1 Better Values of The Reference Current

The complete simulation program will now be used for finding the overall efficiency at full load for the inverter-induction motor system. The load torque will be a fan type, i.e; it will have the full load value only at the maximum of the speed range of operation. The reference cur-

rent will be calculated using equations (4.9) and (4.15), following the technique explained before in section 4.2, for different values of the ratio R given by:

$$T_{max} = R \cdot T_L$$

where: T_{max} is the maximum torque and T_L is the load torque.
The ratio R should be more than 1.0, if the motor is at full load since it will then guarantee some steady state stability margin and a feasible operating point on the stable part of the torque slip characteristics. However, if the motor is lightly loaded, then lower values of the reference current can be used with the result that the motor will be undermagnetized and more efficient operation will be achieved[72-75].

The efficiency is then plotted versus the values of the reference current corresponding to the ratio R range (1.1-2.0) for four frequencies. Accordingly the best value of the reference current that give the maximum efficiency in this range can be found. Throughout, this study the hysteresis current deviation was kept constant at 0.25 p.u. since it was found to have a secondary effect on the motor efficiency (EATA). However, it has an effect on the overall efficiency (EATA0) since it has a direct relation with the average number of commutations per cycle. The results are shown in Figures (6.1,2,3&4) for 60, 45, 30 and 15 Hz respectivly.

6.2.2 Results

For the results shown in Figure 6.1 at 60 Hz, the motor stalls with the lowest value of I_R (i.e; R=1.1), since the motor is running at full load at this frequency. This ratio does not give enough steady state stability margin, and therefore, it is not plotted. Although the variation in the reference current is significant (from 0.98-1.26), EATA and EATAO remained almost constant, and this indicates that it is quite hard to obtain an optimum reference current value at this frequency. However this constant performance is quite interesting, since it encourages the use of a high reference current value without being worried that the efficiency will be impaired. Of course the use of a high reference current is recommended from the stability point of view.

For the results shown in Figure 6.2 at 45 Hz, since the motor now is working at almost half of its full load capability, an attempt has been made to reduce the reference current even more to achieve better efficiency. However, this attempt was not successful, and the motor stalled. The general observation that can be drawn from Figure 6.2 is that, the lower the reference current the higher the efficiency. This indicates that the maximum torque point should be the optimum. However, due to the stability margin requirements, some compromise should be made and a higher value of I_R should be used. The main reason behind this performance is the magnetizing branch iron losses which increase significantly as the reference current is increased. This is indicated from the air gap flux which increases gradually with I_R until a ratio R=1.5, where it attains a constant level. At this level the motor operation is more stable, although less efficient, and beyond this point the charac-

teristic is like the one at 60 Hz. At this high range of I_R the motor operates slightly overmagnetized, but is more stable. This overmagnetization is due to the fact that, the controller at this frequency tends to behave as a voltage source inverter with a constant number of commutations per cycle[32], (as will be discussed in more detail in Chapter 7).

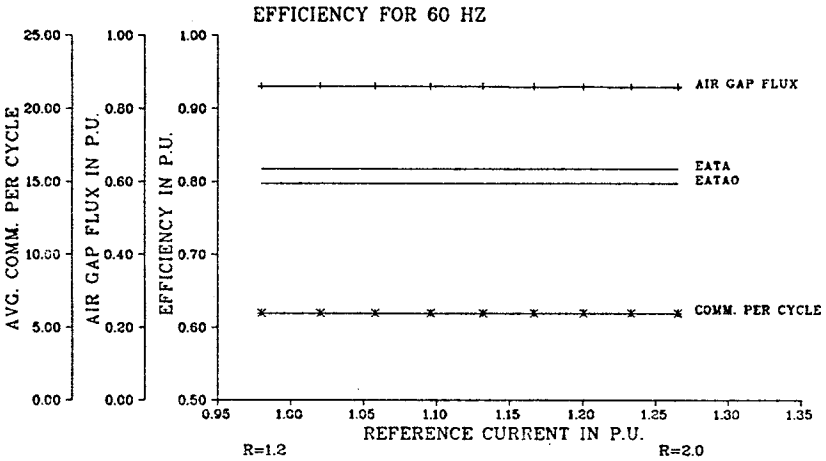

Figure 6.1: Average Values Over 100 Cycles (60 Hz)

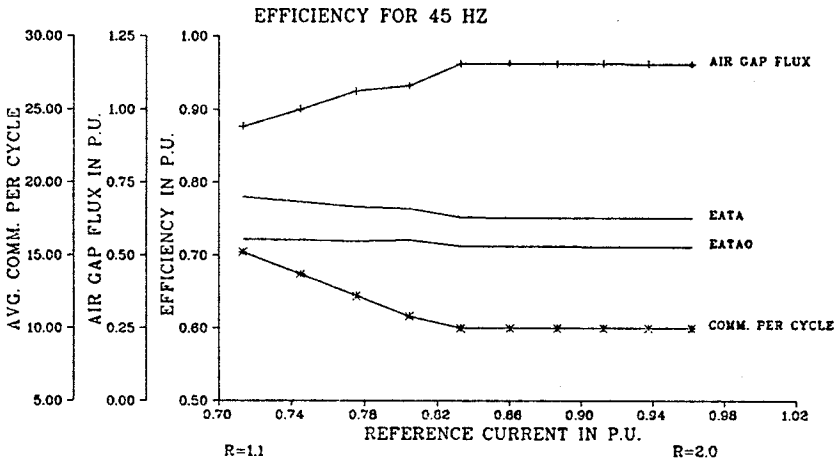

Figure 6.2: Average Values Over 100 Cycles (45 Hz)

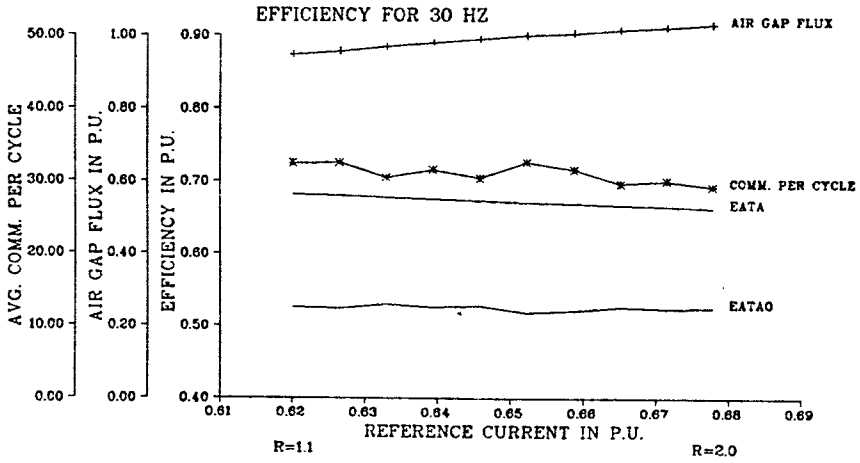

Figure 6.3: Average Values Over 100 Cycles (30 Hz)

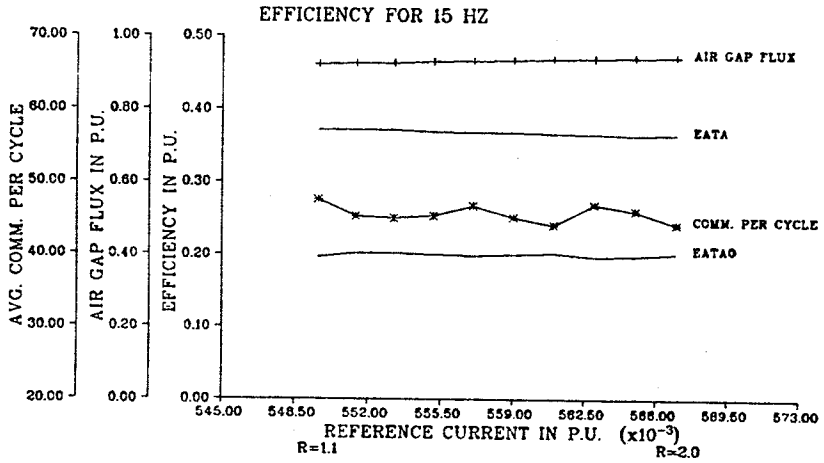

Figure 6.4: Average Values Over 100 Cycles (15 Hz)

Form the results shown in Figures 6.3&4, the general observation is that using lower value of reference current gives a better efficiency, again since the motor now is more lightly loaded. Therefore, due to the fact that, the efficiency of the motor can be improved by reducing the air gap flux iron losses[72-75], the efficiency is calculated at these two frequencies at lower values of the reference current to undermagne-

TABLE 6.2

REDUCING AIR GAP FLUX

f	I_R	$[V_m/f]$	N_c	EATA	EATAO
30	0.58120	0.87277	33.3100	0.69695	0.53147
30	0.51662	0.75685	29.8816	0.71362	0.55094
15	0.50137	0.85329	44.3006	0.39906	0.21179
15	0.44565	0.77720	46.6732	0.42358	0.21443

where:
f is the frequency
and the following variables are given an average value over one hundered cycles:

EATA is the motor efficiency
EATAO is the overall efficiency of the inverter-induction motor system
N_c is the number of commutations per cycle
$[V_m/f]$ is the average of the instantaneous air gap flux

tize the motor. These results are shown in Table 6.2. From Figures 6.3&4 as well as from Table 6.2, it can be noticed that the overall efficiency is effected by the number of commutations per cycle and that the air gap flux is reduced to about 0.85 and 0.75 p.u., by reducing the

reference current to 90% and 80% of the value obtained from the constant current analysis respectively. It should also be noticed that, both EATA and EATAO have been considerably increased by reducing the reference current values, which confirms the previously obtained results[72-75], about undermagnetizing the motor when lightly loaded.

6.2.3 Concluding Remarks

The calculations of the efficiency from a simple open loop study show that, at 60 Hz it is quite difficult to find an optimum value for the reference current, since the efficiency was found to be constant over a wide range of the reference current.

At the lower frequencies, the same study indicated that the optimum point should be at the maximum torque point where the torque to current ratio is maximum. Generally, with a fan type load torque, the lower the reference current the better the efficiency. However the stability requirements necessitate the use of high and safe values of the reference current. The result that the efficiency is improved by reducing the air gap flux is also, confirmed in the case of the current controller.

In order to find optimum values of the controller parameters, the previous calculations may be repeated for some different values of, ΔI, in a range from 0.23 to 0.33 p.u.. This range of, ΔI, should keep the number of commutations per cycle comparable to that obtained from the other PWM strategies, in the frequency range of interest, as was discussed before in Chapters 4 and 5.

Chapter VII

THE FLUX LINKAGE CONTROLLER

In Chapter 5, the load variations were small and there was no change in the control parameters to cater for these transients. It was noted that, higher load variations may cause the inverter induction motor system to move into the unstable region of the torque slip characteristic. The torque slip characteristic of the inverter-induction motor system with a reference current controller strategy is approximately that of the induction motor when fed from a constant current source as shown before in Figure 4.3. Any sudden increase in the mechanical load necessitates a larger slip and therefore a decrease in the input impedance of the motor. Since the input current is constant, the voltage at the motor terminals should therefore decrease leading to a decrease in the input power available. Hence the response to a higher demand for power is a decrease in input power, which means that the motor should stall. A controller that will sense the flux linkage and adjust the amplitude of the reference current accordingly, is to be investigated so as to prevent the undesirable decrease of the input voltage.

Plunkett has introduced a direct method of flux and torque regulation using sensing coils and several feedback loops[76]. Although, the direct regulation of the air gap flux and torque is an ideal control[42], such a control is more than enough for the purpose under consideration,

(i.e; pump and fan drives). Therefore, an indirect way*, cheaper, and easier to implement for regulating both parameters, should be considered as long as good dynamic behaviour, reliability and the other performance indices are not seriously impaired[41]. If direct flux and torque measurements are to be used, clearly sensing means become a problem, especially in the severe environments where pumps and fans are installed. Besides, installing search coils around the proper teeth, is not an easy job to be done in the field. Let us recall that, the objective is to retrofit the existing induction motor with an inverter control suitable for pump and fan drives. Therefore, in the adapted scheme, the flux level will be estimated from the terminal input voltage and a programmed nonlinear relation between the flux and the frequency will be used. One major advantage of the direct flux and torque regulation is the elimination of the need of a tachometer to sense the speed. However, with a microprocessor control,[35] storing the aforementioned nonlinear relation between the frequency and the flux will eliminate the need of a tachometer, in the adapted scheme. The proposed scheme although less accurate, is easier to implement, cheaper, provides resonable reliability and therefore more suitable for the purpose.

In the proposed scheme, the reference current controller is equipped with a flux linkage regulator that maintains the air gap flux almost constant at all loading conditions, the characteristic of the system will be similar to that of a motor fed from a constant voltage per hertz source which is stable in the sense explained before. The

---

* There are several indirect methods of controlling the torque, other than measuring it, such as stator current, slip frequency, flux etc.

purpose of this Chapter is to check the stability of the regulated flux scheme, during high and sudden load changes. During steady state operation the flux linkage controller may also be used to keep the reference current as small as possible so as to maintain a minimum level of losses within the motor[71]. The ramping up of the speed could also be done automatically with the help of such a controller which will vary the reference current as required during frequency changes.

7.1 THE CALCULATION OF THE FLUX LINKAGES

There are quite a few methods for measuring or estimating the air gap flux linkage in an induction motor.[76-78] Some of these possible methods, and that used for this controller will be discussed next:

1. The estimation of the air gap flux:[78]

   The air gap flux can be estimated from the motor terminal voltage and the stator phase current using a model of the motor. This method is quite involved, and is expected to require a fast microcomputer for processing, since more calculations are needed and the response time constant of the controller should be kept as small as possible.

2. The use of search coil:[76,77]

   The air gap flux can be measured directly by sensing coils wound around a motor stator tooth. As the aim of this study is to retrofit existing induction motors driving pumps and fans with an efficient variable speed controller, the idea of using search coils will not be considered.

3. The method adapted for the study: The direct integration of the output voltage of the inverter is the method adapted for the estimation of the air gap flux. Although this method is approximate, it is used because it is easier to implement, should be cheaper, provides reliable and stable operation, and therefore is more suitable for the purpose. The instantaneous flux linkage may be given by;

$$\lambda_{ins} = \int_0^T v \, dt \qquad (7.1)$$

where; T is the period, of one cycle of the inverter frequency.

The integration of the inverter phase voltage will give the waveform of flux linkage, at the terminals of the motor as shown in

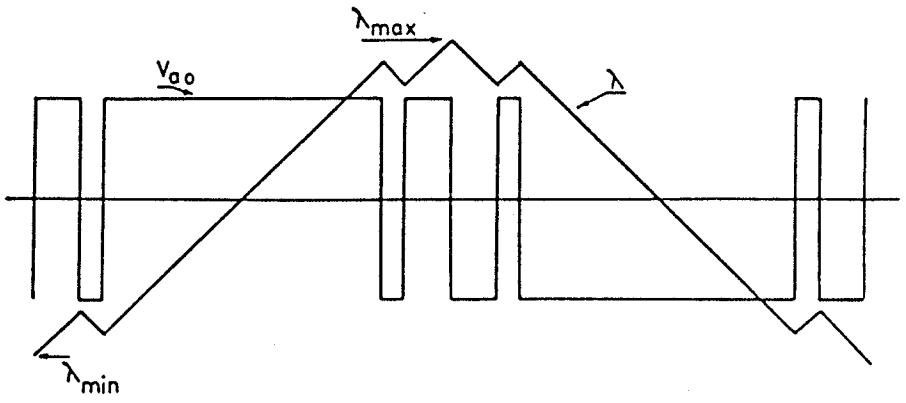

Figure 7.1: The Integrated Flux linkage Waveform

Figure 7.1. The maximum and minimum values of the flux linkage are found and stored. At the end of the cycle, or half cycle the maximum flux in the gap may be given by;

$$\lambda = (1/2).(\lambda_{max} - \lambda_{min}) \qquad (7.2)$$

This method gives an estimate of the total flux at the motor terminals, and is easier to implement practically. The microprocessor may be programmed to add the values of the bus voltages, (+ve) or (-ve), according to switchings between the two buses.

This last method will be used for sensing the value of, λ_{est}, which is to be added as a negative feedback signal to the flux reference value, λ_R. The difference (Error) between these two quantities is then fed to a "PI" controller, the function of which will be explained in the next section.

7.2 THE PI CONTROLLER

The algorithm of a PI controller is the sum of the response of two components; proportional and integral, having independent gains K_p and K_I as shown in Figure 7.2. The algorithm of each component can be derived separately.

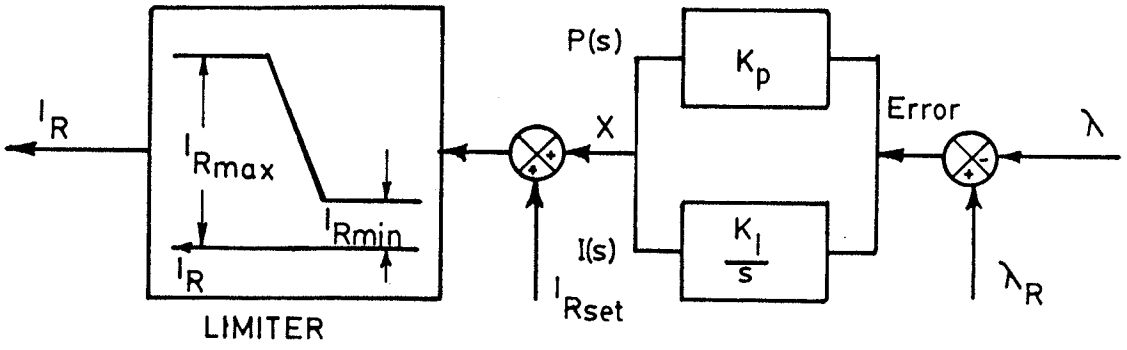

Figure 7.2: The "PI" Controller

7.2.1 The Proportional Block

A proportional controller is the simplest, however, it is not recommended to be used alone, as it always produces a steady state error. The steady state error may be made as small as desired by increasing the gain, but it never reaches zero. Besides, when there is a time delay, no matter how small, an increase in gain will ultimately lead to instability. The consequence of dead time lag (time delay), therefore is instability when the overall gain is one or more. If it is used alone as shown in Figure 7.3, its control law is given by:

$$I_R = K_p \cdot \text{Error} + I_{Rset} \qquad (7.3)$$

Where;

Error= $\lambda_R - \lambda$

λ : is the measured or calculated flux linkage from the processor.

λ_R: is the reference value of the flux linkage.

I_{Rset}: is the set value of the reference current.

I_R: is the reference current value produced by the controller.

A steady state error results when the load is changed from that initially set by the value of I_{Rset} in equation (7.3). Therefore, I_{Rset} is necessary if only a proportional controller is used. On the other hand it can be set to zero if a "PI" controller is used. However in the simulation, I_{Rset} has been set to the no-load current value in the complete scheme (Figures 7.2&4) to speed up the stabilization of the system during the initialization of the process of checking the integrated flux in the three phases (as will be explained later in Section 7.5). In a real system, again, I_{Rset} may be set to zero because the integrator action should ultimately nullify any steady state error.

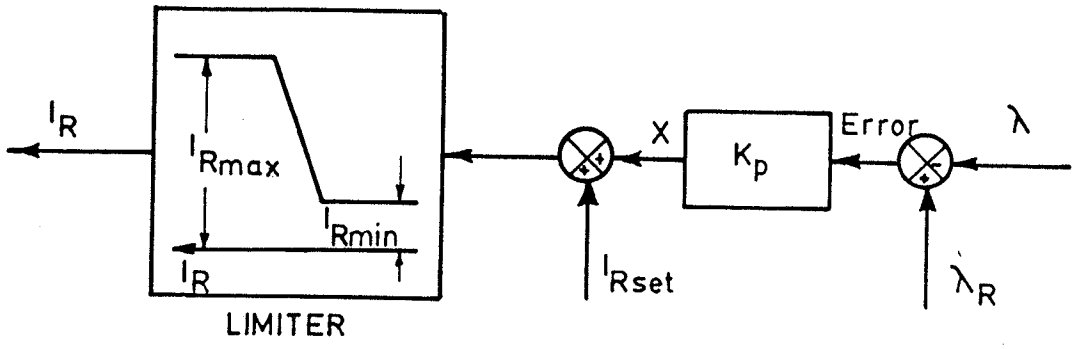

Figure 7.3: The Proportional Controller

7.2.2 The Integral Block

The Laplace form of this block may be given as follows:-

$$(I(s)/Error) = (K_I/s) \tag{7.4}$$

Therefore, the difference equation is;

$$I_n = I_{n-1} + K_I \cdot Error_n \quad ; \quad K_I = K \cdot T_s \tag{7.5}$$

Where T_s is the sampling period. In our specific problem T_s could be one half, one third or one sixth of a cycle. In the case with an integral controller or a "PI" combination, it is both intuitively and mathematically correct to conclude that the integral control will completely null the error and correct the offset, given enough time, since the controller continues to drive the value of the reference current, I_R, so long as any error exists.

7.2.3 The Complete Algorithm of the "PI" Controller

The complete digital computer simulation equations for the "PI" controller are given by:-

$$K_{po} = \text{Error} \cdot K_p \tag{7.6}$$

$$K_{Io} = K_{Io} + \text{Error} \cdot K_I \tag{7.7}$$

$$X = K_{po} + K_{Io} \tag{7.8}$$

$$I_R = I_{Rset} + X \tag{7.9}$$

The addition of a "PI" input flux-linkage controller to a simple implementation of the reference current controller[35], is shown in Figure 7.4. The three phase reference currents are compared with the actual currents in hysteresis comparators. The output of the comparator is fed to the firing circuits which control the firing instants of the commutating and main thyristors for each phase. The magnitude of the reference current I_R is fed to the comparator circuits from the "PI" controller, automatically. The current deviation ΔI is set manually. The "PI" controller can be made as shown in Figure 7.4 using an analog integrator or it can be incorporated into the microprocessor software by just feeding the commutation instants from the firing circuits to the microprocessor as shown by the dotted line. By doing so, a lot of hardware can be saved.

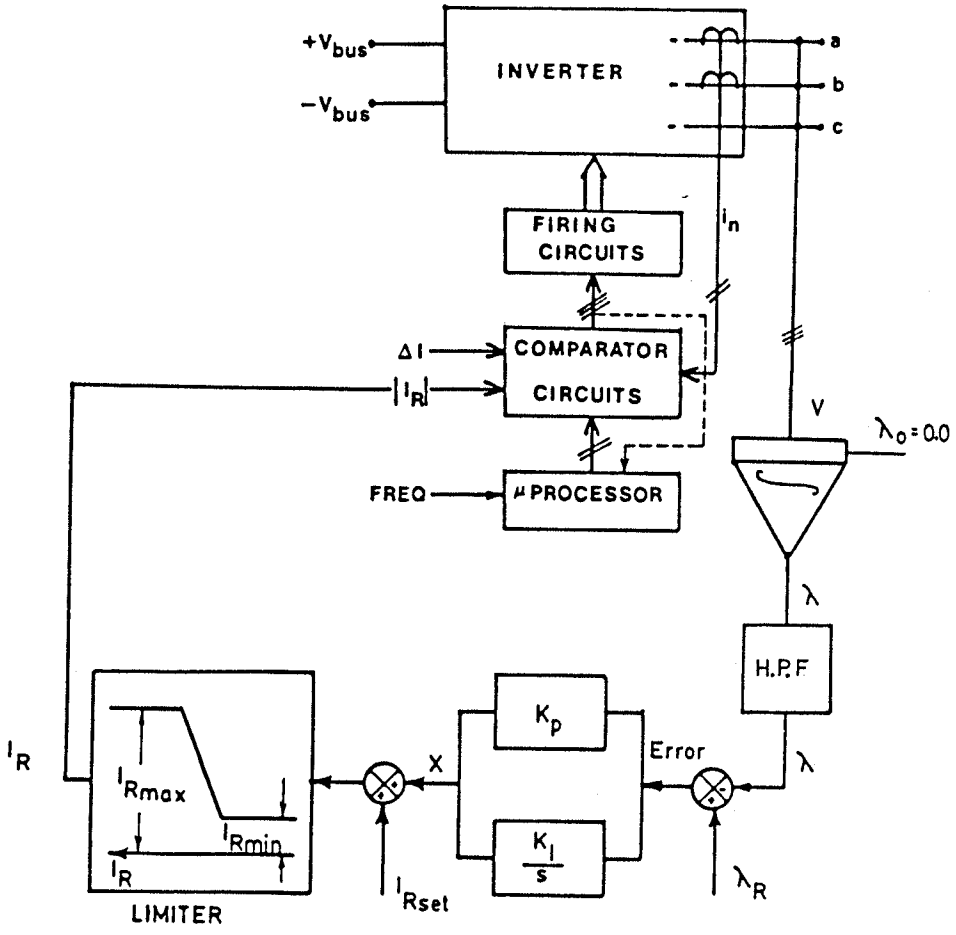

Figure 7.4: The Complete Control Diagram

7.3 THE CALCULATION OF THE FLUX REFERENCE

The reference value of flux, λ_R, in Figure 7.4, according to which the controller will operate, is a critical value and should be estimated very carefully. If this value is set far from the measured feedback values of flux, the controller may not operate properly. A preliminary study on the performance of the inverter-induction motor system under different loading conditions is conducted. The objective of this study is to change the value of I_R for different loading conditions. The general expression for the load torque T_L used throughout this study is :

$$T_L = C_{do} + C_{d1}\ Nu + C_{d2}\ Nu^2 \qquad (7.10)$$

where, Nu is the rotor speed in p.u., C_{do} is the constant load term and will be set to zero throughout the study. C_{d1} is the friction coefficient, (Appendix C), and C_{d2} is the fan load term and will be changed from zero at no load (NL), to 1.28 p.u at double full load (DFL). The full load (FL) is at C_{d2}=0.64 p.u.. General relations, if any, between the fundamental voltage to frequency ratio as well as the actual air gap flux and the load torque are also sought. The values of the reference current required for providing the necessary (V_m/f) ratio or the design flux density in the air gap of the motor for the different loading conditions can be obtained from equations (4.9) and (4.15) as explained before in Chapter 4. The calculated reference current values are then to be used to calculate the integrated flux, the fundamental voltage to frequency ratio (V_1/f) and the air gap flux (V_m/f) as well as the number of commutations per cycle from one hundred consecutive sample cycles using the simulation program of the unregulated flux system. The air gap flux is the average of the instantaneous flux over one cycle, where;

$$\text{Instantaneous Flux} = M\sqrt{(i_{ds}+i_{dr})^2+(i_{qs}+i_{qr})^2} \qquad (7.1$$

and, all other parameters are defined in Appendix B. An average of one hundred calculated values of each performance index will be plotted versus the load torque. Taking the average over one hundred cycles is necessary at the low frequencies, since the calculated indices changes considerably from one cycle to the other.

7.3.1 The Different Flux Levels

In fact the integrated flux has a higher level than the (V_1/f) and that the (V_1/f) has a higher level than the (V_m/f). This may be explained by considering the operation from the controller when it makes only two commutations per cycle (i.e produces a square wave). The relation between the integrated flux,(λ_{est}) and the fundamental voltage to frequency ratio (V_1/f) may be obtained from Figure 7.5 as follows:-

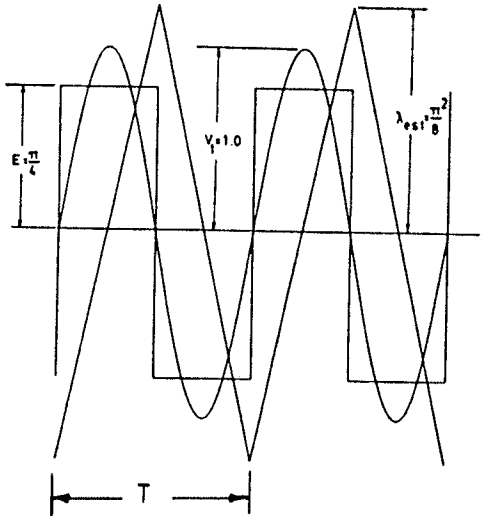

Figure 7.5: The Relation Between the Different Flux Levels

$$T = \frac{2\pi}{\omega} \quad , \qquad \omega \text{ is frequency in p.u. } = f$$

$$\lambda_{est} = \frac{E\,T}{4} = \frac{E\pi}{2\omega}$$

$$\frac{V_l}{f} = \frac{4\,E}{\pi\omega}$$

Therefore,

$$\text{Ratio} = \frac{\lambda_{est}}{(V_l/f)} = \frac{\pi^2}{8} = 1.2337 \qquad (7.12)$$

This explains why the integrated flux value should be different from the (V_l/f). In Figure 7.6 at 60 Hz the voltage is almost square and the average ratio between the integrated flux and the (V_l/f) is 1.1199. The respective average ratios from Figures 7.7-7.9 for the frequencies 45,30 and 15 Hz are 1.1066, 1.09767 and 1.0916 respectively. The difference between the average values of (V_l/f) and (V_m/f) which is due to the stator leakage impedance voltage drop is given in the Figures 7.6-7.9 as well, for the four frequencies of interest.

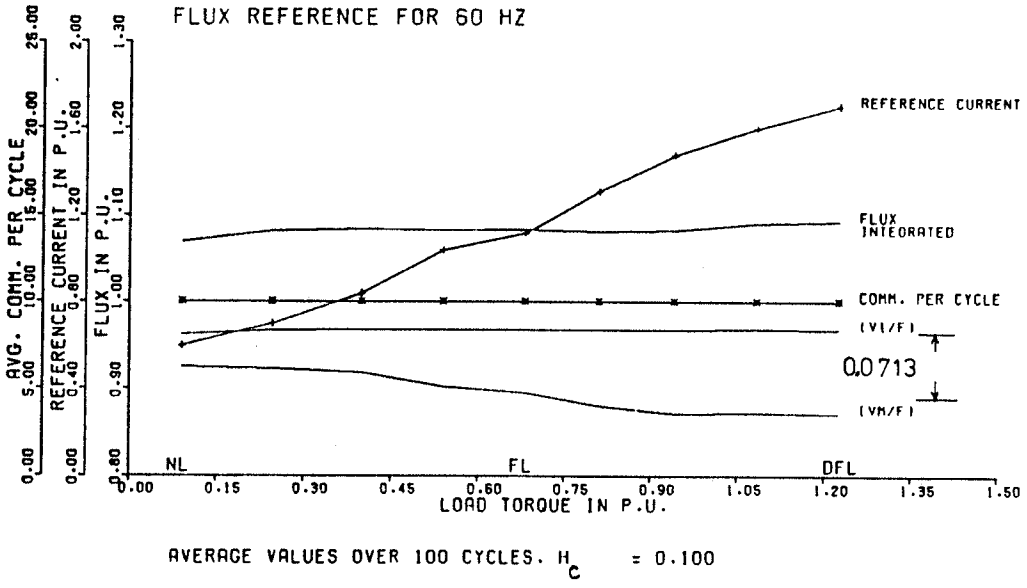

Figure 7.6: Reference Flux Setting for 60 Hz

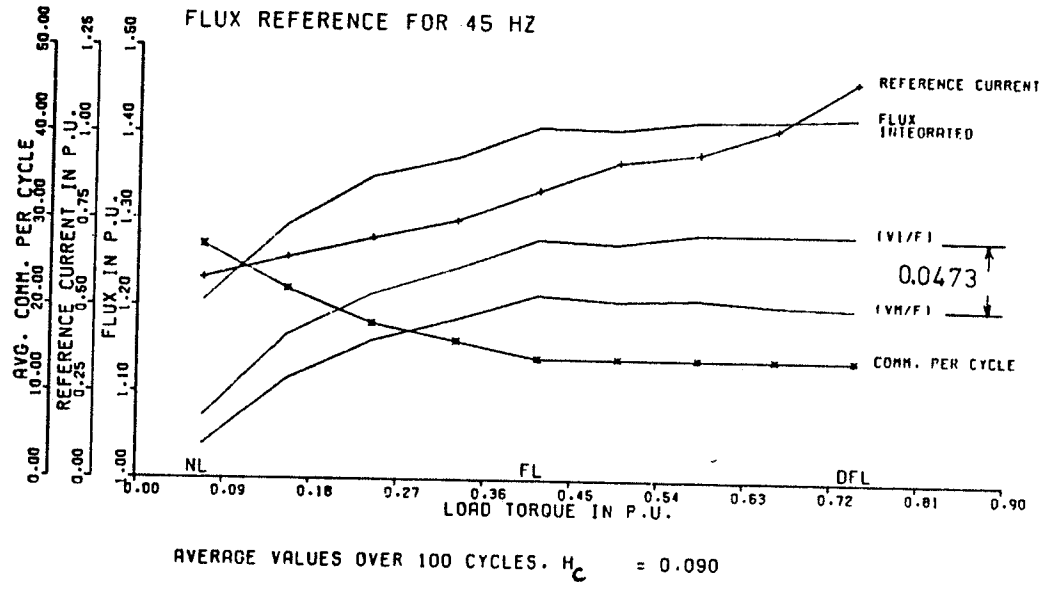

Figure 7.7: Reference Flux Setting for 45 Hz

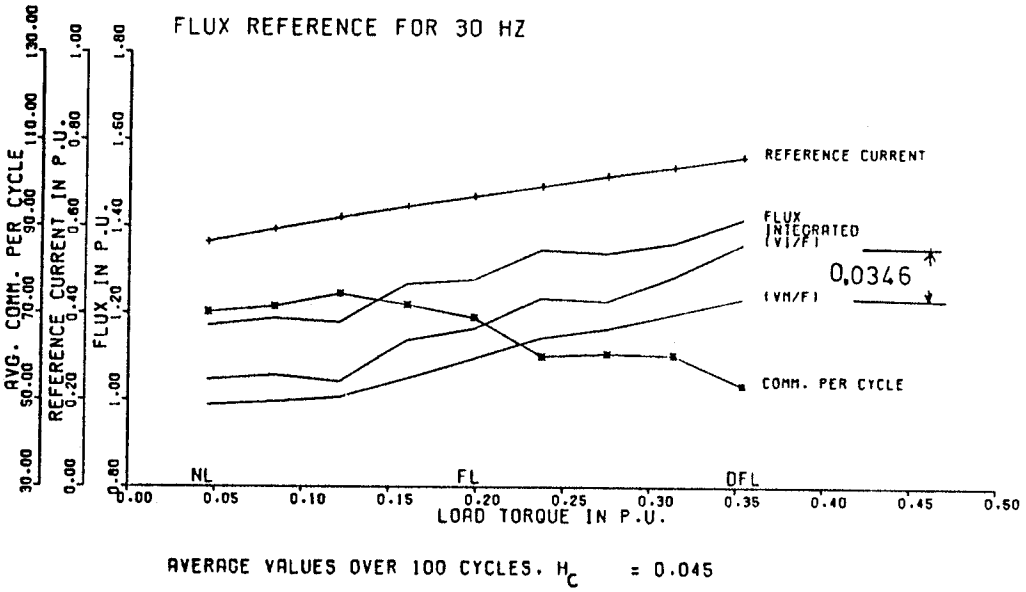

Figure 7.8: Reference Flux Setting for 30 Hz

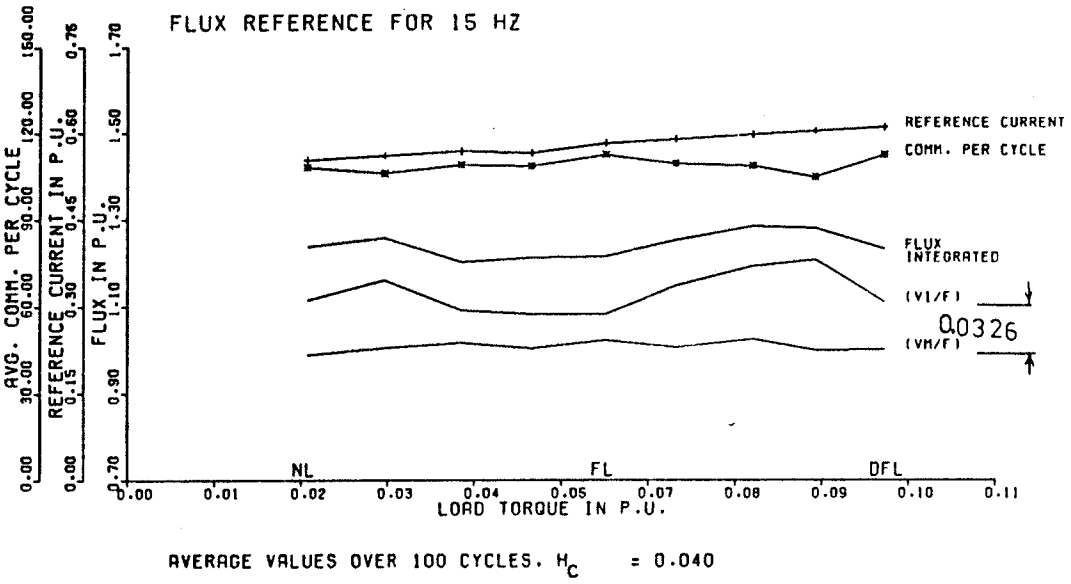

Figure 7.9: Reference Flux Setting for 15 Hz

7.3.2 The Drift Problem

A drift has been noticed in the nonfiltered integrated flux signal, during a preliminary study of the regulated flux system. In fact the integrated flux reference signal is drifting also in the unregulated flux system as it is drifting in the regulated flux study. Therefore, a high pass filter has been added, after the integrator, to the system in Figure 7.4. The first order high pass filter used has a cutoff frequency at 7.5 Hz which is equivalent to 8 p.u. time constant and has the transfer function:

$$\frac{D}{Y} = \frac{sT}{1 + sT} \quad , T = 8.0 \quad \text{(p.u.)} \qquad (7.13)$$

and the associated difference equation is:

$$D_n = \left(\frac{T}{T + H}\right) [\, D_{n-1} + (Y_n - Y_{n-1})] \qquad (7.13a)$$

where,

D is the filtered signal

Y is the original signal (integrated flux λ)

H is the integration increment

This filter was digitally simulated and added to the simulation program to prevent the drift during the calculations of the integrated flux from the unregulated flux study.

The same filter will be used later in the regulated flux system study to remove the drift and to help in stabilizing the system since it will remove the pole from the origin due to the direct integration of the input voltage. Since the same filter is used during the calculation of the reference flux value and during the operation with the regulated flux system the estimated value of the reference flux should be used as it is without any allowance for the attenuation caused by the filter on the high frequency signal. For 15 Hz, (double the cutoff frequency), the first order filter attenuates the drift to only 18 %, which is not sufficient. Consequently a second order filter which attenuates the drift to about 3 %, was used in the unregulated flux study. Hence, the flux reference value obtained from Figure 7.9, should be multiplied by a factor of 1.111, to take into account the extra attenuation in the, 15 Hz, flux signal. This is because in the regulated flux system response traces, (demonstrated in section 7.6), at all frequencies only a first order high pass filter is used. As can be noticed, the use of a first order filter at 15 Hz gave good response to the sudden load changes pattern, even with the drift being reduced to only 18 %. Alternatively a second order filter may be used at all the frequencies. In this case, the reference flux settings calculated from the unregulated system study, at the higher frequencies, will not change significantly and

there will be no need to multiply by a factor at any frequency. Therefore if the 15 Hz range is to be used then a second order filter is recommended. However, it will be more expensive. On the other hand, if the requirements of the pump and/or fan drive necessitate only a limited speed range then, the use of a first order filter should be quite satisfactory.

7.3.3 Comments on the Unregulated Flux Results

At 60 Hz (Figure 7.6) the flux integrated and the (V_1/f) remain almost constant from no load to full load because the number of commutations per cycle is constant over the complete load range.

At 45 Hz (Figure 7.7) from no load (T_L=0.06859) to full load (T_L=0.41574) the integrated flux and the (V_1/f) were increasing with load. However, this is due to the decrease in the number of commutations per cycle from 27 to 14 respectively. From full load to double full load, the number of commutations per cycle is constant and therefore, the integrated flux and the (V_1/f) are constant beyond full load. This indicates that there is a direct relation between the number of commutations per cycle and the flux levels at the high frequencies. The average values of the calculated indices from the unregulated flux study are shown in Table 7.1. It should be pointed out that, the values of the average integrated flux listed in the second column have reversed their sense of change at 30 Hz. This is due to the fact that, the system changes its behavior from constant voltage source to constant current source between 30 and 45 Hz. It should be noticed also that the maximum error between the calculated flux by direct integration(second column), and the actual air gap flux (third column) occurs at the lowest

frequency. The average per unit error is 0.18725, 0.19457, 0.18372 and 0.37275 for the 60, 45, 30 and 15 Hz respectively. This error is due to the explained relation between the different flux levels in Figure 7.5, the drift and the voltage drop on the stator leakage impedance.

TABLE 7.1

THE UNREGULATED FLUX STUDY

f	INTEGRATED FLUX (av.)	$[V_m/f]$ actual	$[V_1/f]$ actual	N_c	H_c
1.0	1.08284	0.89559	0.96687	10	0.10000
0.75	1.36515	1.17058	1.23365	14	0.10000
0.50	1.28742	1.10370	1.17286	68	0.04500
0.25	1.37943	1.00668	1.13727	108	0.04000

N_c is the number of commutations per cycle
H_c is the harmonic loss factor

It should be noticed also that the average air gap flux level at 45 Hz is (1.17058), therefore, many attempts were tried to use lower reference current values so as to produce lower magnetic level in the motor, (this directly means risking the 1.5 ratio between the maximum torque and the load torque which guarantees the same steady state stability margin as at the other frequencies). All these attempts were unfortunately unsuccessful with (the unregulated flux system of the linear model). The reason is as follows; if a lower reference current is used at a high load torque, the magnetizing current will tend to stay constant

since the controller acts as a voltage inverter at this frequency with a substantially constant input voltage. Therefore, the decrease in the reference current will result in a direct decrease in the rotor current which is the torque producing component. Consequently the motor will produce a developed torque lower than the load torque and will eventually stall. This same observation has been repeated several times when the author was trying to lower the reference current in order to obtain an optimum reference current value for the objective of achieving maximum efficiency . There was always one result to such attempts; the motor stalled. In conclusion the operation with a little bit higher flux level is an inherent characteristic of the current controlled induction motor at 45 Hz and occurs if the same steady state stability margin as the other frequencies is to be kept. In order to lessen this effect, a selection of the second frequency as 48 or 50 Hz will produce a lower flux level and should result in a more efficient operation. Nevertheless, the air gap flux level at 45 Hz is not excessive it is still less than 1.25 p.u. In essence this is very similar to operating a 60 Hz designed motor from a 50 Hz supply at the same voltage level. In such an operation the motor overheats slightly but performs satisfactorily. An important point that favours the current controller in this respect is that, the stator current is controlled and cannot be excessive. In fact the current stays confined within the limits of the reference current, even with such a small increase in the flux level.

At 60 and 45 Hz, (Figures 7.6&7), the difference between the integrated flux and the fundamental input voltage to frequency ratio (V_1/f) remains almost constant from no load to double full load and this indi-

cates that the motor is running under constant flux linkage and therefore constant voltage. As the load torque is increased, the input current is increased to furnish the required extra torque, at the same voltage. Therefore the controller acts as a voltage inverter at 60 and 45 Hz.

On the contrary at 30 and 15 Hz, (Figures 7.8&9), despite the fact that the change in the load torque is smaller, it can be noticed that both the integrated flux and the (V_1/f) increase with the load torque. This indicates that quite a different operation from that encountered before at the high frequencies is taking place. Taking into account also that the reference current used at these two frequencies is almost constant from no load to double full load, means that the controller should be working now as a current inverter which supplies an almost constant current and variable input voltage.

It should be noticed also that as the load increases at 30 and 15 Hz, the difference between the integrated flux and the fundamental voltage to frequency ratio (V_1/f) tends to diminish. This is expected due to the fact that, a high number of commutations per cycle is encountered at these low frequencies. Many commutations per cycle make the input voltage very close to the sine wave fundamental component of the voltage ,V_1, or in other words will make this voltage contain only very few high order harmonics. If such an input voltage is integrated the amplitude of the integral will be equal to the fundamental amplitude divided by the frequency. Hence the values of the integrated flux and (V_1/f) tend to be close.

At 30 and 15 Hz again the number of commutations per cycle is also different from one cycle to the other, which means a variable input voltage with load. Another reason for the changes in the input voltage is the change in the locations of the firing angles, which is also very possible to occur. This possibility is emphasized by noticing that, a large number of commutations per cycle does not necessarily means a lower input voltage. The reverse is also true. This observation is a main difference regarding the behaviour of the controller as a voltage inverter and as a current inverter. As a voltage inverter the input voltage has a direct relation with the number of commutations per cycle since the commutation angles keep their relative positions almost constant and are repeated very regularly from one cycle to the other. As a current inverter the input voltage depends on the number and locations of the firing angles, and both change from one cycle to the other.

At all the frequencies, it can be noticed that stator leakage impedance drop decreases as the frequency decreases. This is expected since the leakage reactance depends on the the frequency and because the load torque is a fan type load torque (i;e decreases with frequency). This fact is not directly apparent from Figures 7.6-7.9 since the values plotted are fluxes and not voltages. To obtain correct figures for comparison, the difference between the average values of (V_l/f) and (V_m/f) should be multiplied by the respective frequency. The obtained average voltage differences (stator leakage impedance drop) are ; 0.07128, 0.047308, 0.03458 and 0.032647 (p.u.) for 60,45,30 and 15 Hz respectively. An important note that should be added here is that an increase in the stator leakage impedance drop, with the load torque is a fact shown

in the four Figures 7.6-7.9 at the four frequencies of interest. The used values of the flux integrated in the regulated flux study are: for the 60 and 45 Hz (Figures 7.6&7), the values corresponding to the full load points (1.1 and 1.40747 respectively) and , for 30 and 15 Hz (Figures 7.8&9), the average values over the load transient pattern range. Some other slightly different values were tried as well, the best results are presented.

The importance of the estimation of values of λ_R, lies in the fact that, the reference current controller can work efficiently and stably, if and only if, the proper values of the control parameters are used.

7.3.4 The Implementation of the Flux Reference

There should be some limiting action on the output of the "PI" controller, otherwise the obtained values of, I_R, may go negative or increase without limit to non feasible values (Figure 7.4). The values for minimum and maximum limits of I_R are; IRmin=0.553 which is the no load value of the reference current in Figure 7.9 and IRmax= 1.7 which is the double full load value in Figure 7.6. The value of the reset current was taken equal to the minimum magnetizing current value (i;e IRset=0.526). All the values of the controller parameters are shown in Table 7.2.

The use of a variable value for the flux reference λ_R (Table 7.2) as the frequency changes is required to provide a stable operation. The nonlinear relation between the frequency and the flux reference is in agreement with the schemes of Plunkett[31,32] (see section 7.7 for stabil-

TABLE 7.2

THE USED CONTROLLER PARAMETERS

f	USED FLUX REFERENCE	K_P USED	K_I USED
1.0	1.10000	10.0000	0.10000
0.75	1.40747	10.0000	1.00000
0.50	1.27755	1.00000	0.10000
0.25	1.35000	0.50000	0.05000
Ramp .25-.75	1.40747	05.0000	0.20000

ity discussion). This nonlinear relation has to be found and stored in the microprocessor memory in Figure 7.4. The sinusoidal constant current analysis (Chapter 4), at 30 and 45 Hz (when the controller operates as a current inverter), together with the observation that "at 60 and 45 Hz (when the controller operates as a voltage inverter), all the commutations are squeezed at the sides of the square wave" (Figure 7.11) may be used for the estimation of this nonlinear relation at all the frequencies instead of the actual unregulated flux study.

The values of K_p and K_I are a result of many trials. However, the designer may use only one value for each parameter at all frequencies by compromise and a primary adjustment of the drive. In this particular application and motor, the author recommends the use of K_p=5.0 and K_I=0.2 throughout the whole frequency range. These values are found to

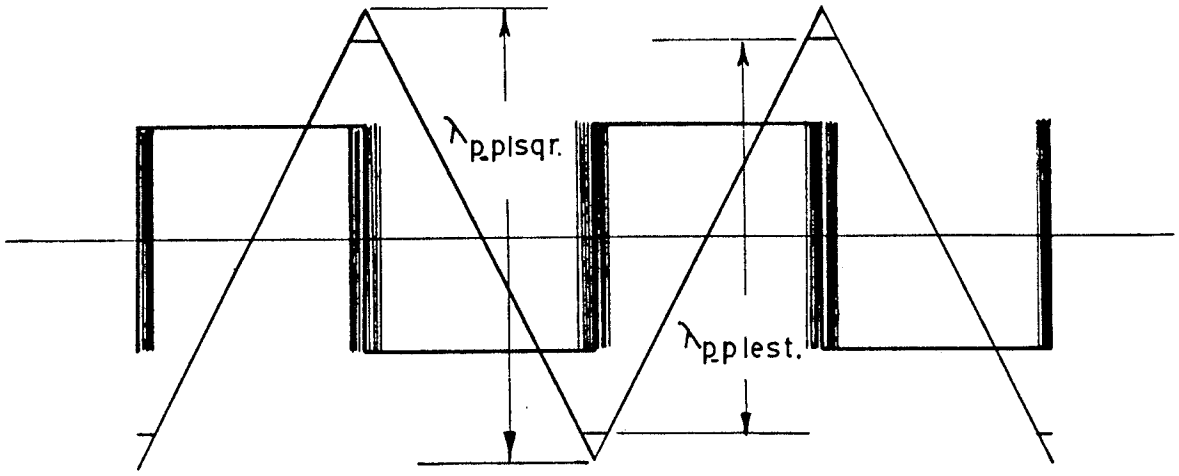

Figure 7.10: Commutations are Squeezed at the Sides of the Square-wave
$\lambda_{p-p|sqr}$ is the peak to peak flux linkage of a square wave.
$\lambda_{p-p|est}$ is the estimated peak-to-peak flux linkage.

be best during the ramping of the speed from 15-45 Hz. Besides, they are a compromise between the best suggested values in Table 7.2.

7.4 THE PATTERN OF THE LOAD TRANSIENTS

The pattern of the load transients is chosen such that it simulates the most liable load changes that may be encountered during the usage of the drive with pumps and fans. The transients are changed sequentially from no-load to 100% load then to 150% load and then to 50% load. These transients and the shape of the reference current amplitude as it follows them at unit frequency are shown in Figure 7.11 for a fan load.

Although load transients substantially mean changes from steady state point for a small period of time and then returning to the same steady state point, the adapted pattern returns to another steady state

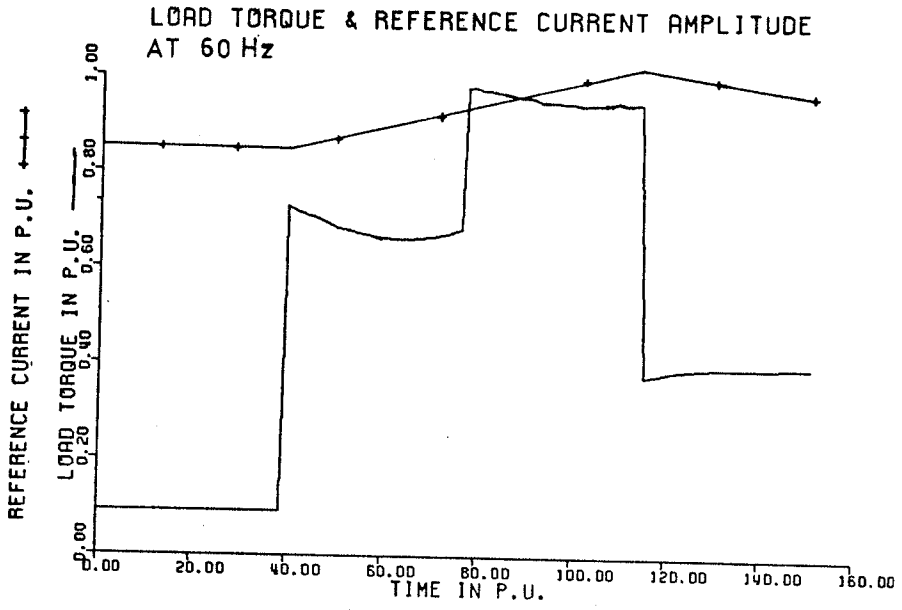

Figure 7.11: The Load Transients Pattern

point loading condition. This demonstrates the ability of the integral control to nullify the steady state error at the other loads as well.

7.5 PERIODICITY OF CHECKING THE FLUX

Two rates of periodically checking of the maximum flux per phase are used. The detection of the zero crossing points of the reference current is used for the location and determination of the begining of each half cycle. These rates are:-

1. Every half cycle using one phase only as shown in Figure 7.12.
2. every one sixth of a cycle using all three phases and checking each half cycle.

Figure 7.12 for the detection of the maximum flux-linkage at the motor input terminals shows that, six peak-to-peak values of λ can be obtained in 3 cycles.

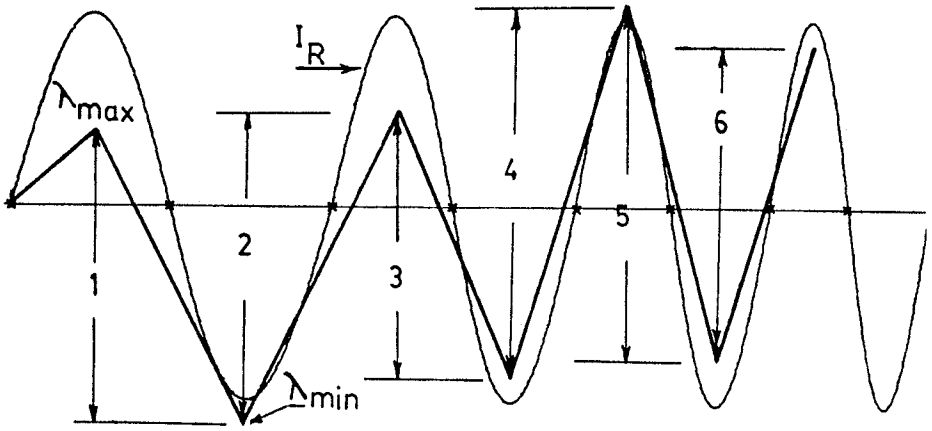

Figure 7.12: Half Cycle Checking

A maximum or minimum value for the flux linkage is detected every half cycle. The peak-to-peak values [Numbers 1 to 6] could be found accordingly. A new peak-to-peak value is acquired each half cycle. Therefore, the beginning and end of each half cycle should be found. A zero crossing detector is essential in the case of changing the frequency ,because, there is no other way to detect the period of a half cycle in this case. If the frequency is constant, the half cycle period is constant and could be detected otherwise easier. Figure 7.12 represents a few cycles of the reference current controller during ramping up of speed.

The periodicity of checking may be increased by detecting the flux linkages in the three phases instead of one phase only as it has been mentioned before. This is done by just repeating the same checking, in the other two phases as well. The effect of increasing the detection periodically is a decrease in the delay time constant T_s. A smaller, T_s, means faster response and better control.

7.6 RESULTS OF THE REGULATED FLUX STUDY

In Figures 7.13-7.17, the automatic action of the "PI" controller is to be demonstrated for frequency and load variations. The general idea that applies to both types of change is that: a simple "PI" controller can automatically adjust the amplitude of the reference current I_R to cope with any frequency or load transients, while maintaining the reference current near optimal values during steady state operation.

7.6.1 Load Variations

Figures 7.13-7.16, for the load variations show the reference current, the air gap flux linkage, the stator phase current,the stator phase voltage, the load torque transients, and the filtered developed torque at the four representative frequencies. The unfiltered developed torque as well as the speed and frequency are shown in Figures (E.1-4) in Appendix E.

At all the frequencies in the four Figures 7.13-7.16 the flux is checked six times each cycle during the load changes. The load transient pattern will be used at all the four representative frequencies. During the period in which the load is increased the number of commutations per cycle is increased in the phase voltage. This decreases the maximum flux linkage value and the "PI" controller orders I_R to increase. The actual current and developed torque follow I_R, up and down until the period of the sudden load increase is elapsed, successfully with a little dip in speed. When the load torque decreases again the number of commutations decreases and the maximum flux increases conseq-

uently. The "PI" controller then acts in the opposite direction and decreases I_R. The actual current and the developed torque are again following I_R successfully. The successful following of I_R to the increase and decrease of load indicates that the used value of the reference flux is good.

The same comments are equally applicable to the cases of 45 and 30 Hz in Figures 7.14 and 7.15. At 15 Hz no changes in the reference current value can be noticed and this is due to the fact that, the load torque level at this frequency is very small and the minimum value of the reference current was enough to handle all the load torque transients even without the slightest change in the reference current.

A filtered torque is also added to show the following of the developed torque to the load torque. The developed torque when not filtered contains high torque pulsations (mainly sixth harmonics) that made it hard to observe how the developed torque is following the load torque. The transfer function of the used low pass filter is:

$$\frac{D}{Y} = \frac{1}{Ts + 1} \quad , \quad T = \frac{1.0}{f} \tag{7.14}$$

The associated difference equation is:

$$D_n = D_{n-1} + (Y - D_{n-1}) \frac{H}{T + H} \tag{7.14a}$$

where,

$D = T_F$ is the filtered torque

$Y = T_e$ is the electromagnetic torque

T is the time constant of the filter

The time constant of the filter was chosen to be equal to the period of one cycle at the respective frequency (T=1.0/f).

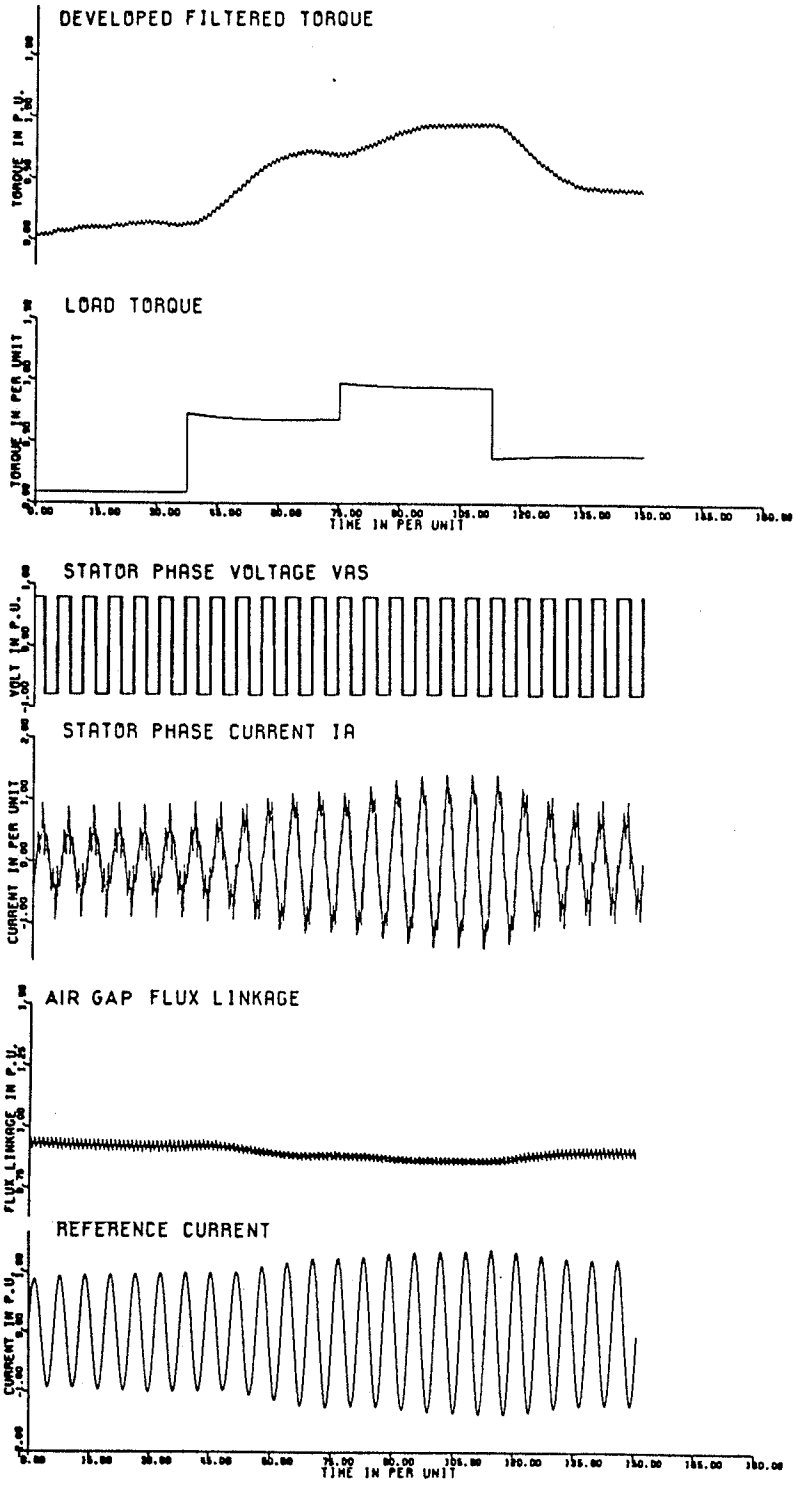

Figure 7.13: Load Transients, f=1.0, K_p=10.0, K_I=0.1 and λ_R=1.10000

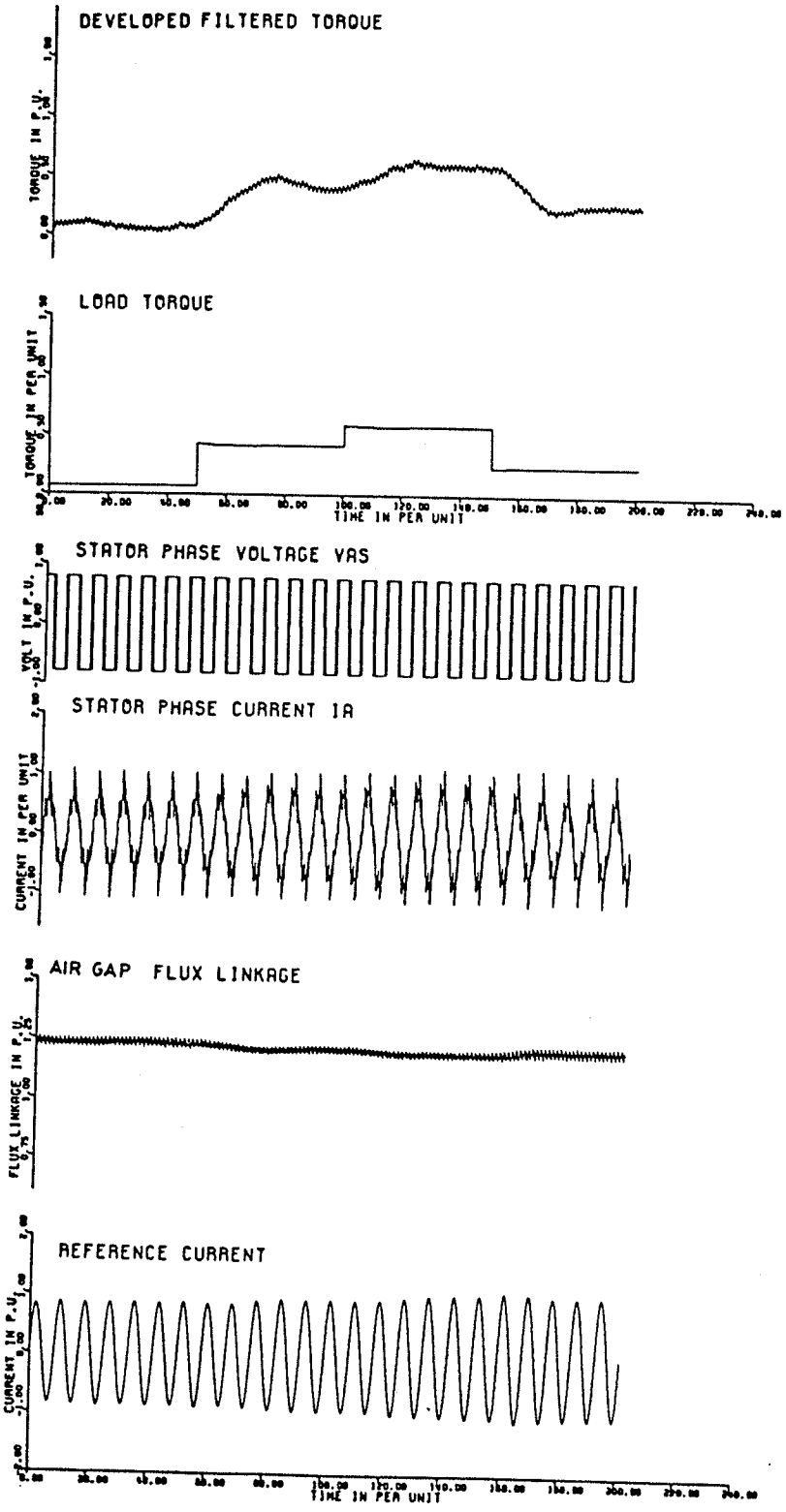

Figure 7.14: Load Transients, f=0.75, K_p=10.0, K_I=1.0 and λ_R=1.40747

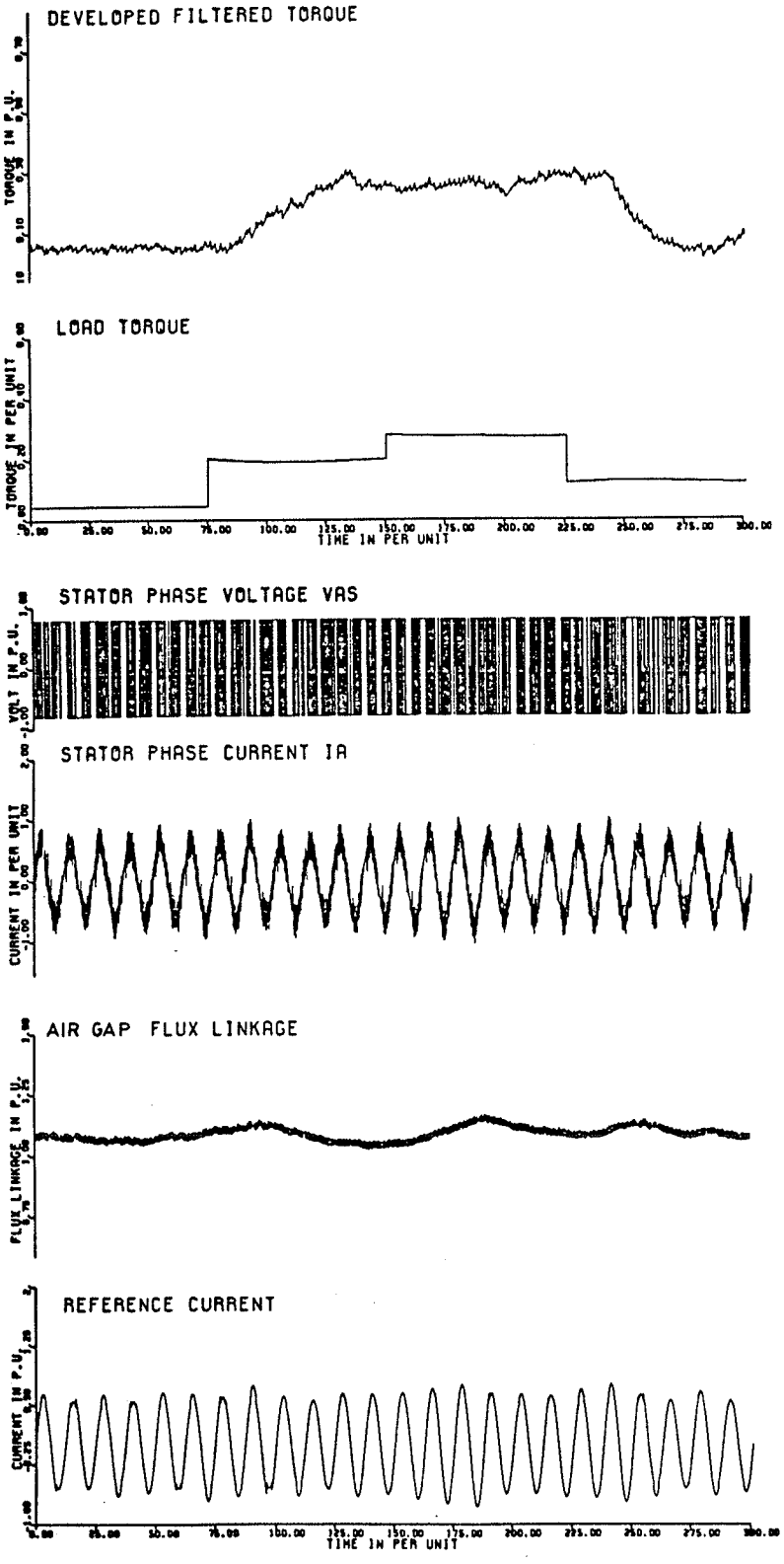

Figure 7.15: Load Transients, f=0.5, K_p=1.0, K_I=0.1 and λ_R=1.27755

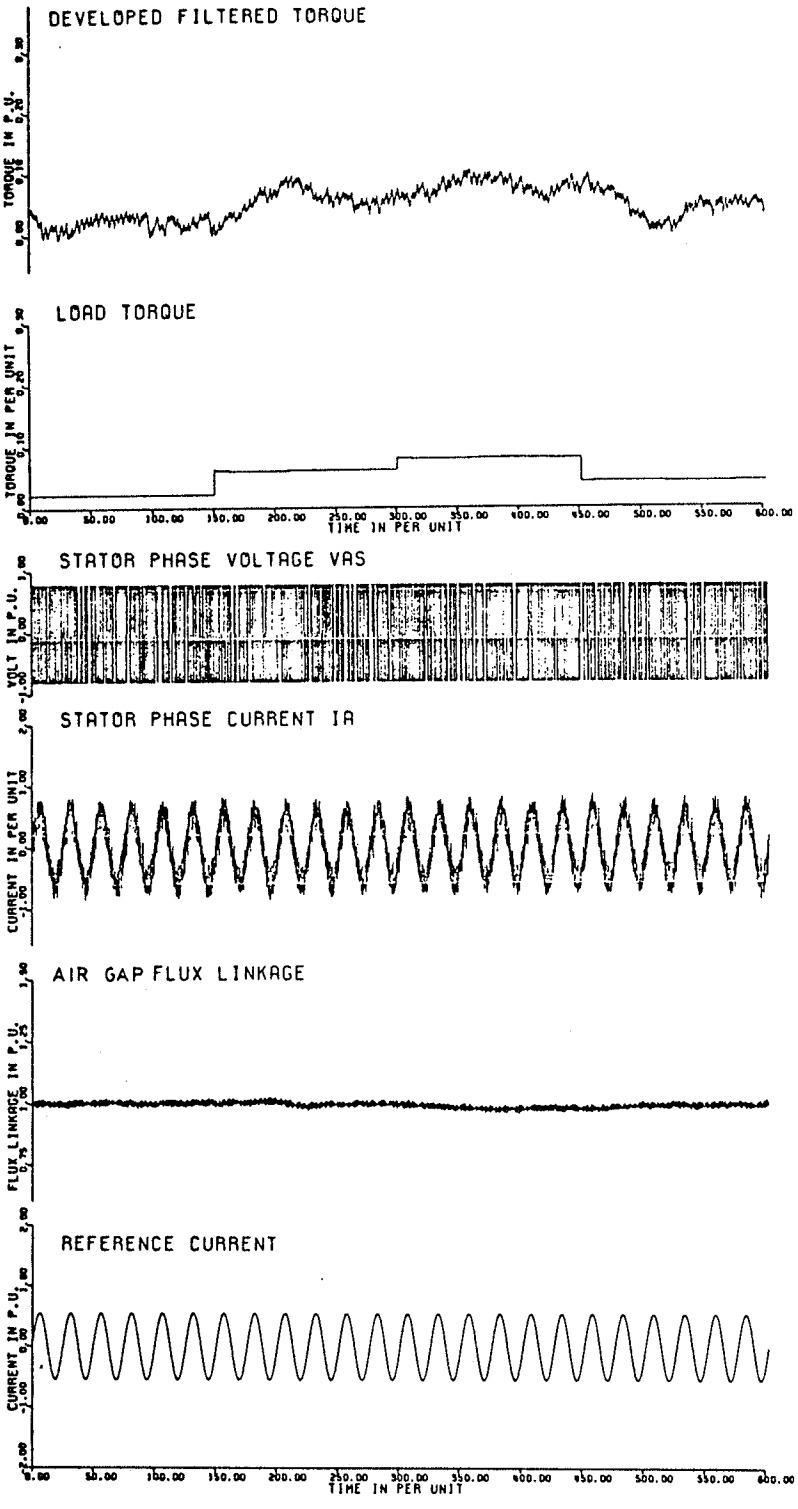

Figure 7.16: Load Transients, f=0.25, K_p=0.5, K_I=0.05 and λ_R=1.35000

7.6.2 The Change of Speed

In Figure 7.17 up to about 100 p.u. time the flux estimated and fed back to the "PI" controller was gradually decreasing during the ramping and there was no response until the flux in the air gap has decreased to about 0.9 p.u. This is due to the integrator action which should have been accumulated with a negative value in the constant term K_{IO}, (equations 7.6-7.9).

Therefore the proportional action has been delayed a few cycles before the reference current starts to increase. Because of this observation a low value of K_I and a long ramping time have been used. The ramping time now is 720 p.u. which is equivalent to 1.9098 seconds. This long time is necessary to achieve acceptable flux level during the ramping in the air gap. The used flux reference value during the ramping is 1.40747 and is constant.

Just before 200 p.u. time a noticeable relaxation in the speed occurs, (a decrease in the amplitude of the actual stator phase current should be noticed as well), with the result that the load torque should decrease. Due to the fact that, the reference current strategy is load dependent, a small blowup in the developed torque was encountered during the following cycle, (similar blowups should also be noticed in the reference current and the actual current at the same time) when the motor tries to speed up to follow the ramping after the speed has been decreased temporarily. This blowup in the developed torque is just an extra accelerating torque . The author has found that using small values of K_p and K_I and long ramping time helps in reducing these blowups con-

siderably. I should point out also here that these blowups (which represent the accelerating torque) at the low frequencies are lower and continue over shorter periods of time than those at the high frequencies because the load torque level increases with the frequency during ramping up a fan load.

The same phenomena repeats itself after that several times until the final speed is reached. Each relaxation in speed is followed by a small blowup in the developed torque (again this is the required accelerating torque). Finally at about 750 p.u. time the final speed is reached and therefore the torque required for acceleration becomes suddenly zero with the result that the developed torque drops almost instantaneously by the amount of the accelerating torque. This sudden drop in the developed torque should be accompanied with an oscillatory response which was slightly underdamped (small machine). Therefore at the final speed, the developed torque oscillates a little bit around the final value of the load torque and finally approaches a new steady state operating point at the new frequency.

In order to achieve a better understanding of the ramping problem let us discuss the idea of the ramping using the sinusoidal constant current torque and voltage slip characteristics. In Figure 7.18, there is two torque slip characteristics one at a certain frequency f_1 and the other at a little bit larger frequency "$f_2=f_1+\Delta f$", the corresponding voltage Characteristics (V_1/f_1) and (V_2/f_2) as well as the load torque T_L are also shown. Assume that the motor is operating at point A then the frequency is ramped from f_1 to f_2. In response the accelerating

torque ΔT_{acc} acts to speed up the motor in the direction of the arrow from point A to point B. Simultaneously the flux level drops from Q_1 to Q_2. Consequently the controller may act and increase the current to IR′ which will increase the torque further. However the flux at this new value could be as large as Q_4 or as low as Q_3 depending on the speed of the motor, whether the speed has reached the new operating point at B or still accelerating between A and B. Due to the new increase in the flux level, from Q_2 to Q_3 or Q_4 or to an intermediate value between Q_3 and Q_4, (the new flux value depends on the rate of ramping and the delay time constants of the system), the controller which is driven by a constant flux reference level, will tend to decrease the reference current again. Nevertheless, during ramping this increase in the frequency will be followed by another increase and the process repeats itself, with the result that no equilibrium state can be achieved as long as the ramping process continues. This phenomena can be noticed from the reference current and the air gap flux traces in Figure 7.17. The decrease in the air gap flux level is followed by an increase in the reference current amplitude and vice versa. Therefore, the air gap flux continues to fluctuate up and down during the ramping and so does the amplitude of the reference current, which is shown to be beating until the ramping ends at about 750 p.u. time.

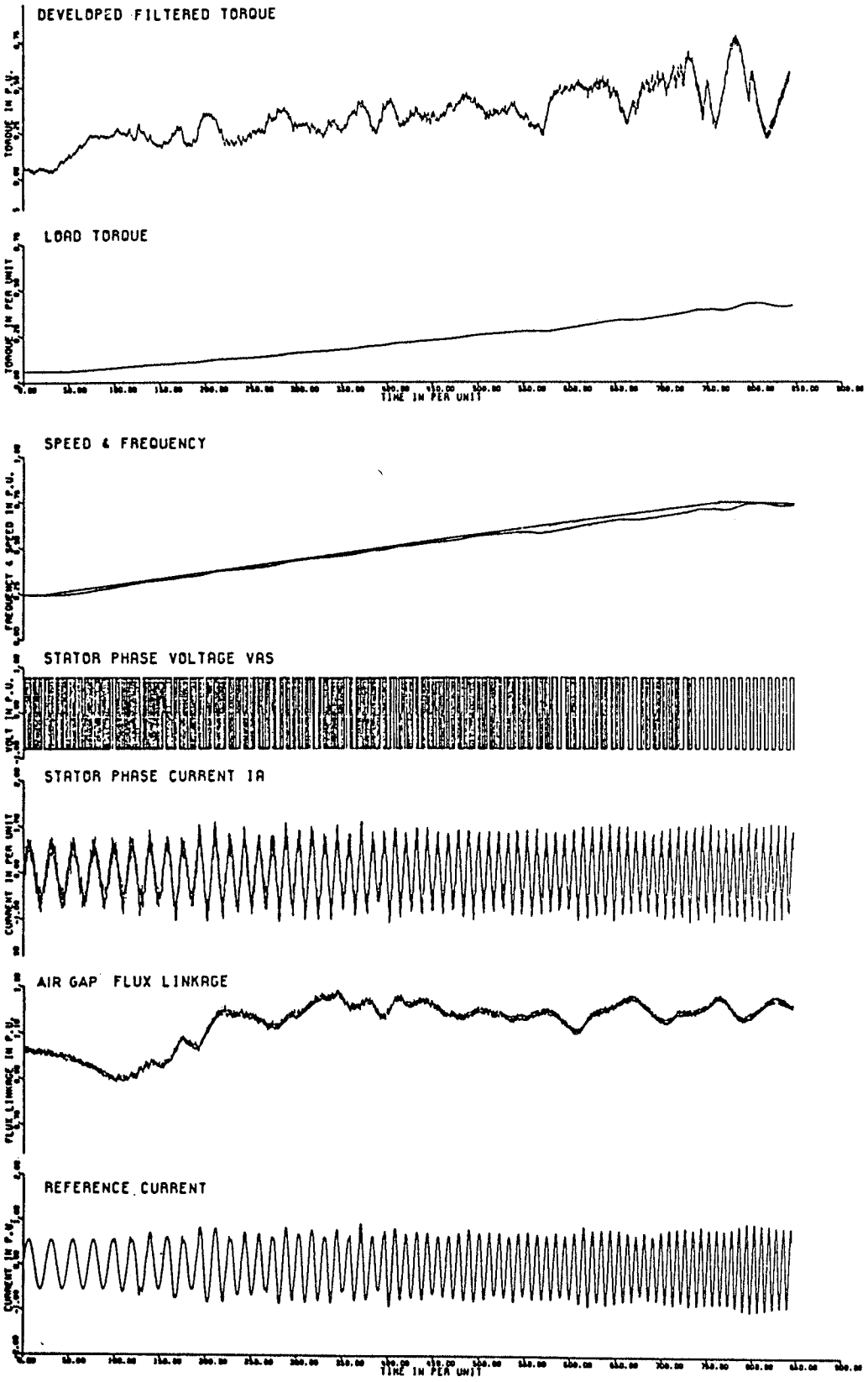

Figure 7.17: Ramping up of Frequency with a Check Every One Sixth of a Cycle, K_P=5.0, K_I=0.2 and λ_R = 1.40747

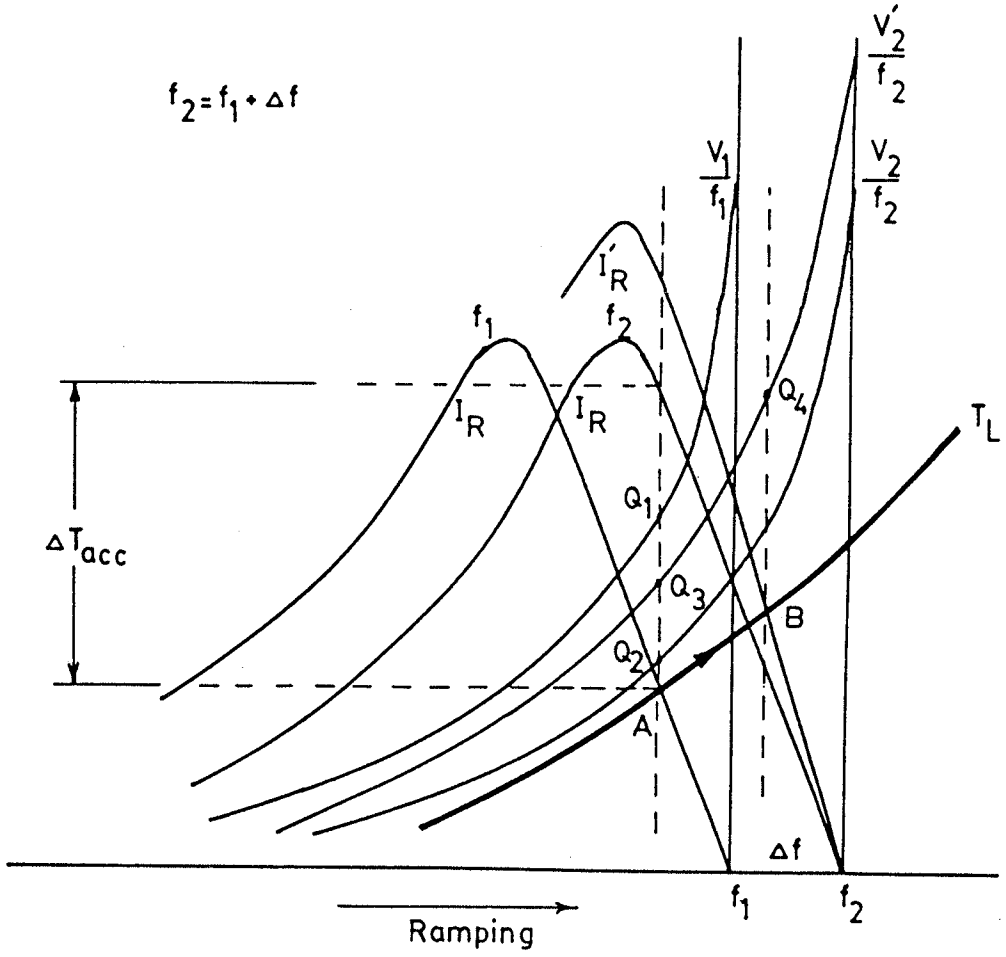

Figure 7.18: Ramping of the Speed

7.7 STABILITY CORRELATION

In a previously controlled current scheme Cornell and Lipo[27] have found that in the current controlled induction motor drive both dynamic and static instabilities exist for open loop operation, but that a well damped closed loop response is possible if slip frequency and current magnitude control are imposed. However, the regulation of the stator current and motor slip frequency requires shaft speed feedback and fast-response current regulation. Therefore, later an alternative of controlling an induction motor was presented by Plunkett, D'Atre and Lipo[79] in which the necessary stabilization of the system was achieved by controlling the motor frequency. The motor frequency command was generated by regulating the motor torque angle. More recently Plunkett and Peak[31,32] presented a novel current controller PWM transistor inverter in which they used the torque angle controller to supply the primary system stability. Plunkett[31] used, in a preliminary scheme the magnitude of the motor current and the angle between the air gap flux and the stator current vectors, as the command inputs. However, although these inputs are satisfactory for a complete control of the drive, they did not allow for an easily generated command signal. For example to increase torque both the angle command and the current command must be increased. However, the relative amount of increase of these signals is a nonlinear function of the desired motor flux level. Afterwards, in another scheme, Plunkett[31] generated a frequency command from the torque angle command. This implies indirectly that, the relation between the frequency command and the flux level command should be nonlinear for the current controller. If this nonlinear relation is found and stored in

the memory of the controlling microprocessor in the proposed scheme (Figure 7.4), then the flux reference will vary according to the stored nonlinear relation as the frequency is changed. Using this nonlinear relation should enable us to dispense with the motor angle loop which provides the necessary stabilization in Plunkett's scheme[79]. Consequently, an "open loop flux linkage controller" (the regulated flux scheme), is therefore expected to work stably. The name open loop comes from the fact that, in the proposed scheme, the loop of the torque angle command is opened.

The author, unfortunatly, did not get a chance to examine the transient stability of the proposed scheme in the frequency domain. However, the transient stability of Plunkett's scheme[31,32] was checked by himself, D'Atre and Lipo[79]. Hence, the author expects that the proposed open loop flux controller with the programmed nonlinearity should be stable as well. Besides, the time domain load changing responses of the proposed scheme indicate a stable and rigid operation, at the four representative frequencies.

Chapter VIII

CONCLUSIONS AND FUTURE RECOMMENDATIONS

8.1 CONCLUSIONS

The aim of this thesis has been the comparison of different PWM strategies, so as to find the most suitable one for controlling the speed of induction motors driving pumps and fans. Three PWM techniques have been compared on the basis of the stator harmonic current content and the electromagnetic torque pulsations. A complete model of the induction motor was suggested and the motor efficiency was compared with different nonsinusoidal supplies. The reference current controller strategy has been found to be good for pump and fan applications. Better values of the reference current has been found to improve the motor performance. Besides, an open loop flux linkage controller has been developed to overcome the low starting torque and the critical stability problems of the drive. The salient conclusions are to be stated according to the different phases of work accomplished throughout the Thesis. These are:

1. The conclusions from the simulation of saturation and eddy currents are:
   a) The simulation of a double cage induction motor, for taking into account the deep bar effects, together with the consideration of the saturation of the mutual and leakage inductances, provided an almost complete representation of the induction motor, which can be used for different performance studies.

b) A practical method for finding the double cage parameters was outlined and the obtained results were used in the simulation model.

c) The simulation results have been verified by laboratory tests of motor starting under no-load conditions, and during loading operation. Excellent agreement was achieved.

2. The conclusions from the induction motor performance subject to PWM waveforms are:

a) The problems of the frequency domain analysis method have been outlined and the need for another approach for the evaluation of the induction motor performance under PWM supplies has been made clear.

b) The time domain analysis was introduced for the evaluation of the induction motor performance indices, such as the harmonic content in the stator phase current and the pulsating torques.

c) The efficiency of the overall inverter-induction motor system has been evaluated and a detailed method for the evaluation of the system losses has been outlined.

3. The conclusions from the study of the reference current controller strategy are:

a) The controller is easily implemented without feedback from the motor.

b) This controller overcomes the two implementation disadvantages usually encountered with other PWM techniques. First; the need for a very precise generation of the input voltage waveform, otherwise these methods would be susceptible to imba-

lance and dc offset problems. Second; the need for extensive lookup-tables and/or transitions between modes or different strategies, (at the high frequency range synchronized transitions are needed which are more difficult to implement).

c) In the reference current controller strategy, the number of commutations per cycle changes automatically with frequency.

d) The disadvantages of the drive as a constant current source are the low starting torque, and the proximity of the maximum torque to the load torque.

e) A method for calculating the reference current at different loading conditions was given.

4. The conclusions in comparing the three PWM strategies and the applicability of the drive are:

a) The time domain analysis can be used effectively in comparing PWM techniques.

b) The reference current controller produces a PWM waveform for induction motor drives which gives performance indices equivalent to other well-known PWM techniques.

c) The reference current controller alleviates the extensive transitions between different modes of operation throughout the whole frequency range.

d) Suggestions for the alleviation of the disadvantages of this drive mentioned before were shown to be satisfactory.

5. The conclusions of seeking a better performance from the recommended strategy are:

a) The accuracy of the time domain snapshot and the sample cycle technique was verified.

b) Better values for the reference current are obtained in respect to improving the efficiency. However, higher values are recommended to insure a stable operation.

c) The result that the efficiency is improved by reducing the air gap flux is also confirmed in the case of the current controller.

6. The conclusions from the study of the flux linkage controller are:

a) A simple flux linkage controller that maintains constant flux in the air gap by adjusting the value of the reference current is found to be good automatic solution for the two aforementioned disadvantages of the drive.

b) The flux reference value settings for the controller were found from an unregulated flux study.

c) The change in the behaviour of the current controlled inverter from a voltage source at frequencies above a frequency between 30 and 45 Hz to a current source at frequencies below this frequency has been emphasized and explained.

d) This dual behaviour and the difficult handling of the problem bang-bang current controller were in agreement with the findings of Plunkett[31], as well as with the remarks of Stemmler.[80]

8.2 FUTURE RECOMMENDATIONS

This thesis is a preparatory work for a practical scheme that, the author expects will be promising. Therefore, the second step to be accomplished is to verify the computational results of the simulation by a test setup. A second extension can be a transient stability study on the system and the system response to small disturbances in load torque with or without the flux linkage controller. Third, a comparative study of the overall efficiency of the PWM strategies can be made, in the time domain, using the complete simulation model and the proposed scheme for efficiency evaluation to confirm the superiority of the reference current controller technique over the other techniques. Some of this work has been contributed in a paper.[81]

REFERENCES

1. Austin,H. and Bonnett 'Understanding efficiency in squirrel-cage unduction motors' IEEE Trans. on IA Vol. 16, No. 4, July/Aug. 1980, pp.467-483.

2. Green,R.M. and Boys,J.T. 'Inverter AC-drive efficiency' IEE Proc., Vol. 129, Pt. B, No. 2, March 1982, pp. 75-81.

3. Morton,W.R. 'Economic of AC adjustable speed drives on pumps' IEEE Trans. on IA vol.11, No.3, May/June 1975, pp.282-286.

4. LeMone, C.P. 'Why utilize adjustable speed drives' Paper #81 presented to the CEA Engineering and operations annual meeting,Vancouver, March 23,1983.

5. Eissa, F.A.M 'Efficient inverter drive for pumps and fans' M.Sc. Thesis in Elect. Enging., The Univ. of Manitoba, October 1981.

6. Mokrytzki,B. 'Pulse width modulated inverters for AC motor drives' IEEE Trans. IGA-3, pp. 493-503, May/June 1967.

7. Bowes, S.R. and Clements, R.R. 'Computer-aided design of PWM inverter systems' IEE Proc., Vol.129, pt.B, No.1, Jan. 1982, pp.1-17.

8. Schonung,A. and Stemmler,H. "Static frequency changers with 'subharmonic' control in conjunction with reversible variable-speed AC drives", Brown Boveri Review, Vol.51,pp.555-576,aug./sep. 1964.

9. Zubec, J., Abbondanti, A. and Nordby, C.J. 'Pulsewidth Modulated Inverter Motor Drives with improved Modulation' IEEE Trans. on Indus. Appl., Vol. IA-11, No. 6, Nov./Dec. 1975, pp.695-703.

10. Bowes S.R. 'New Sinusoidal Pulsewidth Modulated Inverters' Proc. IEE, Vol. 122, No. 11, November 1975, pp. 1279-1285.

11. Nayak, P.H. and Hoft, R.G. 'Optimizing the PWM Waveform of a Thyristor Inverter' IEEE Trans. on Indus. Appl. Sep./Oct. 1975, pp.526-530.

12. Pollack, J.J. 'Advanced PWM inverters techniques' IEEE Trans., IAS, No.2, March/April 1972, pp.145-154.

13. Barton, T.H. 'Pulsewidth Modulation Waveforms : the Bessel Approximation' Conf. Rec. of the Industry Appli. Society, IEEE-IAS-1978, pp.1125-1130.

14. Kliman, G.B. and Plunkett, A.B. Development of a Modulation Strategy for PWM Inverter Drive' IEEE Trans. on Indus. Appl., Vol. IA-15,No. 1, Jan./Feb. 1979, pp. 72-79.

15. Grant, T.L. and Barton T.H. 'Control Strategies for PWM Drives' IEEE Trans. on Indus. Appli., Vol. IA-16, No. 2, March/April 1980, pp. 211-216.

16. Grant, D.A. 'Technique for Pulse Dropping in PWM Inverters' IEE Proc., Vol. 128, Pt. B, No. 1, Jan. 1981, pp. 67

17. Green, R.M. and Boys, J.T. 'PWM Sequence Selection and Optimization: A Novel Approach' IEEE Trans. on Indus. Appli., Vol. IA-18, No. 2, 1982, pp. 146-151.

18. Ohnishi, T. and Okitsu, H. 'A novel PWM technique for three phase Inverter/Converter' Conf. Recor. of IPEC March 1983, pp. 384-395.

19. Azusawa, N. and Shiraishi, H.K. 'Pulse Generator for PWM' Japanese Patent DE 3403802 Al August, 1984.

20. Turnbull, F.G. 'Selected Harmonic Reduction in Static DC-AC Inverters' IEEE Trans. Comm. Electronics, Vol. 83, No. 73, pp. 374.

21. Patel,H.S. and Hoft,R.G. 'Generalized technique of harmonic elimination and voltage control in thyristor inverters' part I, IEEE Trans. Ind. Appl., Vol.IA-9, pp.310-317.

22. Patel,H.S. and Hoft,R.G. 'Generalized technique of harmonic elimination and voltage control in thyristor inverters: part II voltage control techniques' IEEE Trans., 1973, Vol. IA-10, No.5, pp. 666-673.

23. Buja, G.S. and Indri, G.B., 'Optimal pulse width modulation for feeding AC motors', IEEE Trans. Ind. Appl., Vol. IA-13,no.1,pp.38-44,Jan./Feb. 1977.

24. Bellini,A. and Figalli,G. 'On the selection of the commutating instants in induction motor drives' IEEE Trans. IA-15, No.5, pp.501-506, Sept./Oct. 1979.

25. Buja, G.S. 'Optimum Output Waveforms in PWM Inverters' IEEE Trans. an Indus. Appl., Vol. IA-16, No.6, 1980, pp. 830-836.

26. Lipo, T.A. and Cornell E. 'State variable steady state analysis of a controlled current induction motor drive' IEEE Trans. IA-Vol.11, pp.704-712, Nov./Dec. 1975.

27. Cornell,E. and Lipo,T.A. 'Modelling and design of controlled current induction motor drive system' IEEE Trans. Vol. IA-13, pp.321-330, July/Aug. 1977.

28. Forsythe, J.B. and Dewan, S.B. 'Output Current Regulation with PWM Inverter Induction Motor Drive' IEEE Trans. on Indus. Appl., Vol. 11, No. 5, 1975, pp.517-525.

29. Walker, L.H. and Espelage, P.M. 'A High Performance Controlled-Current Inverter Drive' IEEE Trans. on Indus. Appl. Vol. IA-16, No. 2, 1980, pp. 193-202.

30. Palaniappan R.G. and Vithayathil J. 'A Control Strategy for Reference Wave Adaptive Current Generation' IEEE Trans. on Industrial Electronics and Control Ins., Vol. IECI-27, No 2, 1980, pp. 92-96.

31. Plunkett,A.B. 'A current-controller PWM transistor inverter drive' IEEE Conf. Record of Industry Applications Society pp.785-792, 1979.

32. Peak, S.C. and Plunkett, A.B. 'Transistorized PWM Inverter-Induction Motor Drive System' IEEE Trans. IA-Vol.19, No.3, May/June 1983, pp.379-387.

33. Bose, B.K. 'Adjustable Speed AC Drives - A Technology Status Review' Proc. IEEE, Vol. 70, No. 2, Feb. 1982, pp. 116-135.

34. Menzies,R.W. and Mahmoud,A.M.A., 'Comparison of optimal PWM technique with a Bang-Bang reference current controller for voltage source inverter fed induction motor drives' IEEE IAS Annual Meeting Conference Record, Mexico City, October 1983, pp 685-692.

35. Menzies,R.W. , Mahmoud,A.M.A. and Au-Yeung,H. 'Design and operation of a reference current controller for producing PWM waveforms' IEEC&E of IEEE september, 1983. Toronto, Canada, pp. 88-91.

36. Brod, D.M. and Novotny, D.W. 'Current Control of VSI-PWM Inverters' University of Wisconsin, Madison, WEMPEC Research Report 84-6, June 1984.

37. Ziogas, P.D. 'The Delta Modulation Technique in Static PWM Inverters' IEEE Trans. on Indus. Appl., Vol. IA-17, No. 2, 1981, pp. 199-204.

38. Adams, R.D. and Fox, R.S. 'Several Modulation Techniques for PWM Inverters' IEEE Trans. on Indus. Appl., Vol. IA-8, No. 5, 1972, pp. 636-643.

39. Sen, P.C. and Premchandran, G. 'Improved PWM Control Strategy for Inverters and Induction Motor Drives' Conf. Rec. of IEEE Indus. Appl. Annual Meeting, 1982, pp. 823-830.

40. Murai, Y. and Tsunehiro, Y. 'Improved PWM Method for Induction Motor Drive Inverters' Conf. Rec. of IPEC, 1983, pp. 407-416.

41. Bose, B.K. 'Adjustable Speed AC Drive Systems' New York, IEEE Press, 1981.

42. Lipo, T.A., Novotny, D.W., Plunkett, A.B. and Stefanovic, V.R. 'Dynamics and Control of AC Drives' Course Notes, Univ. of Wisconsin Extension, 1984.

43. Murphy J.M.D. 'Thyristor Control of A.C. Motors' Pergamon, 1973.

44. Mokrytzki, B. 'The Controlled Slip Static Inverter Drive' IEEE Trans. Indus. Gen. Appl., Vol. IGA-4, No.3, 1968, pp. 312-317.

45. Miles, R.A. and Novotny D.W. 'Transfer Functions for Slip Controlled Induction Motor' IEEE Trans. on Indus. Appl., Vol. IA-15, No.1, Jan./Feb. 1979, pp.54-62.

46. Blaschke Felix 'The Principle of Field Orientation as Applied to the New TRANSVEKTOR Closed-Loop Control Systems for Rotating-Field Machines' Siemens Review, Vol. 34, pp. 217-220, May 1972.

47. Gabreil R., Leonhard W. and Nordby, C. 'Field Oriented Control of a Standard AC Motor Using Microprocessors' IEEE IAS Annual Meeting Conf. Rec., 1979, pp. 910-916.

48. Klingshirn,E.A. and Jordan,H.E. 'Polyphase induction motor performance and losses on nonsinusoidal voltage sources' IEEE Trans. on PAS, Vol.87, No.3, March 1968, pp.624-631.

49. Jacovides,L.J. 'Analysis of induction motor drives with a nonsinusoidal supply voltage using Fourier analysis' IEEE Trans. on IA, Vol.9, No.6, November/December 1973, pp. 741-747.

50. Chalmers,B.J. and Sarkar,B.r. 'Induction motor losses due to non-sinusoidal supply waveforms' IEE Proc. Vol.115, No.12, December 1968, pp. 1777-1782.

51. Hancock, N.N., 'The parameters used in matrix and tensor analysis of Electrical Machines', Int.J.Elect.Enging. Educ., Vol.5, pp.584-594, 1976.

52. Lipo,T. A. & Consoli, A., 'Modelling and simulation of induction motors with saturable leakage reactances', Conf. Rec. IEEE,IAS 1981 pp.527-535

53. Chalmers, B.J. and Dodgson, R., 'Saturated leakage reactances of cage induction motors', Proc. IEE, Vol. 116, No.8, August 1969, pp. 1395-1404.

54. Agarwal, P.D. and Alger,P.L., 'Saturation factors for leakage reactances of induction motors', Trans. of IEEE Feb. 1961, pp. 1037-1042.

55. Alger,P. L., "Induction machines their behaviour and uses", GORDON and BREACH , New York 1970 pp.265-286

56. Adkin's, B. and Harley, R. G., The general theory of alternating current machine', Book, Chapman and Hall London pp. 240-243

57. de Mello,F. P. & Walsh,G. W., 'Reclosing transients in induction motors with terminal capacitors', pp.1206-1213 AIEE Trans. Feb. 1961 PAS,Vol.80.

58. James,M.L. and Smith,G.L. 'Applied numerical methods for digital computation' Book 1967, Harper & Row Publishers.

59. TEK Products Catalog 1982, A6303/A6302.

60. Tektronix Instruction Manual 'AM 503 Current Probe Amplifier' January 1981, pp. 2-1

61. Nelson, R.H., Lipo, T.A. and Krause, P.C. 'Stability Analysis of Symmetrical Induction Machine' IEEE Trans. on PA&S, Vol.88, No.11, November 1969, pp.1710-1717.

62. Murphy,J.M.D. and Egan,M.G., 'An analysis of induction motor performance with optimum PWM waveforms' Proc. of ICEM Athens, pp.642-656, 1980.

63. Murphy,J.M.D. and Egan,M.G., 'A comparison of PWM strategies for Inverter-fed induction motors' IEEE Trans. on IAS, Vol.19, No.3, May/June 1983, pp. 363-369.

64. De Buck,F.G., 'Losses and parasitic torques in electric motors subjected to PWM waveforms' IEEE Trans. on IAS, VOl.15, No.1, Jan./Feb. 1979, pp. 47-53.

65. Abrams A.B 'Discussion to paper by Klingshirn[10]' pp. 631

66. Kusko,A. and Galler,D. 'Control Means for minimization of losses in AC and DC motor drives' IEEE Trans., Vol.IA-19, No.4, July/Aug.1983, pp.561-570.

67. Slemon,G.R. and Straughen,A., 'Electric Machines' Adison-Wesley, 1980.

68. Alger,P.L , Angst,G. and Davis,E.J 'Stray-load losses in polyphase induction machines' AIEE Transactions, Vol.78, Part.III, June 1969, pp. 349-357.

69. General Electric 'SCR manual' Fifth Edition 1972.

70. Bhagwat,P.W. and Stefanovic,V.R., 'A versatile commutation circuit for PWM inverters' IEEE Trans. Ind. Appl., Vol. IA-18, No.2, pp. 127-137.

71. Mahmoud,A.M.A and Menzies,R.W. 'Feasibility of Optimization of the Current Controlled Induction Motor Parameters in the Time Domain' The Second Canadian Universities Conference on CAD/CAM, Montreal, 1984.

72. Mohan, N. 'Improvement in efficiency of induction motors by means of voltage control' IEEE Trans., PA&S, Vol.99, No.4, July/Aug. 1980.

73. Kirschen, D., Novotny, D.W. and Suwanwisoot, W. 'Minimizing Induction Motor losses by Excitation Control in Variable Frequency Drives' IEEE, IAS, Annual Meeting 1983, Conf. Rec. pp. 526-533.

74. Tsivitse,P.J. and Klingshirn,E.A 'Optimum voltage and frequency for polyphase induction motors operating with variable frequency power supplies' IEEE Trans., on IGA-7, No.4, July-Aug.1971, pp.480-487.

75. Rowan, T.M and Lipo, T.A. 'A Quantitative Analysis of Induction Motor Performance Improvement by SCR Voltage Control' In Conf. Rec. 1982 IEEE PESC, pp. 312-321.

76. Plunkett A.B 'Direct torque and flux regulation in a PWM inverter-induction motor drive' IEEE Trans. Ind. Appl., vol. IA-13, no.2, pp.139-146, Mar./apr. 1977.

77. Lipo, T.A. 'Flux Sensing and Control of Static AC Drives by the Use of Flux Coils' IEEE Trans. on Magnetics Vol. MAG-13, No.5, Sep. 1977, pp. 1403-1408.

78. Abbondanti, A. 'Method of Flux Control in Induction Motors Driven by Variable Frequency Variable Voltage Supplies' IEEE/IAS International Semiconductor Power Converter Conference, 1977, pp. 177-184.

79. Plunkett,A.B. , D'Atre,J.D. and Lipo,T.A. 'Synchronous Control of Static AC Induction Motor Drive' IEEE Trans. on Indus. Appl., Vol. IA-15, No.4, July/Aug. 1979, pp. 430-437.

80. Stemmler, H. 'Remarks on the Problem Bang-Bang Current Controller' A personal letter received by the author from Dr. H.Stemmler on Oct 22, 1982, Dept. IEE CH-5300 Turgui Switzerland.

81. Mahmoud, A.M.A. and Menzies, R.W. 'A Complete Time Domain Model of the Induction Motor for Efficiency Evaluation' accepted for presentation in the 1985 Summer Meeting, July 14-19, 1985, Vancouver B.C. CANADA.

82. Harris, M.R., Lawrenson, P.J. and Stephenson, J.M 'Per-unit Systems with Special Reference to Electrical Machines' Cambridge University Press, 1970.

Appendix A

DOUBLE CAGE PARAMETERS

This appendix will clarify the theoretical basis of obtaining the induction motor double cage parameters from no-load and locked rotor tests.

A.1 PROCEDURE

A.1.1 Locked Rotor Test

A locked rotor test is performed in which I_{sc}, V_{sc}, P_{sc}, are recorded by the appropriate ammeter, voltmeter and wattmeter, respectively. Also, the locked rotor torque may be recorded using a torque transducer. The torque measurement is not necessary for determining the parameters. It can be used as an extra check on the obtained parameters. Recording these electrical quantities for a range of short circuit current from 0.25 p.u. to about 2.0 p.u. produces a curve between the input short circuit line current and the equivalent reactance of the motor. The stator leakage reactance may also be produced as a function of the input current by considering it roughly as half of the equivalent reactance, in this limited range of input current. This limited range is quite enough to allow for the leakage saturation in the no-load saturation calculations, to be explained next.

A.1.2 No-load Test

A no-load saturation test is performed, in which V_o, I_o, P_o are recorded. The magnetizing reactance X_m and the no-load core resistance R_{e+h} are calculated using the relation between the stator leakage reactance and the input current (now I_o), obtained from the previous test. Doing so will allow for the leakage saturation, as a function of the current going through the magnetizing reactance only, i.e; I_m, to be taken into account since only this current is simulated afterwards in the dynamic simulation program.

A.2 THE EQUIVALENT REACTANCE SHARING

The objective now is to find out how the equivalent reactance is divided between the stator and rotor leakages. Notice, that although it was formerly divided evenly between them, the saturation of the leakage inductance was considered. The separation of the equivalent reactance into stator leakage and rotor leakage may be done using the no-load saturation curve by the following procedure:-

1. Transfer the reference from input voltage to the magnetizing reactance branch as shown in Figures A.1 and A.2 . This is to be done on a set of data taken under full load conditions, V_1, I_1, P_1 and s_{f1} are necessary.
2. By assuming a reasonable value for V_m calculate the rotor reactance from both sides of the magnetizing branch as shown in Figures A.1 and A.2, the correct value of V_m is obtained when;

   $$X_{21} = X_{22} \qquad (A.1)$$

   where,

   X_{21}: is the rotor reactance calculated as $X_{21} = X_{eq} - X_1$

X_{22}: is the rotor reactance calculated from rotor circuit.

X_{22}=Imaginary(V_m/I_2)

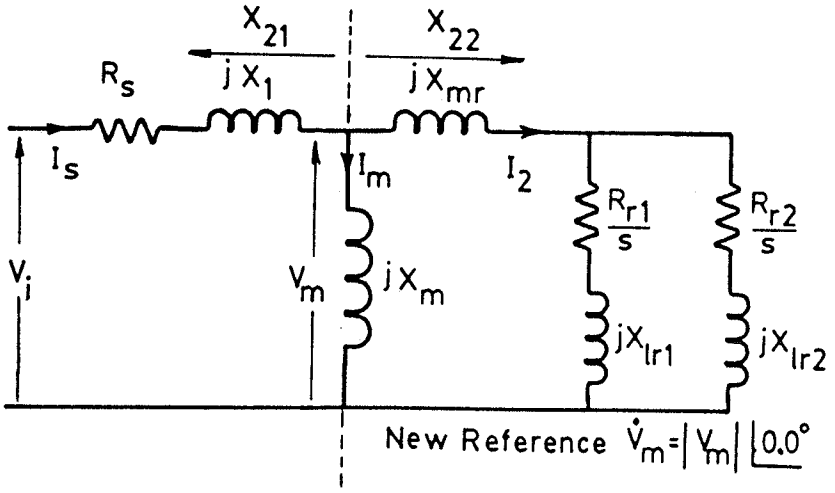

Figure A.1: The Equivalent Circuit of the Double Cage Induction Motor.

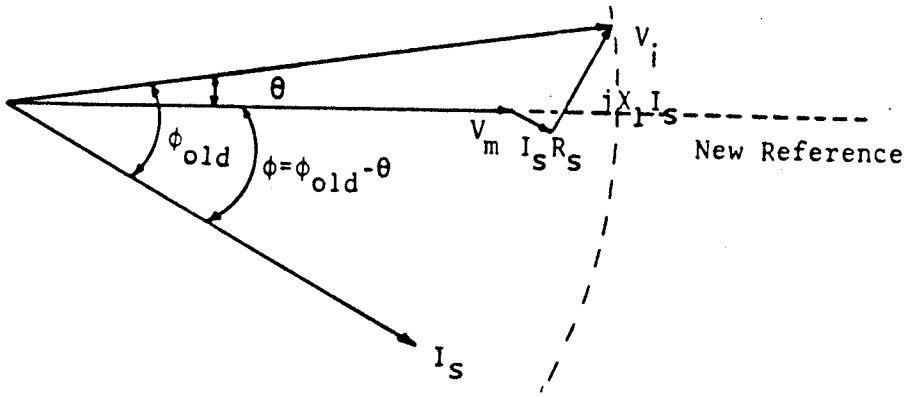

Figure A.2: Phasor Diagram of Change of Reference from V_1 to V_m for each Step V_m is Incremented. V_1, I_1 and ϕ_{old} are Constants

A.3 THE PROGRAM ALGORITHM

Figure A.3 is the flowchart of the Main program.

Figure A.4 is the flowchart of the Motor routine.

The Main program calls Bisection* to find the value of the magnetizing voltage V_m for which $F=X_{21}-X_{22}=0.0$. The search for the zero point of the function F is done by the Bisection technique[58]. To find the values of X_{21}, and X_{22} at each new value of V_m the Bisection calls the subroutine Motor which calculates the new value of F. Motor calls another subroutine Mag, to find the saturation values of R_{e+h} (the iron core loss resistance) and X_m for each new value of V_m.

---

* This is an intermediate routine between the Main program and the routine Motor.

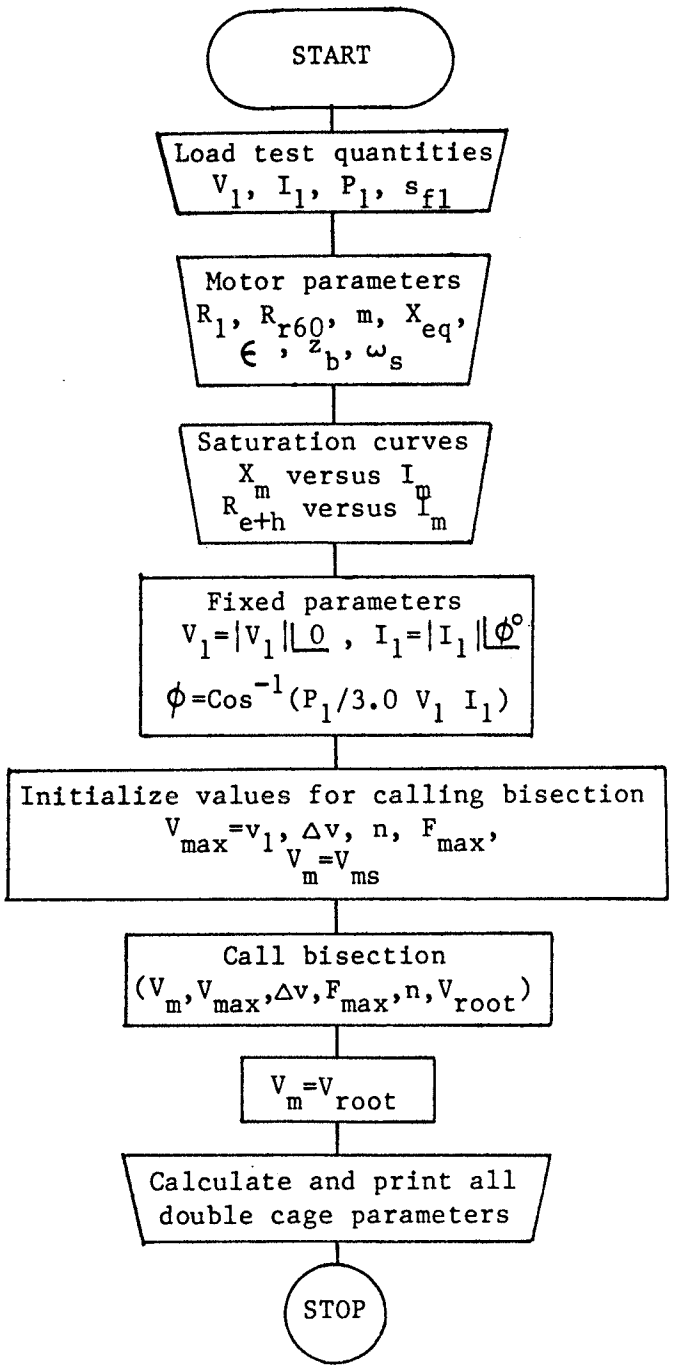

Figure A.3: Flowchart of the Main Program

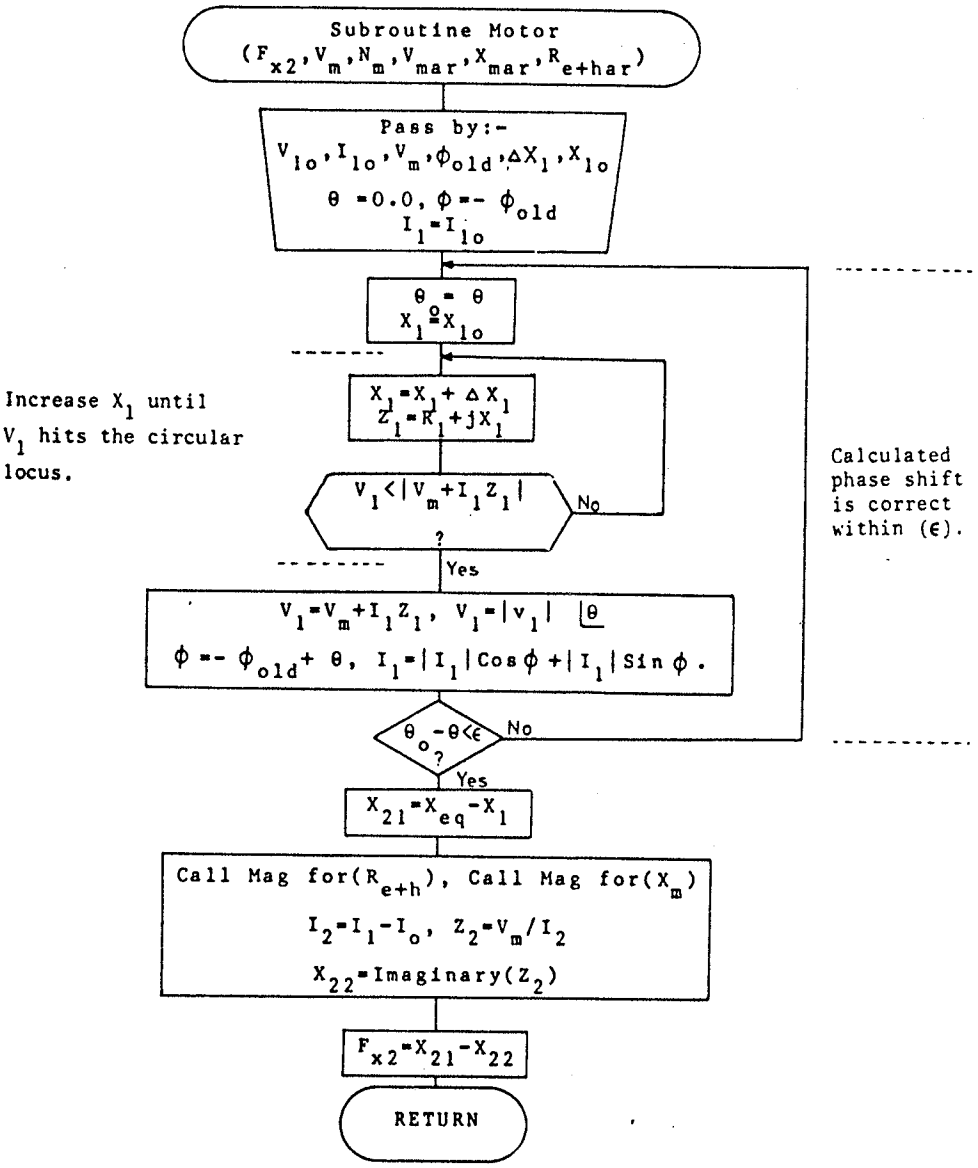

Figure A.4: Flowchart of Subroutine Motor

A.4 THE CALCULATIONS OF THE DOUBLE CAGE PARAMETERS

After finding the exact sharing of stator and rotor equivalent leakage reactances, V_m, Z_2, $X_2=X_{21}=X_{22}$ are known. therefore,

$$R_2=\text{Real}(Z_2) \tag{A.2}$$

$$R_o=R_2 s \tag{A.3}$$

$$\Delta R=R_{r60}-R_o \tag{A.4}$$

$$X_o=\Delta R(m^2+1.0)/m \tag{A.5}$$

Let,

$$k_{ct}=(1.0+R_o/mX_o) \tag{A.6}$$

Therefore,

$$R_B=k_{ct} mX_o \tag{A.7}$$

$$R_A=k_{ct} R_o \tag{A.8}$$

$$X_A=k_{ct}^2 X_o \tag{A.9}$$

The effective leakage reactance of both cages at starting X_{st} is decreased from X_o by $\Delta X_{s=1}$ where,

$$\Delta X_{s=1}=\frac{R_B^2 \; X_A^3}{(R_A+R_B)^2 \; [(R_A+R_B)^2+X_A^2]} \tag{A.10}$$

$$X_s=X_o-\Delta X_{s=1} \tag{A.11}$$

$$X_{mr}=X_2-X_s \tag{A.12}$$

R_{r60} : The starting equivalent rotor resistance.
R_o : The running equivalent rotor resistance.
X_o : The running equivalent rotor reactance.
X_{st} : The starting equivalent rotor reactance.
m : Independent parameter equal to approximately 1.0 for deep bar rotors.
ΔR : Change in rotor resistance from (starting) to (running).
ΔX : Change in rotor reactance from (starting) to (running).
X_{mr} : The mutual rotor reactance.
$R_A=R_{r1}$, $R_B=R_{r2}$, $X_A=X_{r1}$ in Figure A.1

Appendix B

INDUCTION MOTOR ANALYSIS

B.1 ASSUMPTIONS

1. The induction motor used in this analysis is an idealized symmetrical induction motor, in which:
   - The air gap is uniform.
   - The magnetic circuit is linear.
   - Three identical stator windings are distributed so as to produce a single sinusoidal MMF wave rotating in the air gap when excited by balanced sinusoidal currents.
   - The rotor coils or bars are arranged so that the rotor MMF wave can also be considered a space sinusoid having the same number of poles as the MMF wave of the stator.
2. The machine is inverted inside-out, the double cage will be the fixed member and the frame of reference (stationary) will be fixed to it; the three phase wound winding will be the rotating member as shown in Figure B.1.
3. The angle 'θ' is measured counterclockwise between the X-axis and the phase 'a' of the wound rotating winding.
4. The double squirrel cage will be represented as two phase windings as shown in Figure B.1.

5. All the parameters are assumed to be constant with respect to frequency or magnetic saturation.
6. Since the double squirrel cage is treated as two phase windings, then, there will be no mutual coupling between phases, however, there will be mutual M_r between the two windings of different cages on the same axis.

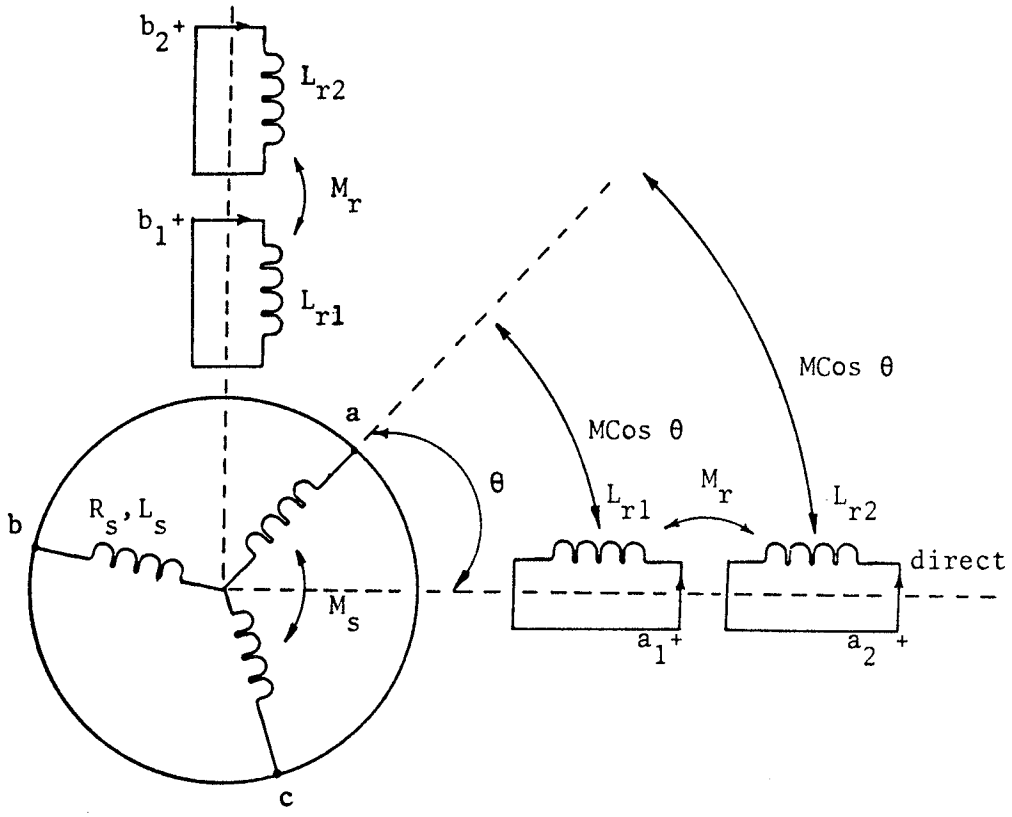

Figure B.1: The Double Cage Model.

Let,

L_s self inductance of the wound winding per phase.

L_{r1} self inductance of the outer cage winding per phase.

L_{r2} self inductance of the inner cage winding per phase.

M_s mutual inductance between phases of the wound winding.

M_r mutual inductance between any two windings, each belongs to a different cage, on the same axis.

M_m peak value of the wound to double cage mutual inductance which occurs when the axes of the two phases concerned coincide. Otherwise, the instantaneous value is proportional to the cosine of the instantaneous angle between the two axis.*

The flux linkage equations may be derived from figure B.1 as follows:

The wound winding

$$\lambda_a = L_s i_a + M_s i_b + M_s i_c + M[(i_{D1}+i_{D2})\cos\theta + (i_{Q1}+i_{Q2})\sin\theta]$$
$$\lambda_b = L_s i_b + M_s i_c + M_s i_a + M[(i_{D1}+i_{D2})\cos\theta_2 + (i_{Q1}+i_{Q2})\sin\theta_2]$$
$$\lambda_c = L_s i_c + M_s i_a + M_s i_b + M[(i_{D1}+i_{D2})\cos\theta_3 + (i_{Q1}+i_{Q2})\sin\theta_3]$$

(B.1-3)

The double cage winding

$$\lambda_{D1} = L_{r1} i_{D1} + M_r i_{D2} + M[i_a\cos\theta + i_b\cos\theta_2 + i_c\cos\theta_3]$$
$$\lambda_{Q1} = L_{r1} i_{Q1} + M_r i_{Q2} + M[i_a\sin\theta + i_b\sin\theta_2 + i_c\sin\theta_3]$$
$$\lambda_{D2} = L_{r1} i_{D2} + M_r i_{D1} + M[i_a\cos\theta + i_b\cos\theta_2 + i_c\cos\theta_3]$$
$$\lambda_{Q2} = L_{r1} i_{Q2} + M_r i_{Q1} + M[i_a\sin\theta + i_b\sin\theta_2 + i_c\sin\theta_3]$$

(B.4-7)

where,

$$\theta_2 = (\theta - 120.0^\circ)$$
$$\theta_3 = (\theta + 120.0^\circ)$$

(B.8-9)

---

* It should be kept in mind that, for the equivalence between the 3-phase and 2-phase MMF,

$$N_q = N_d = (3/2)N_a = (3/2)N_b = (3/2)N_c$$

Hence, M which is the maximum mutual between the 2-phase winding and the wound winding should be $(3/2)M_m$.

The voltage current relations

- First cage

$$v_{D1}=R_{r1}i_{D1}+p\lambda_{D1}$$
$$v_{Q1}=R_{r1}i_{Q1}+p\lambda_{Q1}$$

(B.10-11)

- Second cage

$$v_{D2}=R_{r2}i_{D2}+p\lambda_{D2}$$
$$v_{Q2}=R_{r2}i_{Q2}+p\lambda_{Q2}$$

(B.12-13)

- Wound stator winding

$$v_a=R_s i_a+p\lambda_a$$
$$v_b=R_s i_b+p\lambda_b$$
$$v_c=R_s i_c+p\lambda_c$$

(B.14-16)

The suffixes (a,b,c) indicate the three phase quantities of the wound stator winding. The suffixes (d,q), (D1,Q1) and (D2,Q2) indicate the stator, the first cage and the second cage, direct and quadrature quantities respectively. In the case of a single cage motor, the suffixes (ds,qs) and (dr,qr) indicate the stator and the rotor, direct and quadrature quantities respectively. Substituting (B.1-7) into (B.10-16) the voltages can be obtained as direct functions of the currents. Putting this results in a matrix form gives,

$$
\begin{bmatrix} v_{D1} \\ v_{Q1} \\ v_{D2} \\ v_{Q2} \\ v_a \\ v_b \\ v_c \end{bmatrix} = \begin{bmatrix} R_{r1}+L_{r1}p & 0 & M_r p & 0 & MpCos\ \theta & MpCos\ \theta_2 & MpCos\ \theta_3 \\ 0 & R_{r1}+L_{r1}p & 0 & M_r p & MpSin\ \theta & MpSin\ \theta_2 & MpSin\ \theta_3 \\ R_{r2}+L_{r2}p & 0 & M_r p & 0 & MpCos\ \theta & MpCos\ \theta_2 & MpCos\ \theta_3 \\ 0 & R_{r2}+L_{r2}p & 0 & M_r p & MpSin\ \theta & MpSin\ \theta_2 & MpSin\ \theta_3 \\ MpCos\ \theta & MpSin\ \theta & MpCos\ \theta & MpSin\ \theta & R_s+L_s p & M_s & M_s \\ MpCos\ \theta_2 & MpSin\ \theta_2 & MpCos\ \theta_2 & MpSin\ \theta_2 & M_s & R_s+L_s p & M_s \\ MpCos\ \theta_3 & MpSin\ \theta_3 & MpCos\ \theta_3 & MpSin\ \theta_3 & M_s & M_s & R_s+L_s p \end{bmatrix} \begin{bmatrix} i_{D1} \\ i_{Q1} \\ i_{D2} \\ i_{Q2} \\ i_a \\ i_b \\ i_c \end{bmatrix} \tag{B.17}
$$

It can be seen that $Z_{rs}=Z_{sr}^{t}$ and that the part of Z_{rs} or Z_{sr} representing one cage is a replica of the part representing the other. Consequently the three-phase wound stator quantities may be transformed to the 2-phase quantities and to the d-q or commutator transformation quantities with respect to one cage only. The other cage will follow similarly with the only exception that the mutual between the two cages should be included when a double cage rotor is considered, as indicated in the matrix equations (B.17).

B.2 CONSIDERING ONE OF THE TWO CAGES ONLY

The impedance matrix may be thought as;

$$[Z]=\begin{bmatrix} Z_{rr} & Z_{rs} \\ Z_{rs} & Z_{ss} \end{bmatrix} \qquad (B.18)$$

then,

$$Z_{rr}=\begin{array}{c} \\ D_1 \\ Q_1 \end{array}\begin{array}{c} \begin{array}{cc} D_1 & Q_1 \end{array} \\ \begin{bmatrix} R_{r1}+L_{r1}p & 0 \\ 0 & R_{r1}+L_{r1}p \end{bmatrix} \end{array} \qquad (B.19)$$

$$Z_{ss}=\begin{array}{c} \\ a \\ b \\ c \end{array}\begin{array}{c} \begin{array}{ccc} a & b & c \end{array} \\ \begin{bmatrix} R_s+L_sp & M_s & M_s \\ M_s & R_s+L_sp & M_s \\ M_s & M_s & R_s+L_sp \end{bmatrix} \end{array} \qquad (B.20)$$

$$Z_{sr}=Z_{rs}{}^{t}= \begin{array}{c} \\ a \\ b \\ c \end{array} \begin{array}{c} \begin{array}{cc} D_1 & Q_1 \end{array} \\ \begin{bmatrix} MpCos\theta & MpSin\theta \\ MpCos\theta_2 & MpSin\theta_2 \\ MpCos\theta_3 & MpSin\theta_3 \end{bmatrix} \end{array} \qquad (B.21)$$

B.2.1 Applying the 3-Phase to 2-Phase Transformation

The objective now is to find out the image of the impedance matrix [Z] in the two phase plane i.e;[Z′].

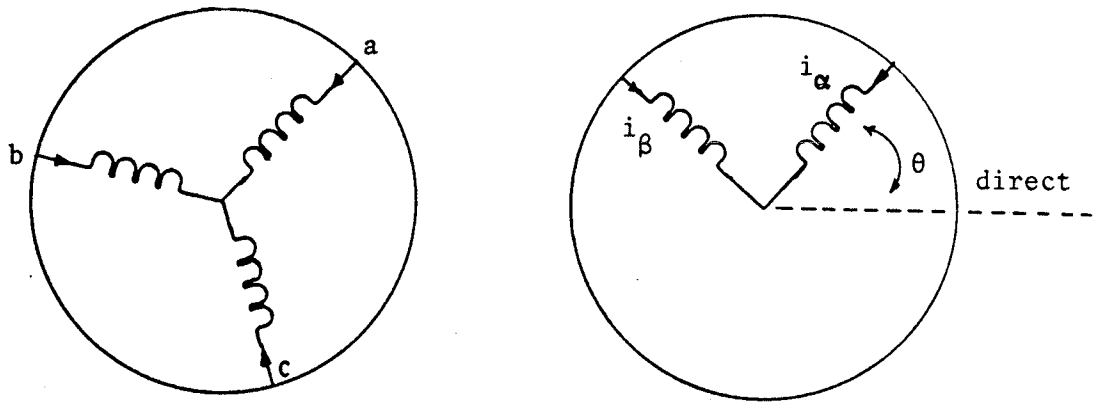

Figure B.2: 3-phase to 2-phase Transformation

In this transformation,

$$Z'_{rr}=Z_{rr} \qquad (B.22)$$

since the double cage rotor was assumed in the two phase representation from the start of this analysis in Figure(B.1).

$$Z'_{ss} = \begin{array}{c} \\ o \\ \alpha \\ \beta \end{array} \begin{array}{c} \begin{array}{ccc} a & b & c \end{array} \\ \begin{bmatrix} R_s+1_o p & 0 & 0 \\ 0 & R_s+L_{ss}p & 0 \\ 0 & 0 & R_s+L_{ss}p \end{bmatrix} \end{array} \qquad (B.23)$$

where,

$$L_{ss}=L_s-M_s$$

and,

$$1_o=L_s+2M_s$$

If the zero sequence is neglected for a 3-wire system, therefore,

$$Z'_{ss} = \begin{array}{c} \\ o \\ \alpha \\ \beta \end{array} \begin{array}{c} \begin{array}{ccc} a & b & c \end{array} \\ \begin{bmatrix} 0 & 0 & 0 \\ 0 & R_s+L_{ss}p & 0 \\ 0 & 0 & R_s+L_{ss}p \end{bmatrix} \end{array} \qquad (B.24)$$

$$Z'_{sr}=Z'_{rs}{}^{t} = Mp \begin{array}{c} \\ o \\ \alpha \\ \beta \end{array} \begin{array}{c} \begin{array}{cc} D_1 & Q_1 \end{array} \\ \begin{bmatrix} 0 & 0 \\ \text{Cos } \theta & \text{Sin } \theta \\ -\text{Sin } \theta & \text{Cos } \theta \end{bmatrix} \end{array} \qquad (B.25)$$

Consequently the total impedance matrix of the wound stator winding and one cage in the two phase representation is:

$$[Z'] = \begin{bmatrix} Z'_{rr} & Z'_{rs} \\ Z'_{sr} & Z'_{ss} \end{bmatrix} \tag{B.26}$$

$$= \begin{array}{c} \\ D_1 \\ Q_1 \\ \alpha \\ \beta \end{array} \begin{array}{c} \begin{array}{cccc} D_1 & Q_1 & \alpha & \beta \end{array} \\ \begin{bmatrix} R_{r1}+L_{r1}p & 0 & MpCos0 & -MpSin0 \\ 0 & R_{r1}+L_{r1}p & MpSin0 & MpCos0 \\ MpCos0 & MpSin0 & R_s+L_{ss}p & 0 \\ -MpSin0 & MpCos0 & 0 & R_s+L_{ss}p \end{bmatrix} \end{array} \tag{B.27}$$

B.2.2 The Commutator Transformation

The objective now is to find the image of the 2-phase matrix [Z′] in the commutator d-q transformation plan i.e;[Z"].

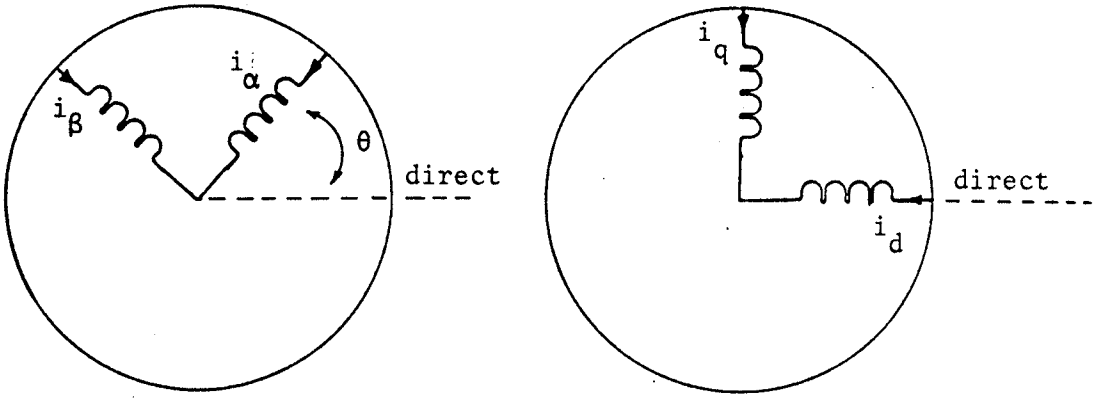

Figure B.3: The Commutator Transformation

Again it should be noticed that,

$$Z''_{rr} = Z'_{rr} = Z_{rr} \tag{B.29}$$

since the double cage rotor was assumed in the d-q axis representation from the start of this analysis in Figure(B.1).

$$Z''_{ss} = \begin{array}{c} \\ d \\ q \end{array} \begin{array}{c} \begin{array}{cc} d & q \end{array} \\ \begin{bmatrix} R_s+L_{ss}p & L_{ss}\,Nu \\ -L_{ss}\,Nu & R_s+L_{ss}p \end{bmatrix} \end{array} \tag{B.30}$$

where, $Nu=p\theta$

$$Z''_{rs} = Mp \begin{array}{c} \\ D_1 \\ Q_1 \end{array} \begin{array}{c} \begin{array}{cc} d & q \end{array} \\ \begin{bmatrix} 1 & 0 \\ 0 & 1 \end{bmatrix} \end{array} \tag{B.31}$$

$$Z''_{sr} = M \begin{array}{c} \\ d \\ q \end{array} \begin{array}{c} \begin{array}{cc} D_1 & Q_1 \end{array} \\ \begin{bmatrix} p & Nu \\ -Nu & p \end{bmatrix} \end{array} \tag{B.32}$$

Through this transformation Z''_{rs} does not equal to Z''^{t}_{sr} because the commutator transformation matrix is a function of 'θ' itself. Now, combining (B.29-B.32) into (B.28) gives;

$$[Z''] = \begin{array}{c} \\ D_1 \\ Q_1 \\ d \\ q \end{array} \begin{array}{c} \begin{array}{cccc} D_1 & Q_1 & d & q \end{array} \\ \begin{bmatrix} R_{r1}+L_{r1}p & 0 & Mp & 0 \\ 0 & R_{r1}+L_{r1}p & 0 & Mp \\ Mp & M\,Nu & R_s+L_{ss}p & L_{ss}\,Nu \\ -M\,Nu & Mp & -L_{ss}\,Nu & R_s+L_{ss}p \end{bmatrix} \end{array} \tag{B.35}$$

The second cage may be implemented in exactly the same manner and the result will be a replica of Eq. (B.35) with R_{r1} and L_{r1} replaced by R_{r2} and L_{r2}. Combining, finally, the two cages and taking into account the mutual between the two cages M_r as indicated in the matrix equation (B.17) gives,

$$\begin{matrix} & D_1 & Q_1 & D_2 & Q_2 & d & q \end{matrix}$$

$$\begin{bmatrix} v_{D1} \\ v_{Q1} \\ v_{D2} \\ v_{Q2} \\ v_d \\ v_q \end{bmatrix} = \begin{bmatrix} R_{r1}+L_{r1}p & 0 & M_r p & 0 & Mp & 0 \\ 0 & R_{r1}+L_{r1}p & 0 & M_r p & 0 & Mp \\ M_r p & 0 & R_{r2}+L_{r2}p & 0 & Mp & 0 \\ 0 & M_r p & 0 & R_{r2}+L_{r2}p & 0 & Mp \\ Mp & M\ Nu & Mp & M\ Nu & R_s+L_{ss}p & L_{ss}Nu \\ -M\ Nu & Mp & -M\ Nu & Mp & -L_{ss}\ Nu & R_s+L_{ss}p \end{bmatrix} \begin{bmatrix} i_{D1} \\ i_{Q1} \\ i_{D2} \\ i_{Q2} \\ i_d \\ i_q \end{bmatrix} \tag{B.36}$$

Appendix C

THE PER UNIT PARAMETERS

Throughout all the calculations made in this thesis two sets of parameters were used, a single cage set and a double cage set. The values of these parameters will be given here for reference. All the values are given in per unit.

C.1 MOTOR #1: SINGLE CAGE PARAMETERS

R_s = 0.05730....Stator Resistance per Phase

R_{rl} = 0.04559....Rotor Resistance per Phase

L_{lsi} = 0.05800....Stator Leakage inductance per Phase "Iron"

L_{lsa} = 0.00000....Stator Leakage Inductance per Phase "Air"

M = 1.84412....Magnetizing Inductance per Phase

L_{ri} = 0.05800....Rotor Leakage "Iron"

L_{ra} = 0.00000....Rotor Leakage "Air"

f_c = 0.09210....Friction Coefficient

J = 188.50000....Polar Moment of Inertia

Motor Ratings 3.0 HP, RPM = 1725, 4 poles,

Volts = 208, Ampere = 10.338, Hz = 60.

The Base Quantities are taken as the peak values of the Motor Ratings[82]

C.2 MOTOR #2: DOUBLE CAGE PARAMETERS

R_s = 0.07040....Stator Resistance per Phase

R_{r1} = 0.09081....1st Cage Resistance per Phase

R_{r2} = 0.15123....2nd Cage Resistance per Phase

L_{lsi}= 0.08527....Stator Leakage inductance per Phase "Iron"

L_{lsa}= 0.00000....Stator Leakage Inductance per Phase "Air"

L_{lr1}= 0.00000....1st Cage Leakage Inductance per Phase

L_{lr2}= 0.26893....2nd Cage Leakage Inductance per Phase

M = 1.87496....Magnetizing Inductance per Phase

M_{ri} = 0.14827....Rotor Mutual "Iron"

M_{ra} = 0.00000....Rotor Mutual "Air"

f_c = 0.05000....Friction Coefficient

J = 136.00000....Polar Moment of Inertia

Motor Ratings 1.5 HP, RPM = 1165, 6 poles,

Volts = 208, Ampere =6.4, Hz = 60.

Base Quantities[82] taken as peak values are:

V_b=169.83 v, I_b=9.05 A, Z_b=18.76 Ohm.

P_b=2305.7 W, T_b=18.35 Nm, $time_b$=2.653 X10^{-3} sec.

Appendix D

THE COMPUTED RESULTS OF THE REFERENCE CURRENT

This Appendix is related to Chapter 4, to show how the two equations (4.9) and (4.15) merge together at about half full load torque.

Figures D.1-4 show the computed reference current for the four representative frequencies 60, 45, 30 and 15 Hz, respectively.

R	CLD2	TL	(4.15) IREF	(4.16) THDEG	(4.14) IROT	(4.9) IREF
1.50000	0.08000	0.17210	0.64806	1.16456	0.36840	0.53738
1.50000	0.16000	0.25210	0.69622	1.16456	0.44587	0.65039
1.50000	0.24000	0.33210	0.74109	1.16456	0.51175	0.74649
1.50000	0.32000	0.41210	0.78330	1.16456	0.57007	0.83156
1.50000	0.40000	0.49210	0.82327	1.16456	0.62295	0.90869
1.50000	0.48000	0.57210	0.86134	1.16456	0.67168	0.97977
1.50000	0.56000	0.65210	0.89775	1.16456	0.71711	1.04604
1.50000	0.64000	0.73210	0.93271	1.16456	0.75982	1.10835
1.50000	0.72000	0.81210	0.96639	1.16456	0.80026	1.16733
1.50000	0.80000	0.89210	0.99891	1.16456	0.83875	1.22348
1.50000	0.88000	0.97210	1.03038	1.16456	0.87555	1.27716
1.50000	0.96000	1.05210	1.06091	1.16456	0.91087	1.32867
1.50000	1.04000	1.13210	1.09057	1.16456	0.94486	1.37826
1.50000	1.12000	1.21210	1.11944	1.16456	0.97768	1.42613
1.50000	1.20000	1.29210	1.14756	1.16456	1.00943	1.47244
1.50000	1.28000	1.37210	1.17501	1.16456	1.04021	1.51734

Figure D.1: Computed Reference Current at 60 Hz

R	CLD2	TL	(4.15) IREF	(4.16) THDEG	(4.14) IROT	(4.9) IREF
1.50000	0.08000	0.11407	0.61054	1.16456	0.29993	0.43751
1.50000	0.16000	0.15907	0.63985	1.16456	0.35418	0.51664
1.50000	0.24000	0.20407	0.66775	1.16456	0.40116	0.58517
1.50000	0.32000	0.24907	0.69446	1.16456	0.44319	0.64648
1.50000	0.40000	0.29407	0.72013	1.16456	0.48157	0.70246
1.50000	0.48000	0.33907	0.74487	1.16456	0.51710	0.75429
1.50000	0.56000	0.38407	0.76879	1.16456	0.55034	0.80278
1.50000	0.64000	0.42907	0.79195	1.16456	0.58169	0.84851
1.50000	0.72000	0.47407	0.81444	1.16456	0.61143	0.89189
1.50000	0.80000	0.51907	0.83630	1.16456	0.63980	0.93327
1.50000	0.88000	0.56407	0.85760	1.16456	0.66695	0.97288
1.50000	0.96000	0.60907	0.87836	1.16456	0.69305	1.01094
1.50000	1.04000	0.65407	0.89863	1.16456	0.71819	1.04762
1.50000	1.12000	0.69907	0.91845	1.16456	0.74249	1.08306
1.50000	1.20000	0.74407	0.93783	1.16456	0.76601	1.11737
1.50000	1.28000	0.78907	0.95682	1.16456	0.78883	1.15067

Figure D.2: Computed Reference Current at 45 Hz

$T_{L(merge)} \equiv$

R	CLD2	TL	(4.15) IREF	(4.16) THDEG	(4.14) IROT	(4.9) IREF
1.50000	0.08000	0.06605	0.57737	1.16456	0.22822	0.33291
1.50000	0.16000	0.08605	0.59145	1.16456	0.26050	0.37998
1.50000	0.24000	0.10605	0.60515	1.16456	0.28919	0.42184
1.50000	0.32000	0.12605	0.61849	1.16456	0.31528	0.45990
1.50000	0.40000	0.14605	0.63152	1.16456	0.33937	0.49504
1.50000	0.48000	0.16605	0.64426	1.16456	0.36186	0.52785
1.50000	0.56000	0.18605	0.65673	1.16456	0.38304	0.55873
1.50000	0.64000	0.20605	0.66895	1.16456	0.40310	0.58800
1.50000	0.72000	0.22605	0.68094	1.16456	0.42221	0.61587
1.50000	0.80000	0.24605	0.69270	1.16456	0.44049	0.64254
1.50000	0.88000	0.26605	0.70426	1.16456	0.45805	0.66815
1.50000	0.96000	0.28605	0.71562	1.16456	0.47495	0.69281
1.50000	1.04000	0.30605	0.72680	1.16456	0.49127	0.71662
1.50000	1.12000	0.32605	0.73780	1.16456	0.50707	0.73966
1.50000	1.20000	0.34605	0.74863	1.16456	0.52239	0.76201
1.50000	1.28000	0.36605	0.75930	1.16456	0.53728	0.78372

Figure D.3: Computed Reference Current at 30 Hz

R	CLD2	TL	(4.15) IREF	(4.16) THDEG	(4.14) IROT	(4.9) IREF
1.50000	0.08000	0.02803	0.54924	1.16456	0.14866	0.21685
1.50000	0.16000	0.03303	0.55307	1.16456	0.16138	0.23540
1.50000	0.24000	0.03803	0.55685	1.16456	0.17317	0.25259
1.50000	0.32000	0.04303	0.56059	1.16456	0.18420	0.26869
1.50000	0.40000	0.04803	0.56429	1.16456	0.19461	0.28387
1.50000	0.48000	0.05303	0.56796	1.16456	0.20449	0.29828
1.50000	0.56000	0.05803	0.57159	1.16456	0.21391	0.31203
1.50000	0.64000	0.06302	0.57520	1.16456	0.22294	0.32520
1.50000	0.72000	0.06802	0.57878	1.16456	0.23161	0.33785
1.50000	0.80000	0.07302	0.58233	1.16456	0.23997	0.35005
1.50000	0.88000	0.07802	0.58585	1.16456	0.24805	0.36183
1.50000	0.96000	0.08302	0.58935	1.16456	0.25588	0.37325
1.50000	1.04000	0.08802	0.59282	1.16456	0.26347	0.38432
1.50000	1.12000	0.09302	0.59627	1.16456	0.27085	0.39508
1.50000	1.20000	0.09802	0.59970	1.16456	0.27803	0.40556
1.50000	1.28000	0.10302	0.60310	1.16456	0.28503	0.41578

Figure D.4: Computed Reference Current at 15 Hz

Appendix E

COMPLEMENTARY RESULTS

This Appendix is related to Chapter 7 to show the actual unfiltered torque as well as the speed and frequency at the four representative frequencies (Figures E.1-4).

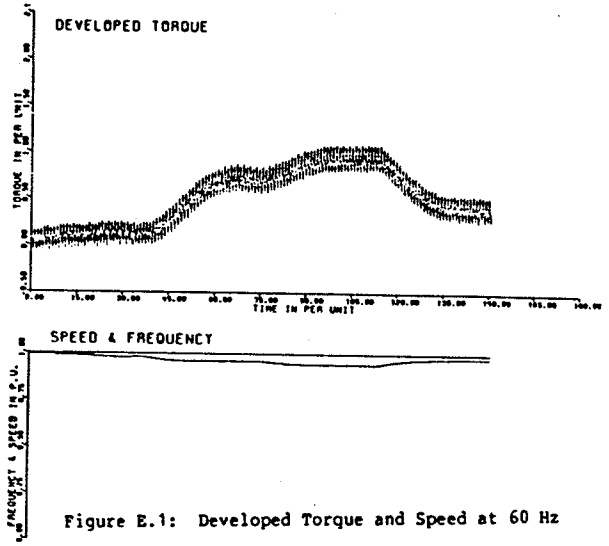

Figure E.1: Developed Torque and Speed at 60 Hz

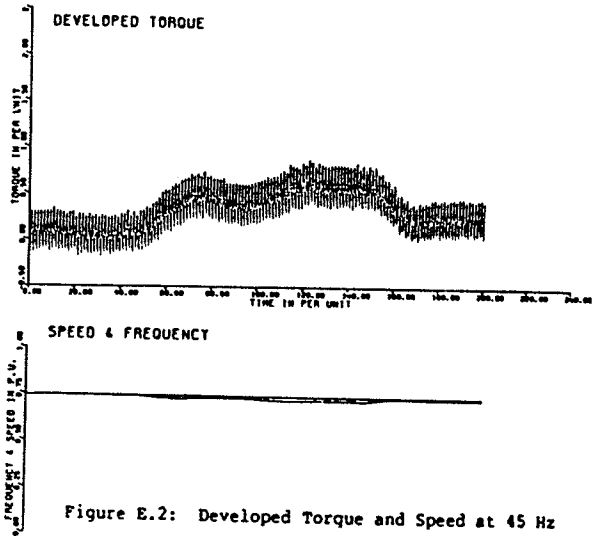

Figure E.2: Developed Torque and Speed at 45 Hz

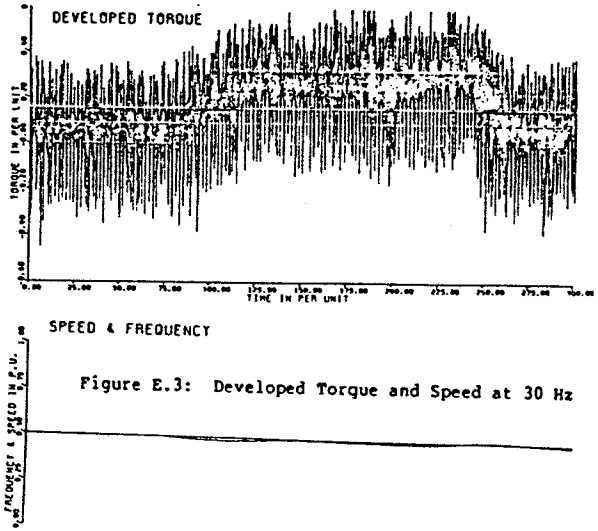

Figure E.3: Developed Torque and Speed at 30 Hz

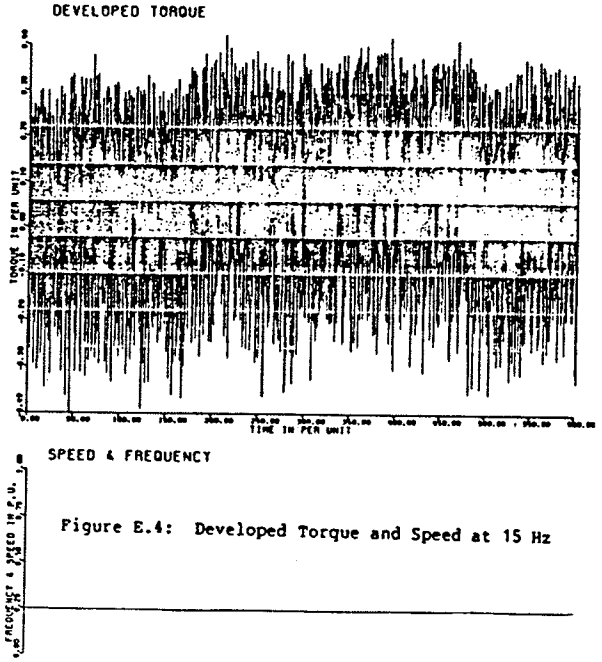

Figure E.4: Developed Torque and Speed at 15 Hz